National Technical University of Athens

School of Naval Architecture and Marine Engineering

Division of Marine Structures

Master Thesis

Buckling and ultimate strength study of a stiffened plate under compression using finite element method

Vasilis Panagiotopoulos

Under the supervision of Professor Manolis Samuelides

Athens, Greece, 2020

Acknowledgements

This work is part of the Postgraduate Studies Program “Marine and Ocean Technology” of the Department of Naval Architects and Marine Engineers, National Technical University of Athens.

It would not have been possible to fulfill this work without the educationally, advisory and emotionally contribution of many different people.

I pay my deep sense of gratitude in my supervisor Prof. Manolis Samuelides (NTUA) for his keen interest and conscientious guidance. His deep scientific knowladge, analytical thinking, patience and and excellent cooperation at all levels have deeply inspired me. It was a great privilege and honor to study under his guidance.

I am greatful to Dimitris Georgiadis (PhD Student, NTUA) for his technical advices and suggestions.

Last, but not least, I would like to excpress my graditude to my parents Christos and Dimitra and my sister Lena, for supporting me with more ways I could possibly ask or even imagine. They always believe in me, even when I doubt, and they give me courage to follow through on my goals. I am really thankful to have them by my side.

Contents

Scope

Hull is mainly composed by a continuous system of frames, plates, stiffeners and girders. Overall failure of a ship's hull is governed by buckling and plastic collapse of the deck, bottom or side shell stiffened plates. Hence, is crucial to accurately calculate the ultimate strength of those elements.

Regulations and guidelines concerning structural integrity of a ship and buckling of its structural components are typically based on text book formulas, modified to take into consideration different buckling modes, interaction between elements, nonlinear behavior etc. This type of approach has limitations concerning complex structural problems. Limitations concerning complex interactions, geometry or loads, could overcome by using Finite Element Method.

The task of this work is to study the buckling and ultimate strength of an isolated stiffened plate and an isolated stiffened plate's element (stiffener and attached plating), as parts of a ship's deck, under compressive loading conditions, which results from the sagging of the hull, using Finite Element Method. The boundary conditions of an isolated structural element of deck (stiffened plate, stiffened plate's element) should represent realistically the behavior of that element as part of the construction. The appropriate boundary conditions for an isolated stiffened plate model were obtained by monitoring displacements on the boundaries of a stiffened plate on the deck of a hull model subjected to longitudinal bending. Those boundary conditions used in the finite element analysis of an isolated stiffened plate model, so that conclusions about collapse mode, ultimate strength, stress distribution and load distribution among stiffened plate's elements to be made. Similarly, the appropriate boundary conditions for an isolated stiffened plate's element were obtained through a stiffened plate model subjected to uniaxial compression, by monitoring the displacements on its elements' boundaries. The obtained boundary conditions used in the finite element analysis of an isolated stiffened plate's element model, so that conclusions about collapse mode, ultimate strength and stress distribution to be made along with a comparison between shell and cubic elements. Using evidences acquired from the study of the aforementioned models, evaluated whether is it possible or not, to predict the buckling behavior of a stiffened plate through the analysis of just one of its elements.

This work fulfilled using Abaqus 6.14

PART 1 Fundamental Theory

1 Stiffened Plates and Stiffened Plate's Buckling

1.1 Stiffened Plates

Stiffened plate structures are widely used in the aerospace, automobile and marine industries. The basic strength members in stiffened panel structures include support members (such as stiffeners, girders, and frames), and plates. The hull structure consists of stiffened panels (bottom construction, side shell construction, upper deck construction, bulkhead, etc). The plate receives loads such as water pressure, stiffeners and girders support the loads from the plate and transverse frames support loads from the stiffeners and girders. Structural members that contribute to the reaction moment of each cross section of the ship during hogging or sagging, receive normal stresses resulting from bending of the ship as a beam.

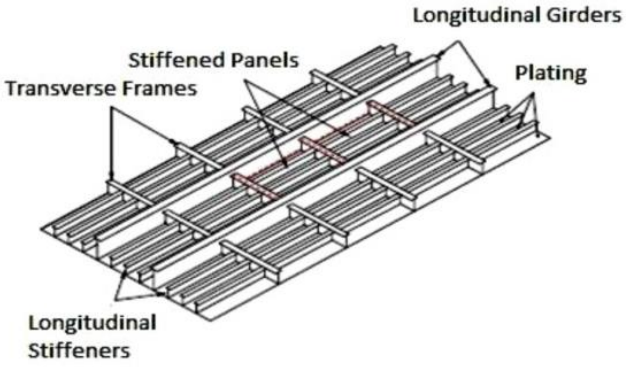

FIGURE 1.1 Typical stiffened plate structure in a ship

In an actual marine structure, an isolated stiffened panel does not exist, but it is a part of a continuous system of plates, stiffeners and frames.

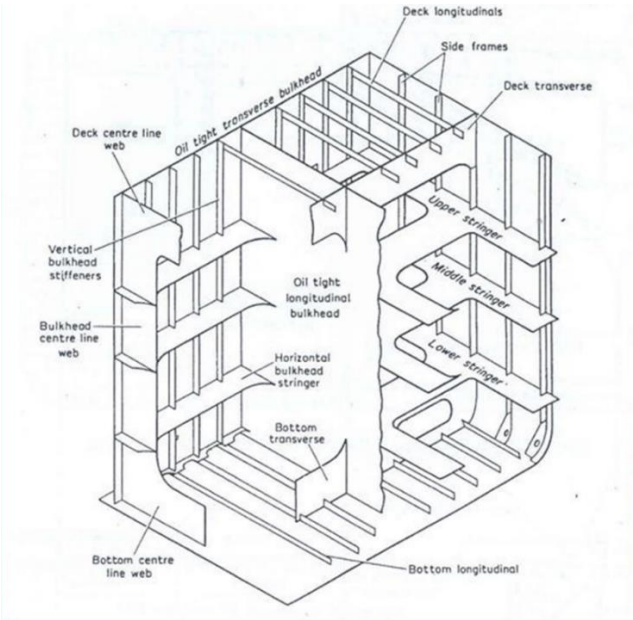

FIGURE 1.2 Part of a longitudinally and transversely stiffened tanker

A variety of sections have been historically used as stiffeners, however the simple flat stiffener, angle stiffener and tee stiffener are almost always used in modern designs. Stiffeners can be attached on one side of the plate (single sided), or on both sides (double sided). Stiffeners can also be doubled up, or even trebled, to form multi-leg stiffeners.

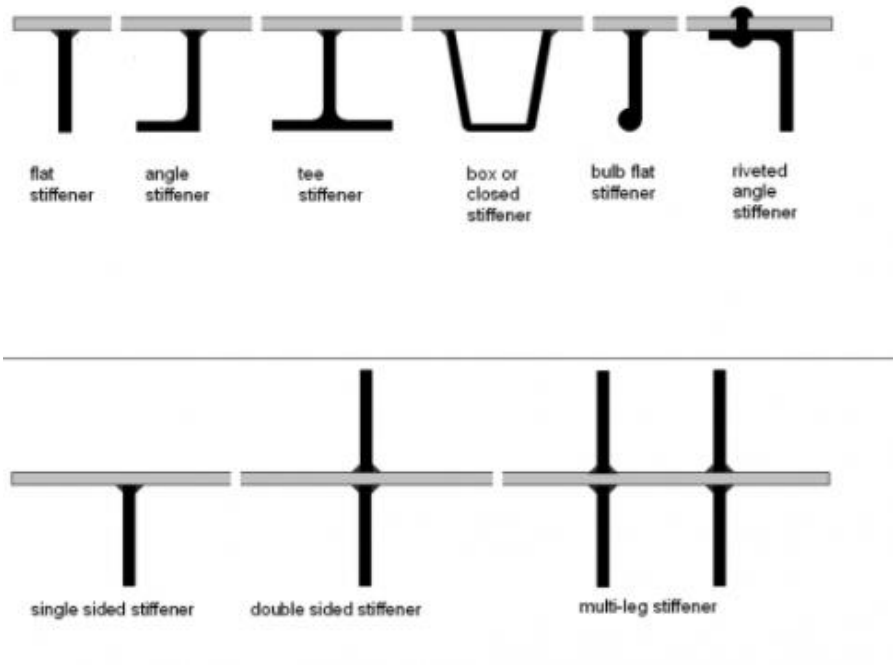

FIGURE 1.3 Stiffener sections

The geometry of a longitudinally stiffened plate is fully described by: plate's length (L), total plate's width (B), span between two stiffeners (s), plate's thickness (t_p), web's height (h_w), web's thickness (t_w) and flange's width (b_f) and flange's thickness for tee and angle stiffener stiffened plate (t_f). Considering that stiffeners are equally spread in transverse direction it's valid that $B = (n+1)\cdot s$, where *n* is the number of stiffeners.

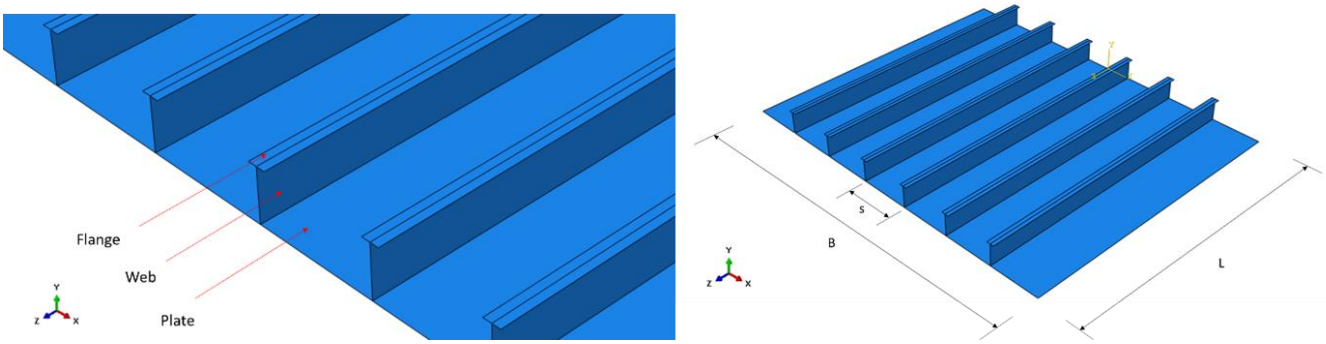

FIGURE 1.4 Tee stiffener stiffened plate principal components and dimensions

1.2 Buckling of Stiffened Plates

1.2.1 Collapse Mode of Stiffened Plates

The overall failure of ship structures is mainly governed by the buckling and plastic collapse of the stiffened panels in the deck, bottom, and sometimes the side shell. Therefore, the accurate and efficient calculation of the collapse strength of stiffened panels is an important task in the design and safety assessment of ship structures.

The possible collapse modes of a stiffened panel can be categorized into the following eight types:

- Overall collapse of the plating and stiffeners as a unit (FIG. 1.4 A)

Plate collapse modes

- Local plate buckling (longitudinal thrust) (FIG. 1.4 B)
- Local plate buckling (transverse thrust) (FIG. 1.4 C)
- Local plate buckling (biaxial thrust) (FIG. 1.4 D)

Stiffener collapse modes

- Beam-column type collapse of stiffeners (FIG. 1.4 E)
- Local buckling of the stiffener web (FIG. 1.4 F)
- Flexural–torsional buckling or tripping of the stiffeners (FIG. 1.4 G)

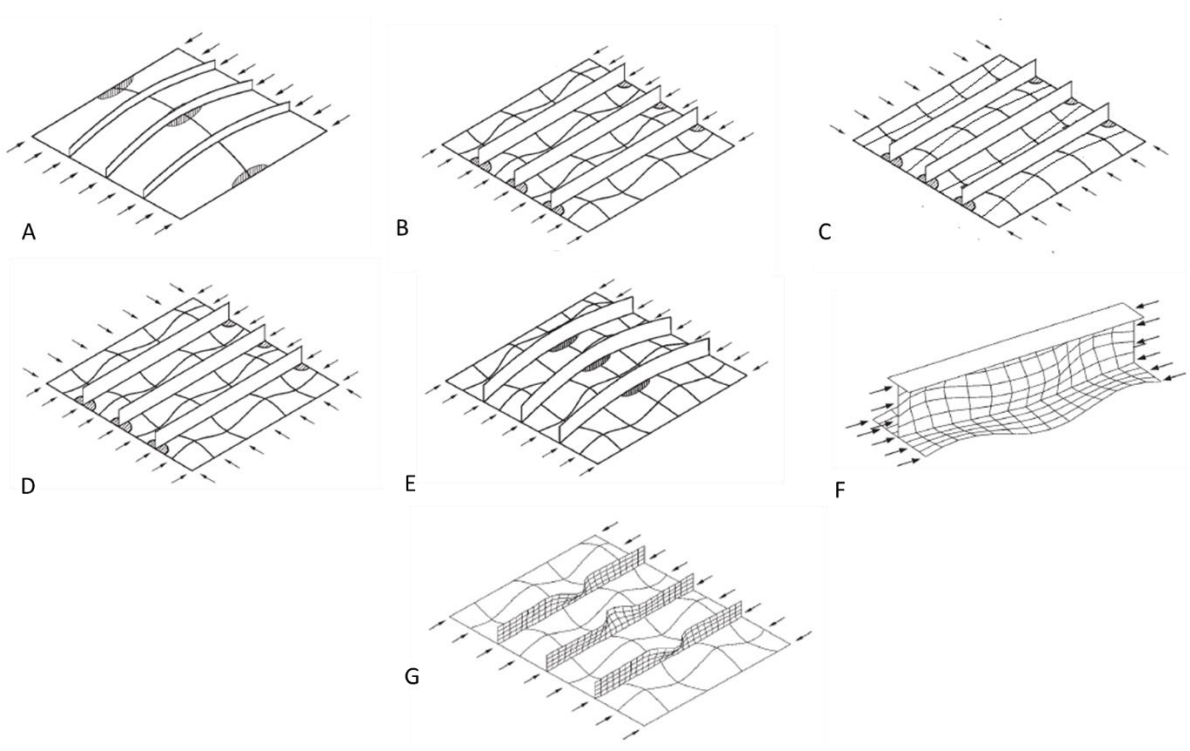

FIGURE 1.5 Collapse modes of stiffened plates

1.2.2 Overall Buckling vs Local Buckling

Stiffened plates can buckle overall or locally. In overall buckling, stiffeners buckle along with the plating. In local buckling either the stiffeners buckle because of inadequate rigidity or stability, or the plate panels buckle between the stiffeners, thus shedding extra load into the stiffeners so that eventually the stiffeners buckle too. Stiffener buckling is synonymous with overall buckling, because if the stiffeners buckle the plating is left with almost no lateral rigidity. Considering this, stiffeners should be at least as strong as the plating, meaning, they should have sufficient flexural and torsional rigidity so that neither overall buckling nor local stiffener buckling occurs before local plate buckling.

A reliable way to ensure that a stiffened plate is designed sufficient is to calculate the overall buckling stress $(\sigma_{\alpha})_{cr}$ and torsional buckling stress of stiffeners $(\sigma_{\alpha,T})_{cr}$ and to compare it with plate buckling stress $(\sigma_{p})_{cr}$.

Owen F. Hughes and Jeom Kee Paik (2010) mention a methodology to determine overall buckling stress of the stiffened plate, beam column buckling stress of the stiffeners and torsional buckling stress of the stiffeners. This methodology will be presented in chapters 1.2.3 and 1.2.4.

1.2.3 Stiffened Plate's Overall Buckling Stress and Stiffeners Beam Column Buckling Stress

A stiffened plate is considered, with stiffeners of the same size and with equal distance between them. Thus, regarding each stiffener and its associated width of plating as a column and assuming any axial load is distributed equally on those columns, it can be assumed that the elastic buckling stress of the stiffened plate, could be approached, calculating the elastic buckling stress of one of those columns, using Euler column buckling formula. Stiffened plates are designed such that plate buckling precedes overall buckling. As soon as compressive stresses acting on stiffened plate reach critical buckling stress of plate between stiffeners and its buckling occurs, the effective width of plate reduces. Overall buckling occurs without plate buckling for the plate between stiffeners taking place, thus for overall buckling, effective width of plate equals actual plate's width. Hence, using Euler buckling column formula considering effective width of plating equals actual plate's width, overall buckling stress for the stiffened plate is obtained. On the other hand, using Euler buckling column formula considering plating will not be fully effective over the width, beam column buckling stress of stiffeners is obtained.

Overall buckling stress of stiffened plates

Overall elastic buckling stress $(\sigma_\alpha)_{cr}$ can be obtained using Euler column buckling formula on one of the aforementioned columns considering plating is fully effective over the width. This column has an equivalent slenderness ratio $(L/\rho)_{eq}$. In short panels the stiffeners are in fact a row of identical parallel columns and concerning buckling, independent. The equivalent slenderness ratio of each column is the actual slenderness of the section.

$$\left(\frac{L}{\rho}\right)_{eq} = \frac{\alpha}{\rho} = \frac{\alpha}{\sqrt{\frac{I}{A + b \cdot t}}} \qquad (1.2.1)$$

Where

$I =$ Moment of inertia of section comprised of stiffener together with plate

$A =$ Cross-sectional area of stiffener only

$b =$ plate's width, $t =$ plate's thickness

Parameter "γ" is the ratio of the flexural rigidity of the combined section to the flexural rigidity of the plating and parameter "Π" is the aspect ratio of the stiffened panel.

$$\gamma = \frac{EI}{Db} = \frac{12(1-v^2)I}{bt^3} \qquad (1.2.2)$$

$$\Pi = \frac{L}{B} = \frac{a}{B} \qquad (1.2.3)$$

Where

$E =$ Young modulus of section comprised of stiffener together with plate

$v =$ Poisson ratio

$I =$ Moment of inertia of section comprised of stiffener together with plate

$D =$ flexural rigidity of the plating, $D = \frac{Et^3}{12(1-v^2)}$ (1.2.4)

In long panels, the stiffeners receive some lateral restraint from the sides of the panel. This could cause them to buckle in more than one half-wave. In this case, the equivalent slenderness ratio is smaller than the value given by equation (1.2.1). The effect occurs for large values of the panel aspect ratio "Π" and for small values of stiffener rigidity relative to the plating "γ". From the work of Sharp (1966), it is possible to derive an aspect ratio coefficient "C_Π" which accounts for this effect as follows:

$$\left(\frac{L}{\rho}\right)_{eq} = C_{\Pi}\frac{\alpha}{\rho} = \frac{C_{\Pi}\cdot\alpha}{\sqrt{\frac{I}{A+b\cdot t}}} \qquad (1.2.5)$$

Where

$$C_{\Pi} = \frac{1}{\Pi}\sqrt{\frac{\gamma}{2(1+\sqrt{1+\gamma})}} \qquad (1.2.6)$$

or

$$C_{\Pi} = 1 \qquad (1.2.7)$$

Whichever is lower. The resulting value of (1.2.5) is then used in the standard column buckling formula

$$(\sigma_a)_{cr} = \frac{\pi^2 E}{\left(\frac{L}{\rho}\right)^2_{eq}} \qquad (1.2.8)$$

Stiffeners beam column buckling stress

Slender panels are normally designed such that plate buckling precedes overall buckling. When the latter occurs, the plate flange of the stiffener will not be fully effective over the width b. Instead, it is necessary to take some reduced effective width b_e.

For elastic or near-elastic buckling, a satisfactory formula was derived by von Karman, Sechler, and, Donnell (1932), idealizing the state of stress within the buckled plate by assuming that, because of buckling, the center portion has no compressive stress, while the edge portions of the plate remain fully effective and carry a uniform stress. This means that the buckled center portion of the plate is discounted completely and the original plate of width "b" is replaced by an unbuckled plate of effective width "b_e". It is clear that axial strength in the stiffener columns "σ_e" and the external applied stress "σ_α" are related by:

$$\sigma_e = \frac{b}{b_e}\sigma_\alpha \qquad (1.2.9)$$

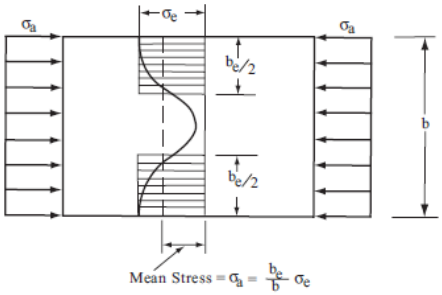

FIGURE 1.6 Post-buckling stress distribution, effective width

To simulate the progressive growth of the buckling, it is further assumed that the (yet unbuckled) effective plate is always on the verge of further buckling, meaning the effective width is taken to be the width at which the equivalent plate would buckle at an applied stress of "σ_e". This implies that

$$\sigma_e = k\frac{\pi^2 D}{b_e^2 t} \qquad (1.2.10)$$

and for the original plate

$$(\sigma_a)_{cr} = k\frac{\pi^2 D}{b^2 t} \qquad (1.2.11)$$

Assuming that "k" is the same for both cases:

$$\frac{b_e}{b} = \sqrt{\frac{(\sigma_a)_{cr}}{\sigma_e}} \qquad (1.2.12)$$

Substituting equation 1.2.11 to 1.2.12:

$$b_e = \pi \cdot t \cdot \sqrt{\frac{k \cdot E}{12(1-v^2)\sigma_e}} \qquad (1.2.13)$$

Having an expression for "b_e" extracted, an expression for the ultimate or collapse load of slender stiffened panels can be obtained. The effective width is used to calculate the equivalent slenderness ratio from equation (1.2.5), using "b_e" as the plate flange width in calculating "I", and "ρ". Those values shall be denoted as "I_e", and "ρ_e" and the resulting value of equivalent slenderness ratio as "$(L/\rho_e)_{eq}$". The axial stress in the stiffener columns is "σ_e" and the critical value of this stress is

$$(\sigma_e)_{cr} = \frac{\pi^2 E}{\left(\frac{L}{\rho_e}\right)_{eq}^2} \qquad (1.2.14)$$

This equation refers to "σ_e" rather than "σ_α". Axial stress in the stiffener is larger than the external applied stress "σ_α" because of the reduced width of the plate. The quantity of interest is the value of "σ_α" corresponding to "$(\sigma_e)_{cr}$". From statics, the two are related by $\sigma_\alpha(bt + A) = \sigma_e(b_e t + A)$, and from this together with equation (1.2.14) :

$$(\sigma_a)_{cr} = \frac{b_e t + A}{bt + A}\frac{\pi^2 E}{\left(\frac{L}{\rho_e}\right)_{eq}^2} \qquad (1.2.15)$$

Because of the presence of "σ_e" in equation (1.2.13), the fore going sequence of calculations must be performed iteratively. A suitable procedure would be:

1. Assume some initial value of b_e (e.g., 0.8b).

2. Calculate "I_e", and then evaluate "$(L/\rho_e)_{eq}$" from equation (1.2.5), using "b_e" in place of "b".

3. Calculate "$(\sigma_e)_{cr}$" from equation (1.2.14). Check that $(\sigma_e)_{cr} > (\sigma_p)_{cr}$.

4. Using this value of "σ_e", recalculate "b_e" from equation (1.2.13).

5. Repeat from step 2 until "b_e" has converged.

6. Calculate $(\sigma_\alpha)_{cr}$ from equation (1.2.15).

1.2.4 Stiffener Tripping Buckling Stress

Under uniaxial load, stiffeners act as columns, but torsional buckling differs from that of a column in three ways:

- Rotation occurs about the line of attachment to the plating and not about shear center
- Plate offers some restraint against this rotation
- The rotation is not necessarily rigid body rotation. Considering a construction with a sturdy plate and stiffeners with slender webs, sideways displacement of stiffener's flange could occur due to web bending.

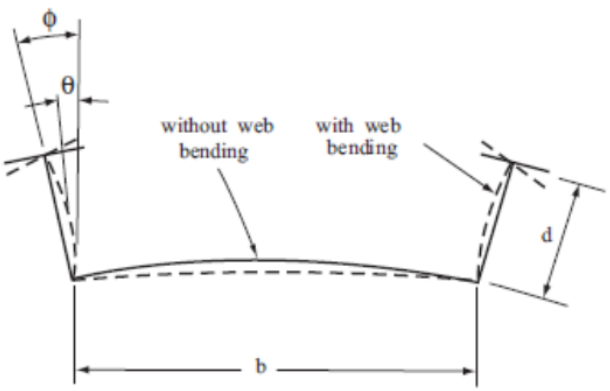

FIGURE 1.7 Effect of web bending

From the basic theory of the torsion of thin-walled sections is known that for all cross-sectional shapes that are composed of thin rectangles which meet at a common point, the shear center is at this point and the warping constant is zero. The differential equation for the torsional buckling of a column about an enforced axis of rotation under the action of an applied axial stress for the above case is

$$EI_{sz}d^2\frac{d^4\varphi}{dx^4}-\left(GJ-\sigma_\alpha I_{sp}\right)\frac{d^2\varphi}{dx^2}+K_\varphi\varphi=0 \qquad (1.2.16)$$

Where

$I_{sz}=$ moment of inertia of the stiffener about an axis through the centroid of the stiffener and parallel to the web

$d=$ stiffener web height + (t_p + t_f)/2

$I_{sp}=$ polar moment of inertia of the stiffener about the center of rotation

$\sigma_\alpha=$ axial stress

$K_\varphi=$ distributed rotational restraint which the plating exerts on the stiffener

If the ends of the stiffener are regarded as simply supported, the solution for ϕ(x) is a buckling mode in which the rotation ϕ varies sinusoidally in m half-waves over the length a. The elastic torsional stress that would cause tripping according to elastic theory, will be denoted as "$\sigma_{\alpha,T}$". From the foregoing equation, it may be seen that $\sigma_{\alpha,T}$ is the minimum value of σ_α that satisfies the following, in which m is a positive integer.

$$EI_{sz}d^2\frac{m^4\pi^4}{a^4}-\left(GJ-\sigma_\alpha I_{sp}\right)\frac{m^2\pi^2}{a^2}+K_\varphi(\sigma_\alpha,m)=0 \qquad (1.2.17)$$

In the absence of other factors, the rotational restraint offered by the plating comes directly from the plates flexural rigidity which causes, in response to the rotation *φ* of the stiffener, a total distributed restraining moment M_R = 2*M* along the line of the stiffener attachment, as shown in FIGURE 1.7. If the individual plate panels are long, that is, if a>> *b*, then we may ignore aspect ratio effects, and by considering a unit strip of plating across the span *b* it may be shown that ϕ= ½*Mb*/*D*. Therefore, the rotational restraint coefficient is

$$K_\varphi=\frac{M_R}{\varphi}=\frac{4D}{b} \qquad (1.2.18)$$

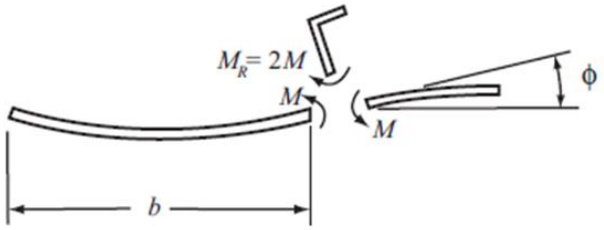

FIGURE 1.8 Restraining moment exerted by plating

1.2.4.1 Plate-Web Interaction

The above assume that displacement of the stiffener is entirely due to rigid body rotation. This is only accurate if the flexural rigidity of the stiffener web is much larger than that of the plate. In practice, some of the sideways displacement of the stiffener flange occurs because of bending of the web, and this effect becomes important if the plating is sturdy or if the stiffener web is slender (FIG. 1.9). Sharp (1966) has presented an expression that accounts for this effect.

$$K_{\varphi} = \frac{4D}{b} C_r C_a \qquad (1.2.19)$$

Where

$$C_r = \frac{1}{1 + 0,4\left(\frac{t_p}{t_w}\right)^3 \frac{d}{b}} \qquad (1.2.20)$$

$$C_a = 1 - \left(\frac{2\sigma_\alpha}{(\sigma_p)_{cr}} - 1\right)\frac{m^2}{\alpha^2} \qquad (1.2.21)$$

C_r is the factor by which the plate rotational restraint is reduced because of web bending and C_a is the factor taking account of stiffened plate's aspect ratio.

From the expression for "C_a", it may be seen that for $\sigma_\alpha=(\sigma_p)_{cr}$, the factor C_a, and hence also the plate rotational restraint K_ϕ, is proportional to $1-(m/\alpha)^2$; that is, the restraint disappears when $m = \alpha$. This reflects the fact that if the plate panel between the stiffeners buckling pattern matches that of the stiffener ($\alpha = m$) then as "σ_α" approaches plates critical buckling strength "$(\sigma_p)_{cr}$", the plate loses its ability to provide any rotational restraint. For stiffened panels of usual proportions, tripping occurs in a single half-wave, $m = 1$, and hence it is

mainly square or short panels in which this loss of stiffness can occur. Final expression of the rotational restraint coefficient is

$$K_{\varphi} = \frac{4D}{b}\left[\frac{1}{1+0,4\left(\frac{t_p}{t_w}\right)^3\frac{d}{b}}\right]\left[1-\left(\frac{2\sigma_{\alpha}}{\sigma_{cr,p}}-1\right)\frac{m^2}{\alpha^2}\right] \qquad (1.2.22)$$

Substituting equation 1.4.22 to 1.4.17 and solving for "σ_{α}" torsional buckling stress can be acquired as the minimum value of σ_{α}

$$\sigma_{\alpha,T} = \min_{m=1,2...}\left\{\frac{1}{I_{sp}+\frac{2C_r b^3 t}{\pi^4}}\left[GJ+\frac{m^2\pi^2}{a^2}EI_{sz}d^2+\frac{4DC_r}{\pi^2 b}\left(\frac{a^2}{m^2}+b^2\right)\right]\right\} \qquad (1.2.23)$$

As mentioned previously, in stiffened panels of average proportions the critical tripping mode is usually the *m* = 1 mode, but of course this cannot be simply assumed, the correct value of *m* must be ascertained in each case. An estimate can be obtained regarding m as a continuous variable, differentiate equation (1.2.23) with respect to "m", and set this equal to zero. The result is

$$m \cong \frac{a}{\pi}\sqrt[4]{\frac{4DC_r}{EI_{sz}d^2b}} \qquad (1.2.24)$$

After obtaining this estimate, torsional buckling stress can be obtained trying the two integer values above and below it to see which value gives the lowest value in equation (1.4.20).

1.2.5 Long Plate Buckling Stress

The elastic buckling strength of a long plate subjected to uniaxial compression can be expressed as:

$$\left(\sigma_p\right)_{cr} = \frac{\pi^2 kE}{12\left(1-v^2\right)}\left(\frac{t}{b}\right)^2 \qquad (1.4.22)$$

Where,

k = plate's buckling coefficient

t = plate's thickness

b = plate's width

Buckling coefficient “k” is determined depending on loading, boundary conditions and plate’s aspect ratio. The effect of boundary conditions on a rectangular plate under uniaxial compression is illustrated in figure 1.8. Assuming a rectangular plate with simply supported edges under uniaxial load, buckling coefficient “k” is expressed as:

$$k = \left(\frac{a}{mb} + \frac{mb}{a} \right)^2 \qquad (1.4.23)$$

Where

$a =$ plate’s length

$b =$ plate’s width

$m =$ number of halfwaves of buckling mode in the direction of load

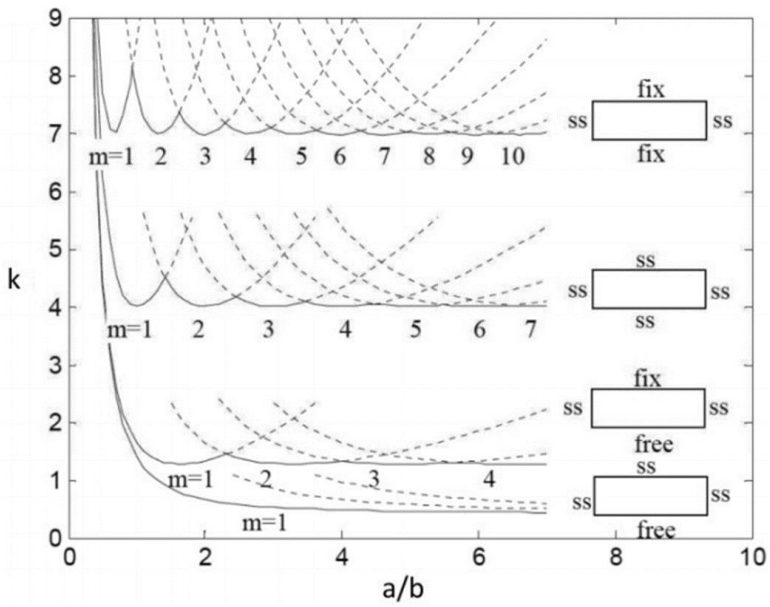

FIGURE 1.9 Effect of boundary conditions on a rectangular plate under uniaxial compression

Stiffened plates are designed so that local panel buckling takes place before overall buckling occurs. For such design, local buckling strength of plate between stiffeners is affected by the interaction between the plate and the stiffener’s web. Assuming simply supported edges is the most representative boundary condition for plate edges in a high level of accuracy, buckling coefficient could be assumed to equal 4 (FIGURE 1.8) However, due to the aforementioned interaction, buckling coefficient’s “k” value is expected to change slightly from the above ideal conditions.

Stiffener’s web could be studied as plates using equation (1.4.22), substituting “t” with web thickness “t_w” and “b” with web’s height “h_w”. When flatbars are used as stiffeners, assuming a plate with three simple supported edges and one free, since plate provides restriction to the web, is representative of the conditions on the web’s boundaries. Hence, the buckling coefficient equals 0.5 (FIGURE 1.8). When tee-stiffeners are used, the

appropriate conditions for the boundaries is to consider four simply supported edges, since stiffener's flange and plate provide restriction to the web, thus "k" equals 4. Due to interactions with plate and flange (tee-stiffeners), buckling coefficient is expected to be slightly different from this of the ideal conditions above.

According to IACS CSR (2019, Part 1, Chapter 8 Section 5, tables 2,3) buckling coefficient for plate's between stiffeners (k_p), for the boundary conditions mentioned could be taken as:

$$k_p = F_{long} \frac{8,4}{\psi + 1,1} \qquad (1.4.24)$$

Where,

$\psi = 1$, for equally distributed load

$F_{long} = c + 1$ for $\frac{t_w}{t_p} > 1$ or $F_{long} = c\left(\frac{t_w}{t_p}\right)^3 + 1$ for $\frac{t_w}{t_p} < 1$

$c = 0,1$ (flatbar stiffeners) or $c = 0,3$ (tee-stiffeners)

According to ABS (2019, Rules for building and classing, Marine vessels, Part 3 Hull construction and equipment, p. 388) for flanged profile stiffeners, the ideal buckling stress of the web is given by:

$$\left(\sigma_{p,w}\right)_{crit} = 3,8\left(\frac{t_w}{h_w}\right)^2 \qquad (1.4.25)$$

2 Buckling Finite Element Analysis

M. Mano (2009, p.125) referring to finite element method, mentions that the finite element method (FEM) is an essential and powerful tool for solving structural problems not only in the field of shipbuilding but also in the design of most industrial products and even in non-structural fields. FEM can be used for a wide variety of problems in linear and nonlinear solid mechanics, dynamics, and ships' structural stability problems, in accordance with the development of computer technology and its popularization. The conventional method in solving stress and deformation problems is an analytical one using theories of beams, columns and plates, etc. As a result, its application is restricted to most simple structures and loads. On the other hand, FEM:

(1) divides a structure into small elements

(2) assumes each element to be a mathematical model

(3) assembles the elements and solves the overall

Hence it is possible for complex structural problems to be solved in a short time. Characteristics of FEM are as follows:

- It does not give an exact solution but solves approximately, because structures are modeled as a combination of simple elements and/or loads.
- It is a kind of numerical experiment without experimental devices, models, or instruments. Hence it is economical and time-saving.
- It can solve actual structural problems by using some models, although their shapes and loads are complex. It is even used for non-structural problems.
- It is used for a wide variety of steel, nonferrous materials and complex materials.
- It relies on computer technology for both hardware and software.

Nevertheless, FEM should be considered only as a practical tool, thus the extracted results must be checked and assessed continuously combined with engineering experience and correct interpretation.

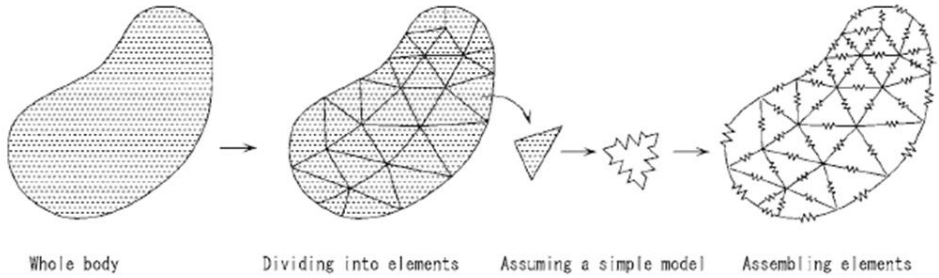

FIGURE 2.1 Basic concept of FEM

2.1 Buckling Linear Finite Element Analysis

Linear buckling analysis (also known as Eigenvalue buckling analysis) predicts the theoretical buckling strength and collapse mode of an ideal elastic structure. It is the first step during the structural stability verification of a construction. However, imperfections and nonlinearities prevent most real-world constructions from achieving their theoretical buckling strength.

Assuming and incremental loading pattern $\{P\}^n$, buckling problem is formulated as an eigenvalue problem

$$[K]^{m,n}\{q_i\}^n = \lambda_i [K_\sigma]^{m,n}\{q_i\}^n \qquad (2.1.1)$$

Where

$[K]^{m,n} =$ stiffness matrix

$[K_\sigma]^{m,n} =$ geometric stiffness matrix or stress stiffness matrix due to the incremental loading pattern $\{P\}^n$

$\{q_i\}^n =$ eigenvector of displacements

$\lambda_i =$ eigenvalue (used to multiply the loads which generated $[K_\sigma]^{m,n}$)

The geometric stiffness matrix is determined by the element geometry and stress conditions, and is independent of the elastic properties. It reflects the increasement of bending stiffness of an element under axial tension or the reduction of bending stiffness of an element under compression.

The analysis is conducted in two steps:

- Static structural analysis for the given load $[K]^{m,n}\{q_i\}^n = \{P\}^n$ where stress stiffness matrix $[K_\sigma]^{m.n}$ is calculated
- Eigenvalue buckling problem (2.1.1) is solved to find λ_i and $\{q_i\}^n$

2.2 Nonlinear Finite Element Analysis

The behavior of real structures differs from this predicted from linear analysis. A nonlinear analysis demonstrates a nonlinear relation between applied forces and displacements. In a model, nonlinearities result in a changing stiffness matrix during the load application, opposed to the linear analysis, where the stiffened matrix remains constant.

Sources of nonlinearities could be:

- Geometrical nonlinearities
- Material nonlinearities
- Boundary nonlinearities

Geometrical nonlinearities

Geometric nonlinearity occurs whenever the magnitude of the displacements affects the response of the structure. This may be caused by: a) Large deflections or rotations, b) “Snap through”, c) Initial stresses or load stiffening.

For example, considering a cantilever beam loaded vertically at the tip. If the tip deflection is small, the analysis can be considered as being approximately linear. However, if the tip deflections are large, the shape of the structure and, hence, its stiffness changes. In addition, if the load does not remain perpendicular to the beam, the action of the load on the structure changes significantly. As the cantilever beam deflects, the load can be resolved into a component perpendicular to the beam and a component acting along the length of the beam. Both of these effects contribute to the nonlinear response of the cantilever beam.

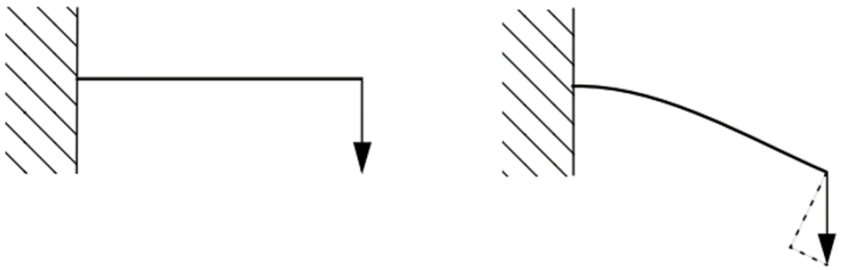

FIGURE 2.2 Large deflection of cantilever beam

One would expect large deflections and rotations to have a significant effect on the way that structures carry loads. However, displacements do not necessarily have to be large relative to the dimensions of the structure for geometric nonlinearity to be important. Consider the “snap through” under applied pressure of a large panel with a shallow curve. In this example there is a dramatic change in the stiffness of the panel as it deforms. As the panel “snaps through,” the stiffness becomes negative. Thus, although the magnitude of the displacements, relative to the panel's dimensions, is quite small, there is significant geometric nonlinearity in the simulation, which must be taken into consideration.

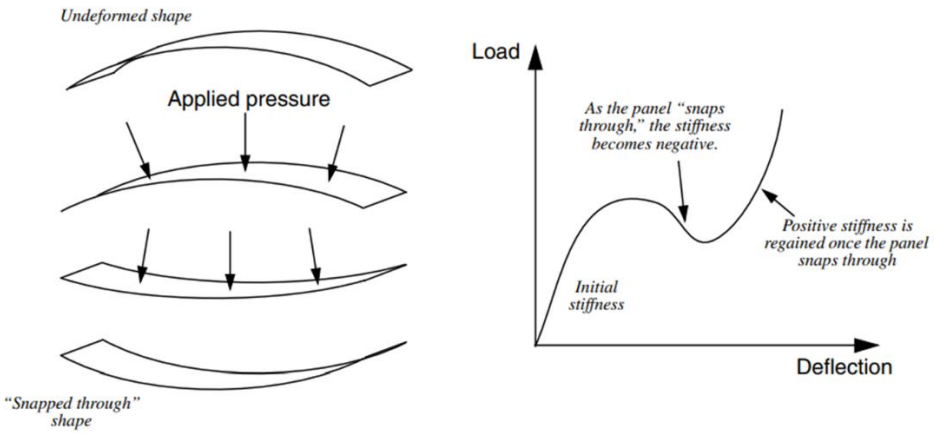

FIGURE 2.3 Snap-through of a large panel

Material nonlinearities

Material nonlinearity involves the nonlinear behavior of a material based on a current deformation, deformation history, rate of deformation, temperature, pressure, and so on. Examples of nonlinear material models are large strain (visco) elasto-plasticity and hyperelasticity (rubber and plastic materials). Most metals have a fairly linear stress/strain relationship at low strain values, but at higher strains the material yields, at which point the response becomes nonlinear and irreversible. Rubber materials can be approximated by a nonlinear, reversible (elastic) response.

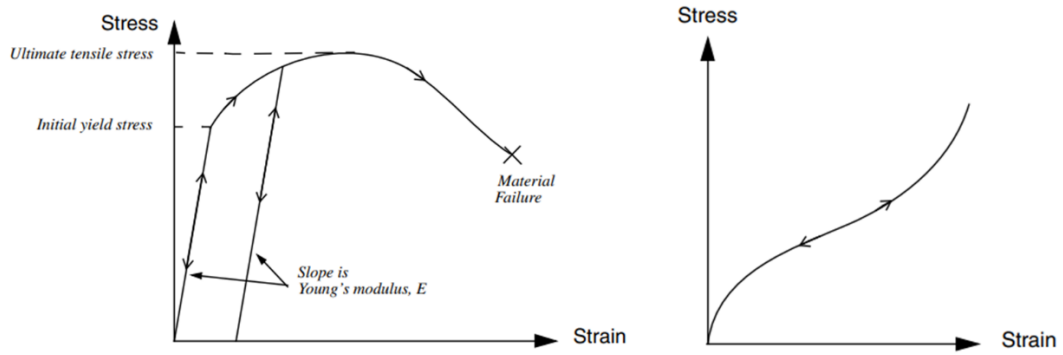

FIGURE 2.4 Stress-strain curve for an elastic-plastic material under uniaxial tension (left), Stress-strain curve for a rubber-type material (right)

Boundary nonlinearities

Boundary nonlinearity occurs if the boundary conditions change during the analysis. Consider a cantilever beam that deflects under an applied load until it hits a "stop." The vertical deflection of the tip is linearly related to the load (if the deflection is small) until it contacts the stop. There is then a sudden change in the boundary condition at the tip of the beam, preventing any further vertical deflection, and so the response of the beam is no

longer linear. Boundary nonlinearities are extremely discontinuous, when contact occurs during a simulation, there is a large and instantaneous change in the response of the structure.

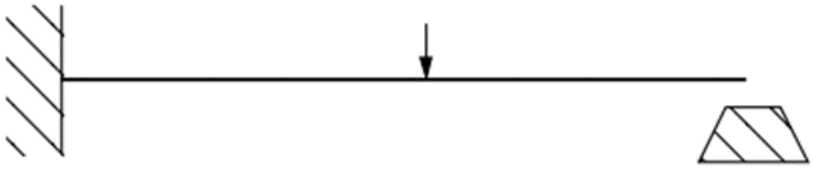

FIGURE 2.5 Cantilever beam hitting a stop.

Generally, the buckling load obtained from a linear buckling analysis is higher than the true buckling load of a structure. The reason is that there are no imperfections included in a linear buckling analysis, which are present in a real life situation. The nonlinear buckling analysis is a simulation procedure that allows for large deformations and geometrical and/or material nonlinearities. There are several ways of modeling imperfections. Sometimes a small out of plane force or translation of some nodes in the normal direction of the plate is sufficient in order to excite the first eigenmode. The most common and structured way to model imperfections is to use the pattern of the first eigenmode (under the assumption that this is the true shape of the buckling mode), obtained from the linear buckling analysis.

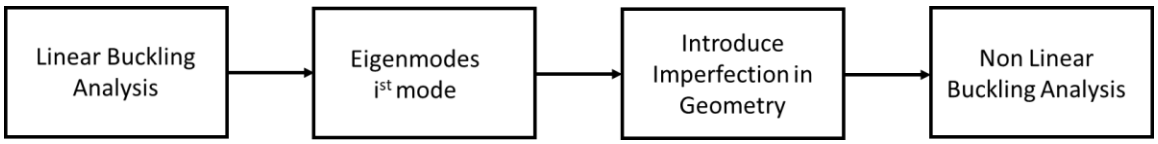

FIGURE 2.6 Nonlinear analysis procedure

A major problem in nonlinear buckling analysis is to quantify and motivate the amount of imperfection that has to be included in the analysis. For this aim an imperfection sensitivity analysis has to be carried out or proposed values to be used. Assuming a stiffened panel, maximum plate displacement magnitude according to IACS CSR is proposed to be the span between stiffeners in mm divided by 200 (s/200) and maximum stiffener displacement magnitude is proposed to be stiffeners length in mm divided by 1000 (L/1000).

In the figure below is depicted the load versus out of plane deflection paths. it is possible to see the effect of imperfections in contrast to an ideal buckling path. Including imperfections reduces the buckling load of a structure (the secondary path has no imperfections).

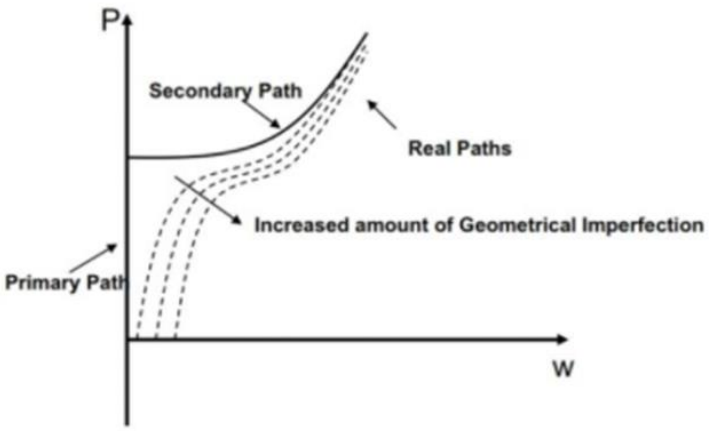

FIGURE 2.7 Imperfection sensitivity analysis

Iteration Methods and Post-buckling Analysis

In nonlinear analysis, the stiffness matrix [K] and/or the load vector $\{f\}$ in the structural equations, $[K]\{u\} = \{f\}$, become functions of the displacements, {u}. This makes it no longer possible to solve the systems of equations directly for the displacements by inverting the stiffness matrix. Consequently, a tangent stiffness matrix, $[K]_t$, is created, which includes both the effect of changing geometry as well as stiffening due to stress. The procedure then becomes to solve $[K]_t\{\Delta u\}=\{\Delta f\}$ by use of an iteration method, e.g. the Newton-Raphson method. It must be noted that convergence is not guaranteed for any iteration method, however stability is improved if load steps are smaller, e.g. applying load incrementally.

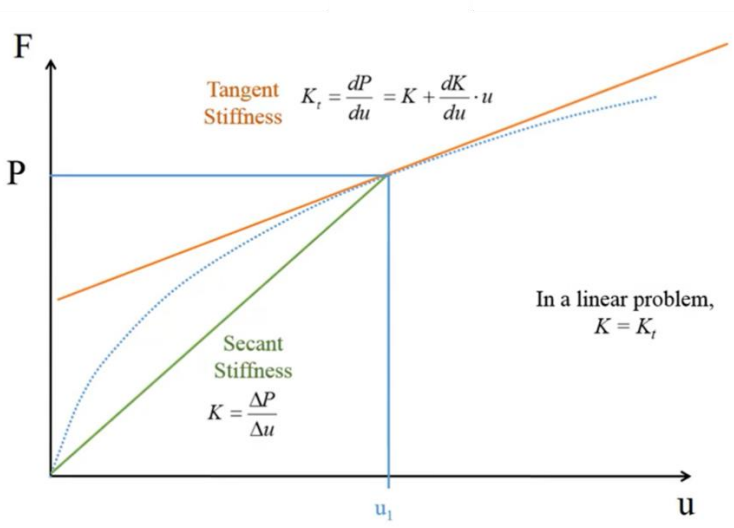

FIGURE 2.8 Secant and Tangent Stiffness

The Newton-Raphson method is the most rapidly convergent process and has a quadratic convergence rate and is also the most commonly implemented solution scheme in commercial FE software. Calculation of Tangent Stiffness Matrix is a computational expensive procedure. Since Newton Raphson method requires to calculate tangent stiffness Matrix after each iteration, modified Newton-Raphson method is often used. In Modified Newton-Rapson method, Tangent Stiffness Matrix is calculated for each increment, leading to a computational cheaper solution. However, using Modified Newton Raphson method on hardening structures could easily lead to diverge.

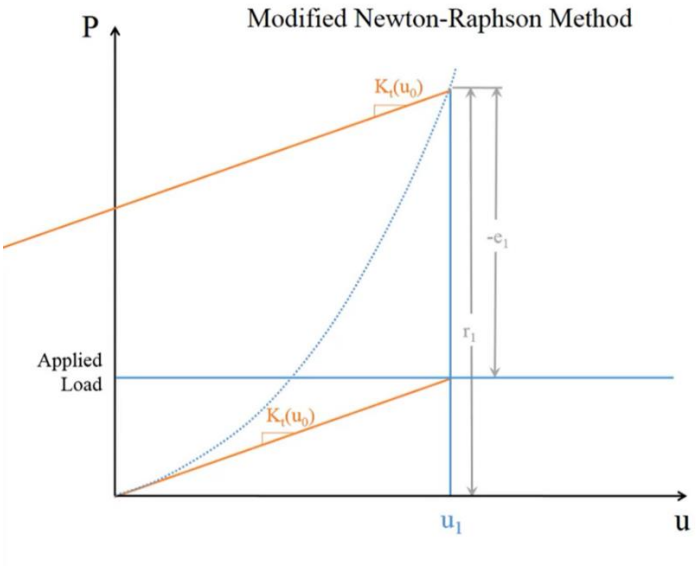

FIGURE 2.9 Diverge of Modified Newton-Raphson Method

It can be of interest to verify if the structure continues to carry the load after it has reached its critical limit or if it looses all its stiffness and collapses. Post-buckling can be divided into two different types. The first type is called stable post-buckling and the second is called unstable post-buckling. The characteristic of stable post-buckling behavior is when the structure continues to carry the load that it is subjected and keep its stiffness. The definition of unstable post-buckling is when the structure loses its stiffness and is no more able to carry the same amount of load. This often leads to that the structure starts to undergo very large geometrical changes for decreased or unchanged loading.

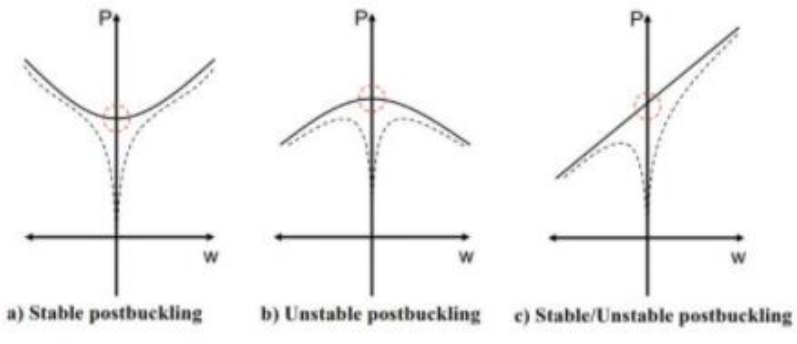

FIGURE 2.10 Post buckling paths

The Newton-Raphson methods perform poorly for bucking problems, where the slope at limit points is exactly equal to 0, also present problems in case of snap-through and snap-back points, failing to predict the complete load-displacement response.

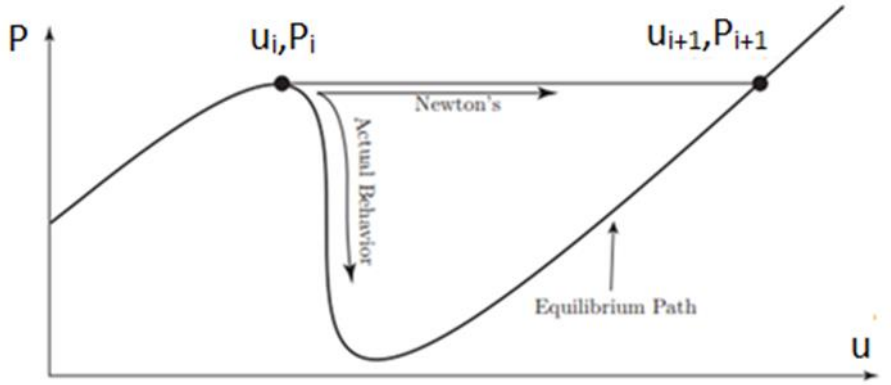

FIGURE 2.11 The Newton's method cannot accurately predict the solution after a limit point is reached

For the post-buckling study, the Riks iteration method is used. It is a variant of the Arc Length method. Unlike the Newton-Raphson method, this method uses an extra constraint and allows the solver to reach the convergence with lower applied load and find the equilibrium. This property of the Riks method makes it possible to trace the behavior after a limit point is reached, even though that the stiffness matrix is not positive definite. The Newton method can also work as a solution scheme when doing post-buckling analysis but only with the requirement that the post-buckling path is stable. This is hard to know in advance, so therefore the Riks method is recommended for this kind of analysis because it is valid for both stable and unstable behavior of the post-buckling paths.

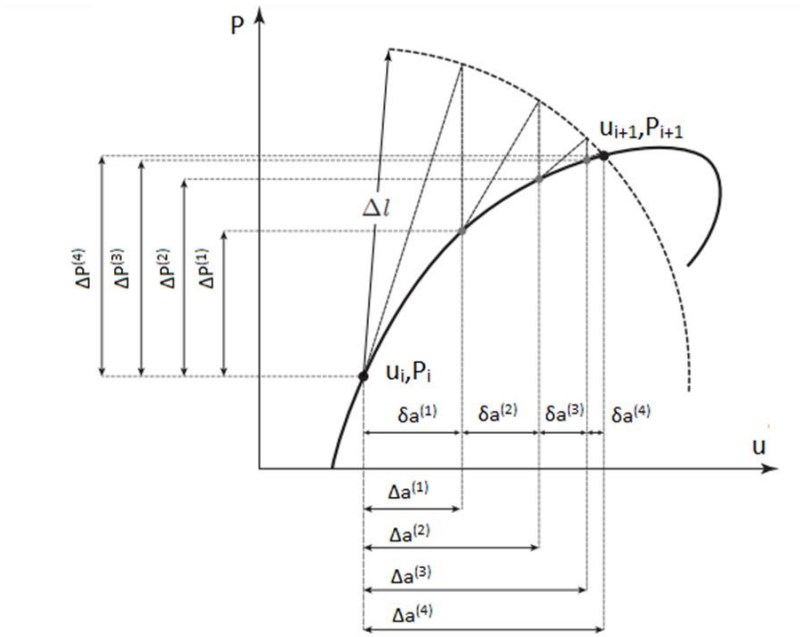

FIGURE 2.12 A representation of Arclength Method

PART 2 FEM Analysis

3 Investigation Strategy

This work focuses on the study of buckling behavior and ultimate strength of a stiffened plate belonging to a ship's deck and the stiffened plate's elements, under compressive loads resulting from the sagging of the hull, using a one span model in the longitudinal direction. Transverse frames of the hull can't be included in a one span model, although they have a great effect on the structure. However, the boundary conditions of an isolated structural element should be such that represent realistically the behavior of that element as part of the construction. Hence, for the appropriate boundary conditions to be obtained, the procedure described afterwards followed. Firstly, a three-span model of a VLCC's hull with a span switch of L/2+L+L/2 subjecting to pure bending were analyzed. From this analysis, observing deformation of the frames and making the essential assumptions, the appropriate boundary conditions for the analysis of a one span model of the same hull were extracted. Analyzing the one-span model of the hull and observing displacements on the boundaries of a stiffened plate on its deck, realistic boundary conditions for deck's stiffened plate were obtained. Boundary conditions obtained for deck's stiffened plate used in the analysis of an identical isolated stiffened plate under compression, so that their validity could be evaluated. Typically, continuous plates consisting of 5 to 10 stiffeners are used in marine structures, therefore a model of stiffened plate with 6 stiffeners subjecting to uniaxial compression were analyzed, so that accurate conclusions about buckling collapse mode, ultimate strength, stress distribution and load distribution among stiffened plate's elements to be made. Observing the displacement in the boundaries of stiffened plate's elements, the boundary conditions for the analysis of a stiffened plate's isolated element were obtained.

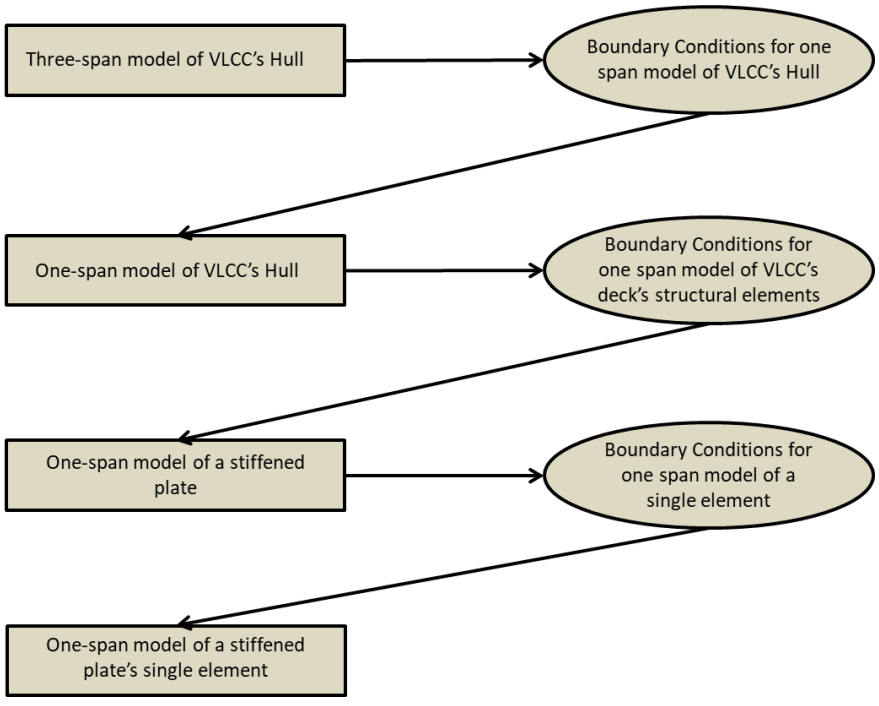

Figure 3.1 Investigation strategy

Finite element models described on table 3.1 used to accomplish the aforementioned procedure.

Model	Longitudinal span	Load	Solver	Element type	Mesh size	Comments on BC	
						Transverse section nodes' transverse displacement (Stiffened Plate)	longitudinal edge nodes' transverse displacement (Stiffened Plate)
VLCC's Hull	3 (L/2+L+L/2)	Pure bending	Dynamic Implicit	S4R	250 mm	_	_
	1 (L)	Pure Bending	Dynamic Implicit	S4R	250 mm	free	_
	1 (L)	Pure Bending	Dynamic Implicit	S4R	250 mm	suppressed	_
VLCC's deck stiffened plate with 24 stiffeners	1 (L)	Uniaxial compression	Dynamic Implicit	S4R	250mm	free	common
	1 (L)	Uniaxial compression	Dynamic Implicit	S4R	250mm	suppressed	suppressed
Stiffened plate with 6 stiffeners	1 (L)	Uniaxial compression	Static, Riks	S4R	50mm	free	common
	1 (L)	Uniaxial compression	Static, Riks	S4R	50mm	suppressed	suppressed
Single element of stiffened plate	1 (L)	Uniaxial compression	Static, Riks	S4R	50mm	free	common
	1 (L)	Uniaxial compression	Static, Riks	S4R	50mm	suppressed	suppressed
	1 (L)	Uniaxial compression	Static, Riks	C3D8R	20*20*4 mm	free	common
	1 (L)	Uniaxial compression	Static, Riks	C3D8R	20*20*4 mm	suppressed	Suppressed

Table 3.1 Models used for the study

4 Hull Analysis

This chapter focuses on the analysis of a VLCC's hull. The goal is to observe the displacement on the boundaries of a stiffened plate with 24 stiffeners on deck, as hull is sagging, so that realistic boundary conditions which represent the behavior of an isolated stiffened plate as structural element of the hull could be obtained. Firstly, a three-span model of a hull will be studied and the behavior of the aforementioned stiffened plate will be observed. At the same time the deformation of the transverse frames will be inspected. Making the appropriate assumptions, based on the results from the analysis of three span model, regarding deformation of frames, two different one-span models of the same hull will be analyzed. One assuming that nodes on transverse section of the model are free to move in transverse direction and one assuming transverse translation of nodes is suppressed. Inspecting the translation on the boundaries of the stiffened plate with 24 stiffeners, two different sets of boundary conditions for the analysis of an isolated stiffened plate emerge. One evolves from the assumption that nodes on the transverse cross-section of one-span model are free to move in transverse direction and the other from the assumption the translation of the same nodes is suppressed. The extracted boundary conditions will be tested and evaluated by analyzing two models of an isolated stiffened plate, identical with this on the deck of the VLCC. One model is considered to have free transverse translation of nodes on transverse section and common transverse translation of nodes on longitudinal edges and the other is consider to have suppressed transverse translation of nodes on transverse section and suppressed transverse translation of nodes on longitudinal edges

4.1 Three-span Hull Model with Transverse Frame

The model represents a VLCC's hull of 58m width and 32m height. In the longitudinal direction, the three-span model consists of 5 parts, 2 transverse frames 15 mm thick, 2 bays of 2.56 m length (L/2) and one bay of 5.12 m length (L). Through the analysis of this model, useful data for the condition structural elements of the deck encounter can be obtained. The investigation will concentrate on the horizontal stiffened plate in the middle of the deck, as hull is imposed to sagging. At the same time the appropriate boundary conditions for the simplified one span hull model will be approached.

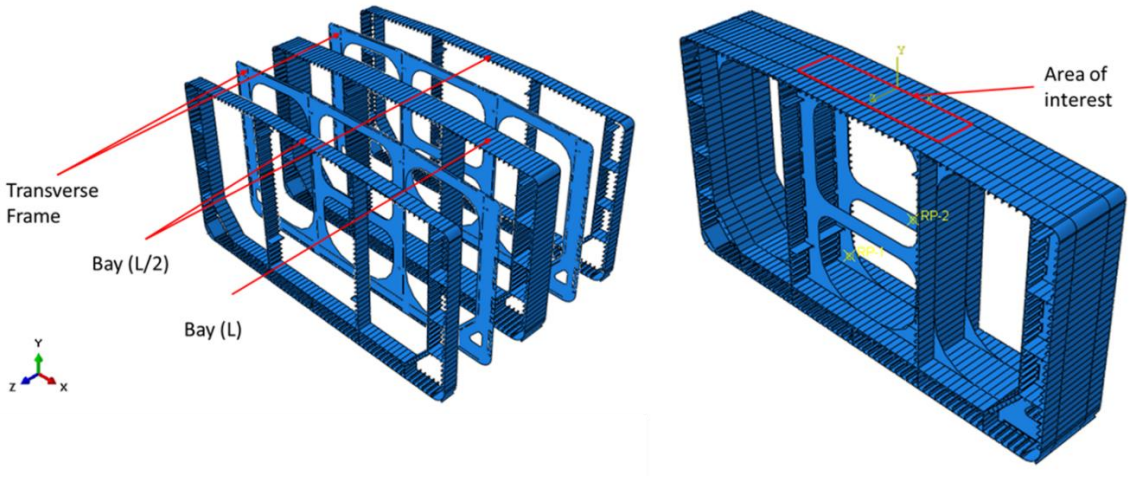

FIGURE 4.1 Parts of model, final assembly and area of interest

4.1.1 Model Geometry, Mesh and Material Properties

Model Geometry

Each bay designed accurately according to the dimensions of a VLCC. There are three stiffener types in the construction (tee-stiffeners, angular stiffeners, tee-stiffeners with angular stiffeners to stiffen webs). Principal stiffener dimensions vary and not all plates of the construction have the same thickness.

The area of interest on deck consists of a 5.12 m long stiffened plate with 23 tee-stiffeners. Span between stiffeners is 910mm. Plates thickness is 17.5 mm. Web's height and thickness is 400mm and 13mm respectively and flange has a width of 130mm and a thickness of 18mm.

Stiffened plate geometry (deck, area of interest)	
s (mm)	910
L (mm)	5120
t_p (mm)	17,5
h_w (mm)	400
t_w (mm)	13
b_f (mm)	130
t_f (mm)	18

TABLE 4.1 Stiffened plate geometry (deck, area of interest)

A typical frame geometry designed with detail to the cut-outs where stiffeners and transverse frame intersects. There are five types of cut-outs on the construction as shown in FIGURE 4.2 and their dimensions depends on the dimensions of the intersecting stiffener. A portion of stiffener's web of about 90% (regarding cut-out type) is connected with the

transverse frame as if they were a single body. Flange of stiffeners with a portion of about 10% of the stiffener's web, in the web-flange connection end, have no interaction with transverse frame.

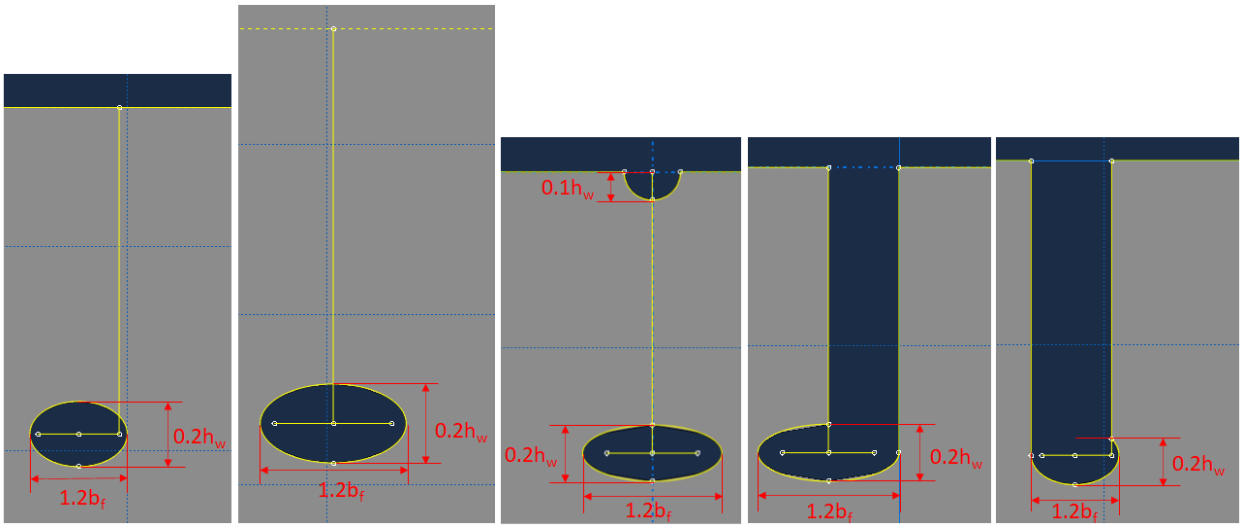

FIGURE 4.2 Types of Cut-outs on Transverse frame

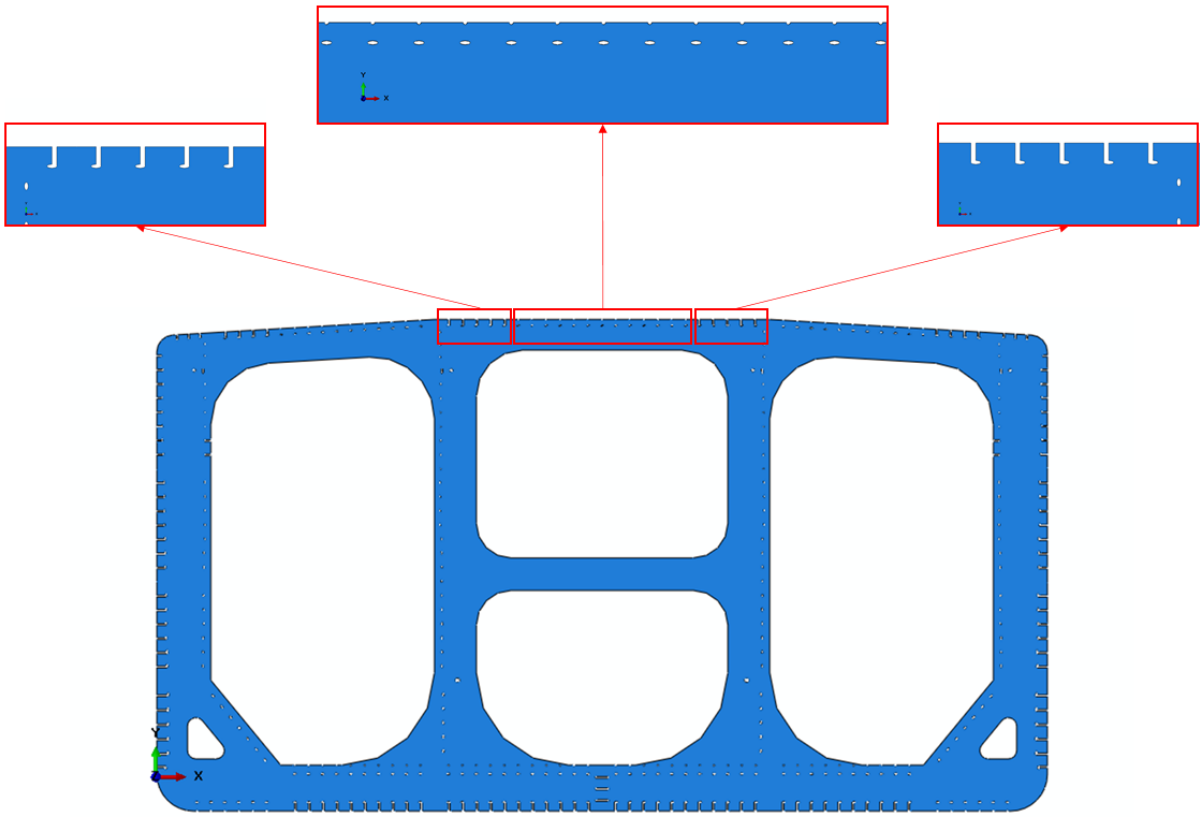

FIGURE 4.3 Transverse frame and details

Very large size of model sets limits to its discretization. Complex cut-outs' geometry together with the use of large finite elements leads to a problematic mesh. To deal with this, geometry of frame's cut-outs simplified as shown in FIGURE 4.4, in such way that intersection between stiffeners and web doesn't affect.

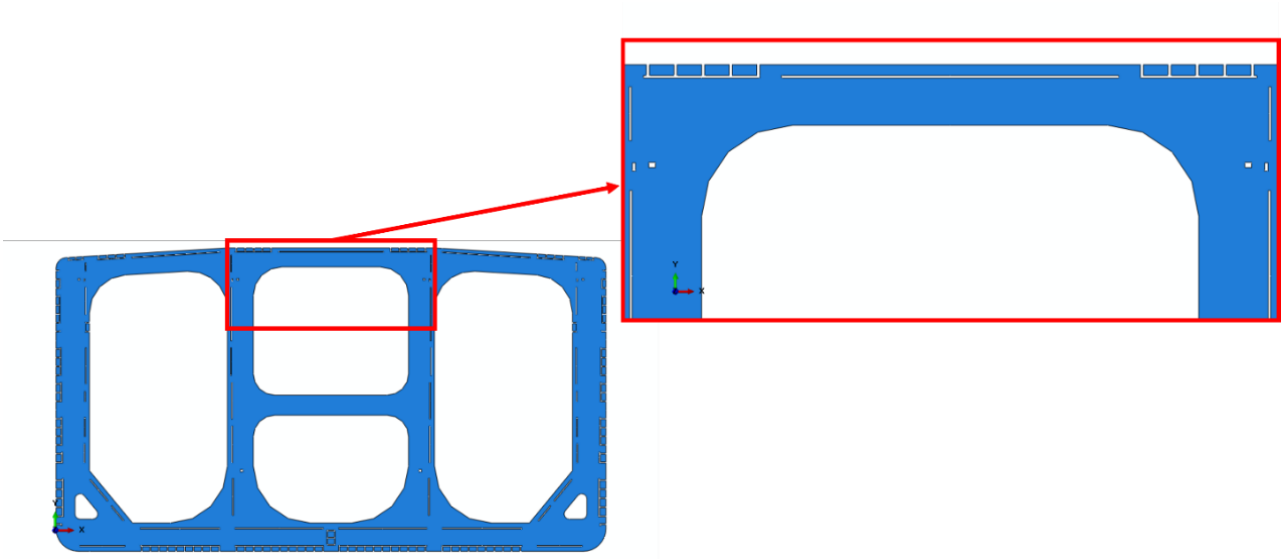

FIGURE 4.4 Simplified geometry of transverse frame and details

Mesh

Discretization of the model should be such that processing time is reasonable and at the same time critical details of geometry, especially those affecting connections of frame and bays, are taken into account. Considering this, use of reduced integration shell elements S4R of 250 mm length is proposed. It should be noted that this mesh isn't dense enough for an ultimate strength analysis of stiffened plate elements that form the hull. For the ultimate strength analysis of stiffened plate structures that involve an elastic-plastic large deflection response, current practice indicates that at least eight four-noded plate-shell elements are required to model the plating in between stiffeners. However, this analysis does not aim to accurately estimate stresses and displacements of construction, but to give an approach of displacements of nodes on the boundaries of a stiffened plate on deck, so that reasonable assumptions to be made leading to realistic boundary conditions that represent the behavior of an isolated element as part of the construction and to create a one span model of the same hull.

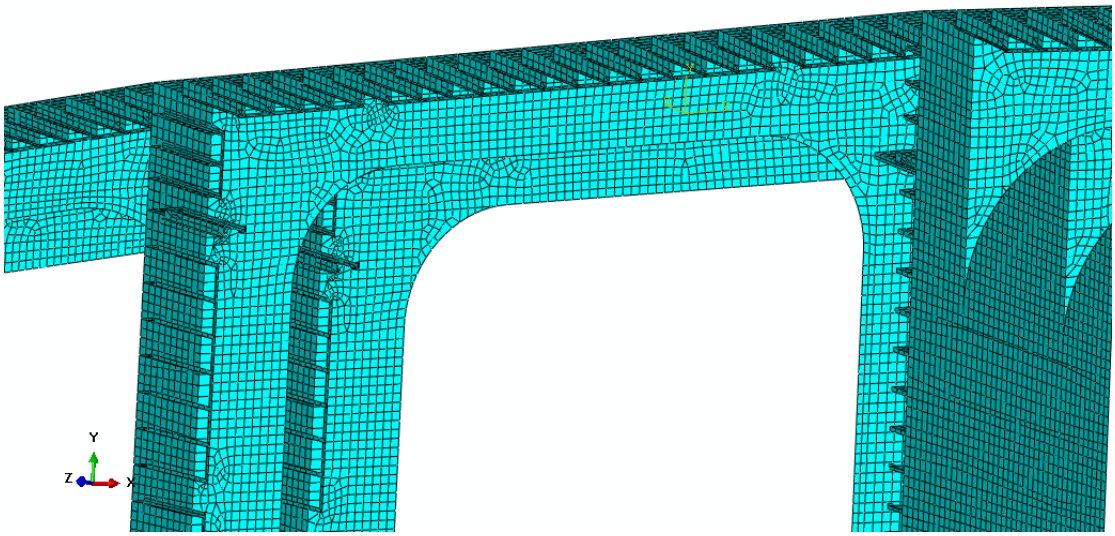

FIGURE 4.5 Mesh of three-span model

Material Properties

Material used is AH32. AH32 steel is a structural high tensile strength marine steel mainly used for making the hull of ship building and ship repairing, offshore oil drilling platforms, the platform pipe joints and other components. It is an isotropic material that has Young's modulus/modulus of elasticity (E) of 206 GPa, Poisson's ratio (v) of 0.3 and Yield strength (σ_y) of 315 MPa.

AH32 steel	
Young's modulus E (GPa)	206
Poisson's ratio v	0.3
Yield strength σ_y (MPa)	315

TABLE 4.2 Material properties of hull

4.1.2 Boundary Conditions

Boundary conditions are applied so that hull is imposed to pure longitudinal bending. To maintain symmetry, at each longitudinal end of the model, one Reference Point (RP) is placed at the center of surface of each cross section. Edge nodes of each cross section are controlled by RPs through kinematic coupling constraint. Coupled degrees of freedom are longitudinal translation, rotation around transverse axis and rotation around vertical axis, meaning edge nodes follow RP's motion as rigid body for the coupled degrees of freedom and at the same time cross section remains plain. One RP is clamped and the other is free to move in vertical and longitudinal directions and rotate around transverse axis. Transverse

frame isn't considered rigid body. To avoid local buckling of transverse frame and considering pure longitudinal bending, transverse frame must remain plane as hull bends, so rotation around vertical and longitudinal axis is forbitten and at the same time an equation has been set on frame's nodes, forcing them to rotate as rigid body around transverse axis.

x=transverse, y=vertical, z=longitudinal							
Location	Translation			Rotation			Constraints
	Ux	Uy	Uz	URx	URy	URz	
RP1	Suppressed	Free	Free	Free	Suppressed	Suppressed	Kinematic coupling with longitudinal edge nodes. Constrained degrees of freedom: Uz, URx, URy
RP2	Suppressed	Suppressed	Suppressed	Suppressed	Suppressed	Suppressed	Kinematic coupling with longitudinal edge nodes. Constrained degrees of freedom: Uz, URx, URy
Transverse Frames	Free	Free	Free	Free	Suppressed	Suppressed	Equation, URx=common

TABLE 4.3 Boundary conditions for three span model of VLCC's hull

4.1.3 Linear Analysis

The model is imposed to pure longitudinal bending by subjecting moment about transverse axis to the free to move/rotate RP.

The first eigenmode located to the deck arises at the horizontal stiffened plate at the middle of the deck (FIGURE 4.6). Z-axis and X-axis are antisymmetry axis. Six half waves are being formed and plate buckling seems to be dominant. Deformation of the plate is higher at the middle and is decreasing as edges of the plate are approached. Stiffeners' webs seem to buckle locally.

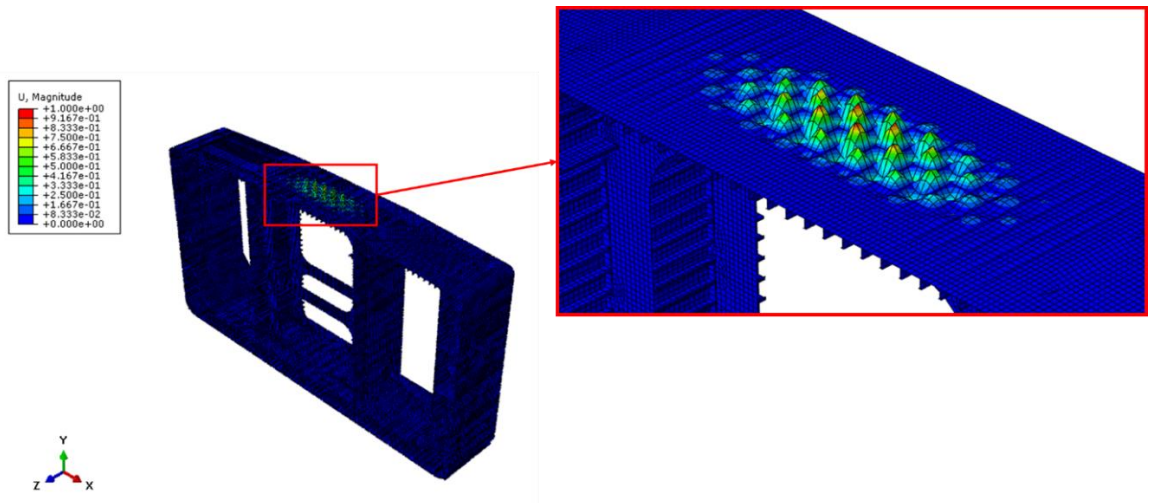

FIGURE 4.6 First antisymmetric buckling mode that forms on deck

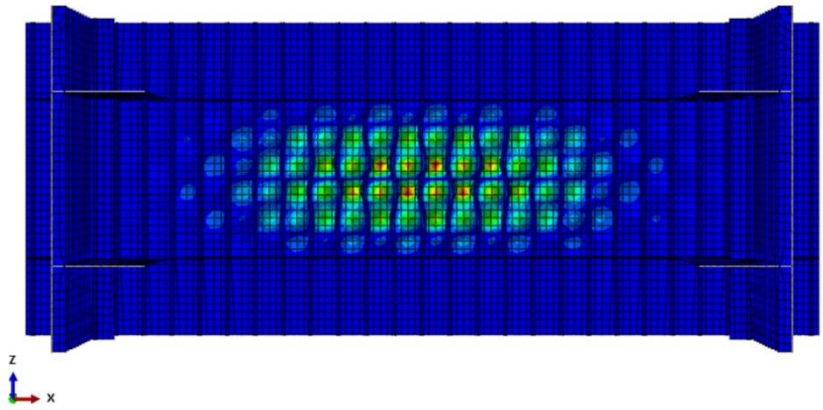

FIGURE 4.7 First symmetric/antisymmetric buckling mode that forms on deck (Z-X plane)

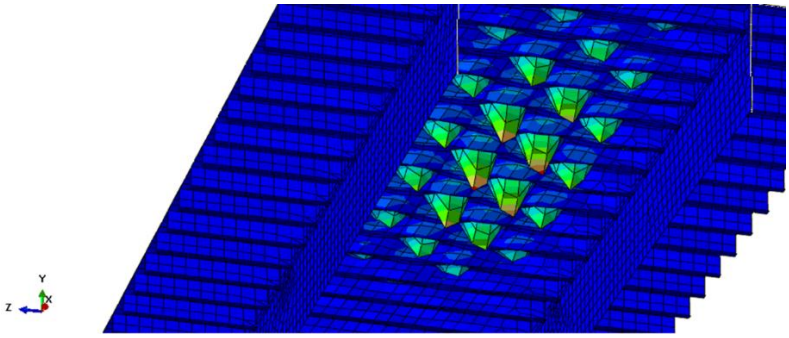

FIGURE 4.8 First symmetric/antisymmetric buckling mode that forms on deck (stiffeners view)

4.1.4 Nonlinear Analysis

The aforementioned eigenmode would be utilized as initial geometrical imperfections of the model, applied with the proposed tolerance level. Since plate buckling is the dominating source of buckling, maximum amplitude of 4.55 mm (s/200) is applied.

The model is imposed to pure longitudinal bending by subjecting rotation about transverse axis to the free to move/rotate RP.

Simulation run using dynamic implicit solver of quasi static type. RP rotates with a radial velocity of 0,0015 rad/s. It is proposed that Kinetic Energy should be less than 5% of Internal Energy of the model, so that could be regarded negligible and the consideration of quasi static loads is true. During the analysis Kinetic energy values remain lower than the proposed maximum value.

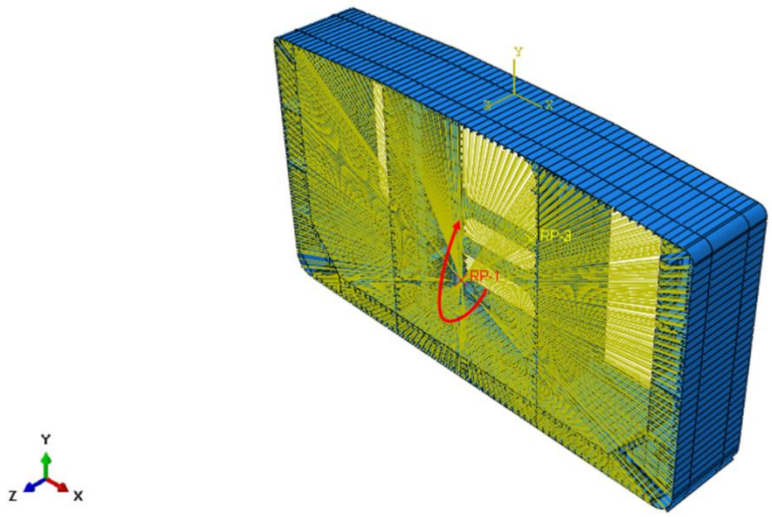

FIGURE 4.9 Rotation of RP

Hourglass energy is work done by the forces calculated to resist hourglass modes. Hourglass modes are nonphysical, zero-energy modes of deformation that produce zero strain and no stress. Hourglass modes occur in reduced integration solid, shell, and thick shell elements, like S4R elements used for this simulation. For this analysis Hourglass Energy values remain under 10% of Internal Energy of model. Values under 5% of Internal Energy are noticed for the first 5 s of the analysis. It should be noted that critical values of the analysis such as maximum reaction moment of Hull or maximum axial stress of the Horizontal Stiffened Plate are reached while Hourglass energy is under the 5% limit.

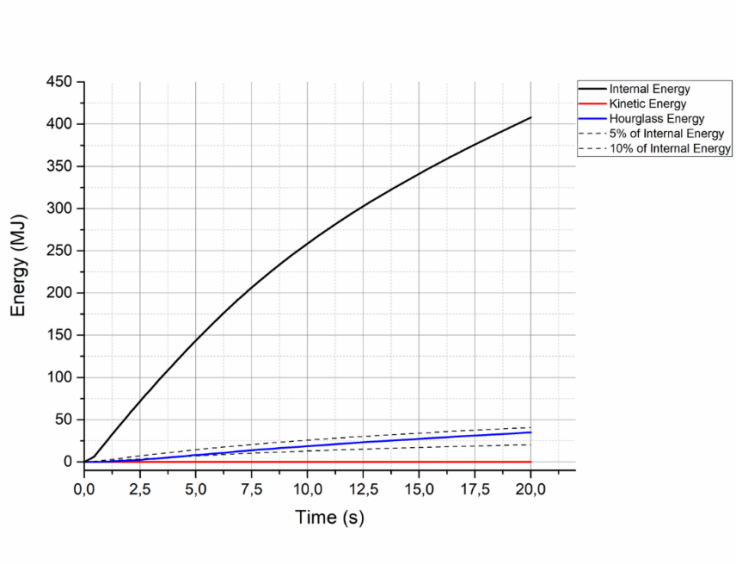

FIGURE 4.10 Internal, kinetic and hourglass energy comparison for 3 span Hull model

During the analysis the Reaction Moment-Rotation curve of the Hull reaches its peak on linear trend and drops slowly. At the same time deck's structural elements are under compression. The Stress-Rotation curve of the horizontal stiffened plate in the middle of the deck reaches its peak on linear trend and drops quickly.

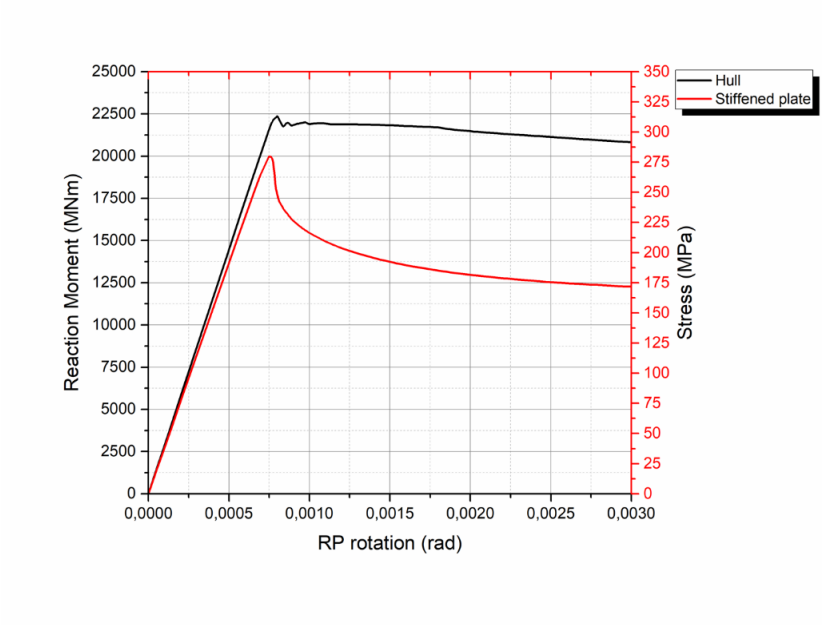

FIGURE 4.11 Reaction moment-RP rotation curve and Stress-RP rotation curve for hull and horizontal stiffened plate on deck

It is noted that maximum Reaction moment of Hull and maximum Stress of the plate do not achieve for the same rotation. Bearing in mind that imperfections are applied only on the Horizontal plate of the deck and not on the whole model, this behavior can be explained. The “imperfect” plate is more vulnerable on compressive loads than the rest of the model. When reaching its critical buckling load and collapses, the other “perfect” parts of Hull under compression, which haven’t reached their critical buckling load, overcome the instability due to the loss of strength capacity of the “imperfect” plate.

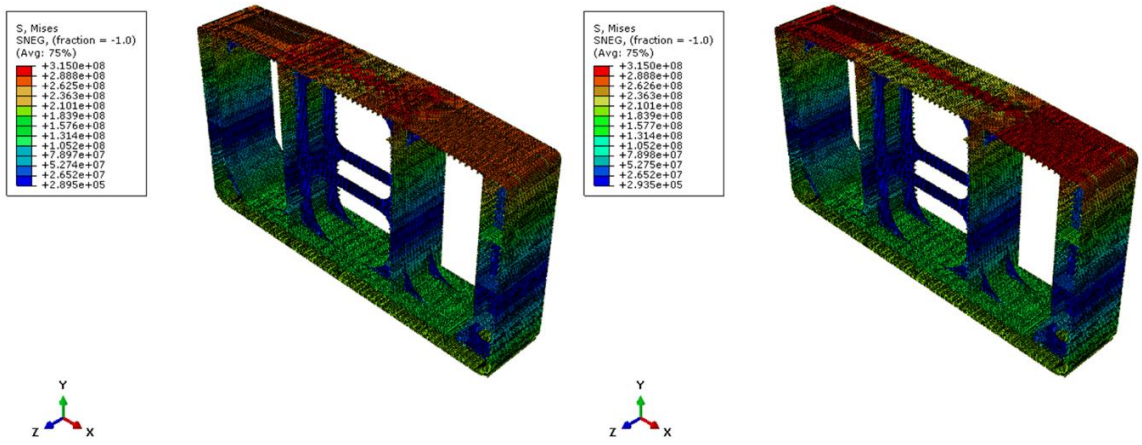

FIGURE 4.12 Von Misses stress on stiffened plate’s collapse step (left), maximum reaction moment of hull step

Stiffened plate loose stability under a combination of local plate buckling and local web buckling (FIGURE 4.13). Local plate buckling is dominant and six halfwaves are being formed to the plating between stiffeners. The same collapse mode predicted through the linear analysis of the model.

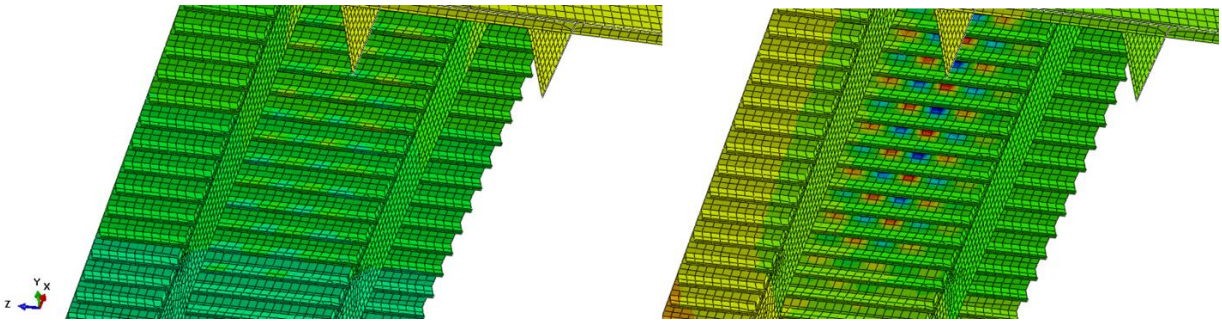

FIGURE 4.13 Transverse (left) and vertical (right) displacement of stiffened plate when it collapses

As hull bends, frame remains plane but its nodes are free to move on their local vertical and transverse direction. As shown in FIGURE 4.14 change in vertical length of frame varies from 2 mm to -1 mm, which can be assumed negligible. Change in transverse length of frame varies from 15 mm near deck to -9.5 mm near bottom. Frame lengthens in transverse direction above neutral axis and shortens below. It's not clear whether this change in length is negligible and it should be investigated.

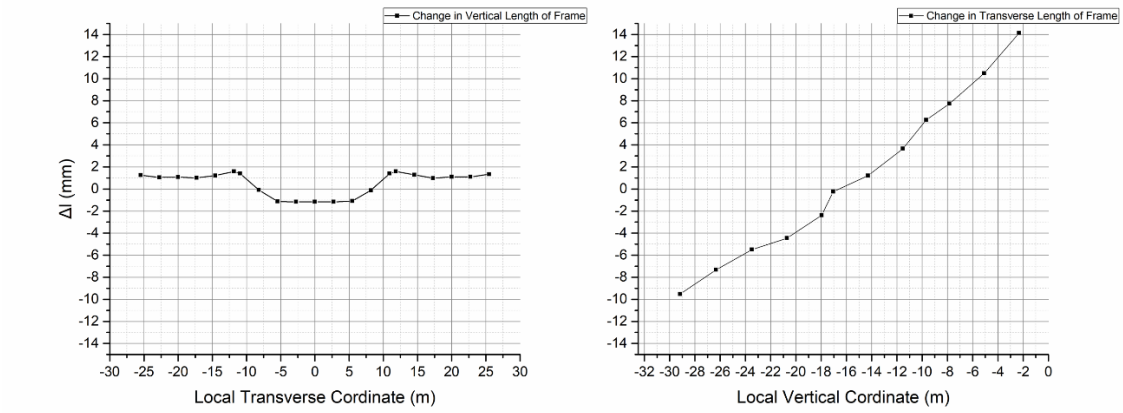

FIGURE 4.14 Change in vertical and transverse length of frame when horizontal stiffened plates buckles

As Hull sags deck is imposed to compression, leading its structural elements to buckle. The “imperfect” horizontal stiffened plate in the middle of the deck, reaches critical buckling stress of 280 MPa for a strain of 0,00152.

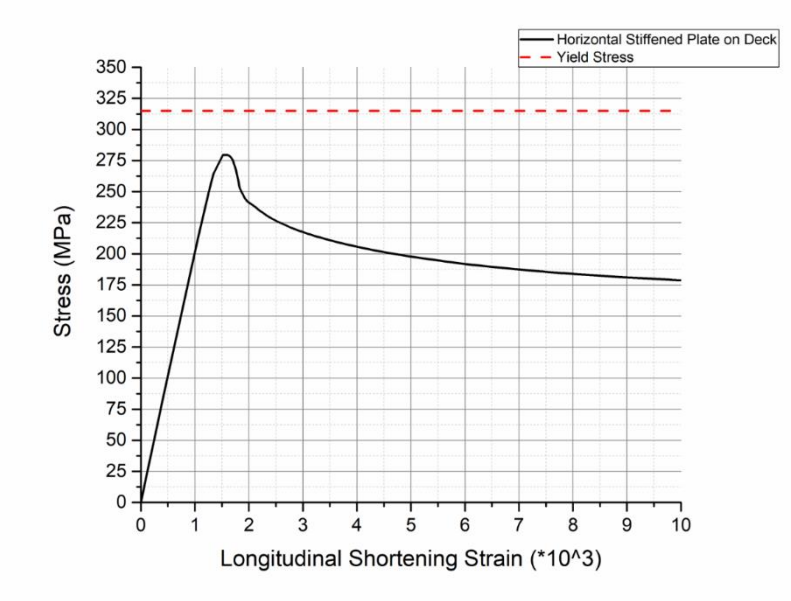

FIGURE 4.15 Stress-strain curve for horizontal stiffened plate on deck

Taking advantage of symmetry, conditions on the boundaries of plate as Hull is imposed to pure bending can be examined using two edges of the plate, one transverse edge and one longitudinal.

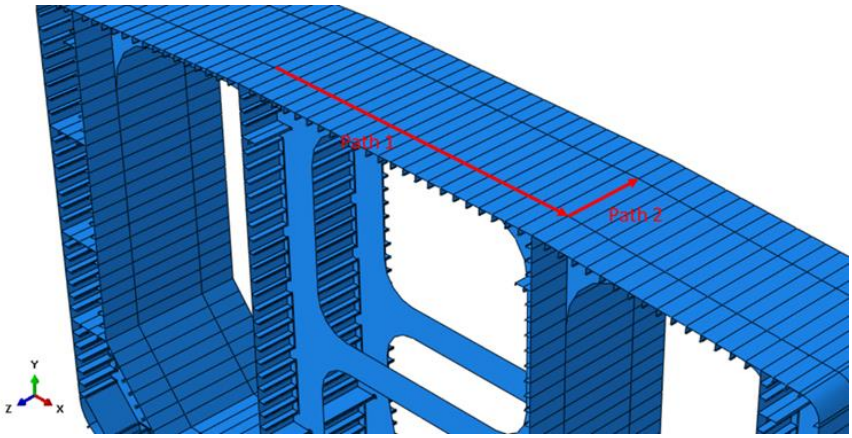

FIGURE 4.16 Edges of plate used to examine boundary conditions

It is observed that as plate shortens, the node on the middle of the transverse edge remains motionless, as excpected due to symmetry. Nodes lying on the left and right of the motionless middle point, move away from it antisymmetricaly. Each node's Transverse Displacement-Strain curve seperatly, reaches its peak with almost linear trend. For each curve seperatly, when buckling occurs peak is reached. Post buckling displacement of all nodes reduces. The furhter away from the motionless middle node a node is, the greater its displacement is.

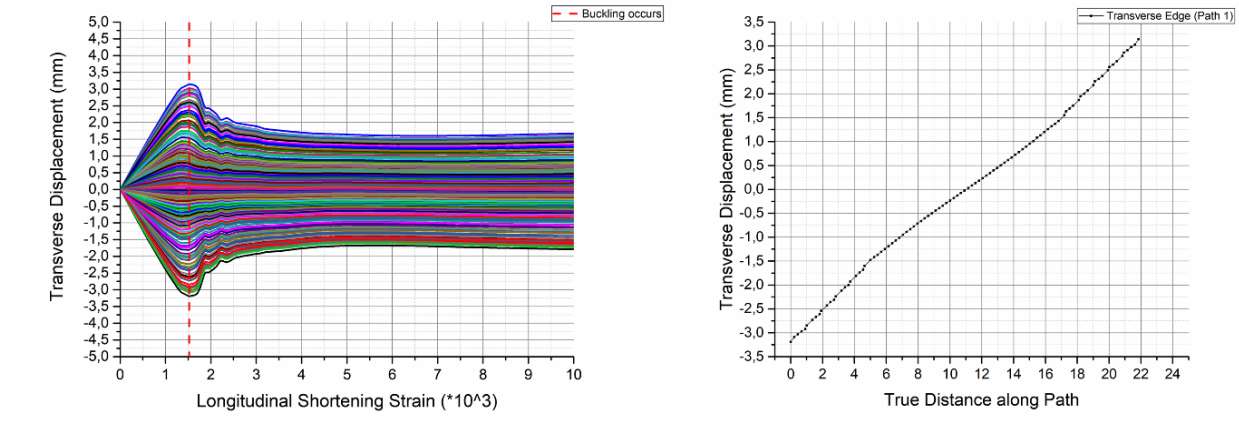

FIGURE 4.17 Transverse displacement-Strain curve of nodes on transverse edge of plate (left), transverse displacement of nodes on transverse edge on stiffened plate's buckling step (right)

As shown in FIGURE 4.18 nodes on longitudinal edge of the plate have common displacement through transverse direction. This behavior remains post buckling, but changes after a while. Post buckling all nodes displacement reduces.

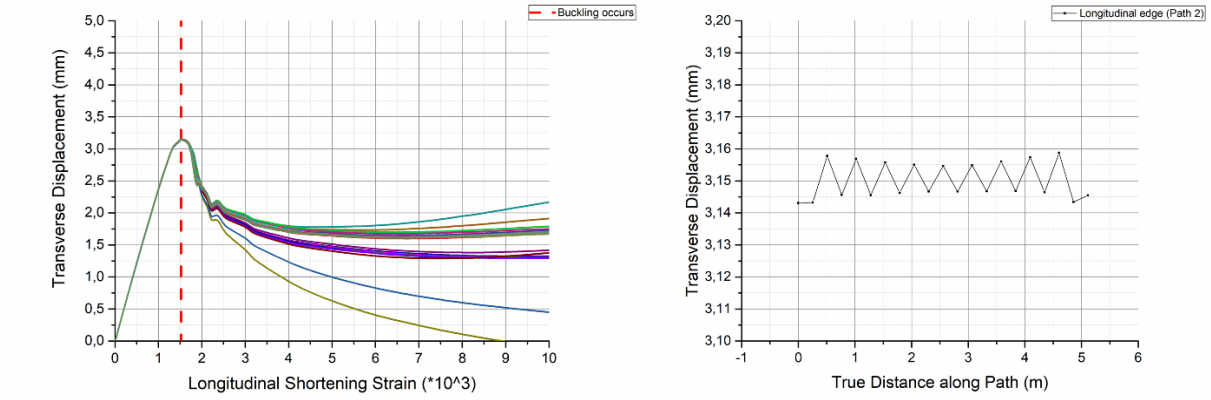

FIGURE 4.18 Transverse displacement-Strain curve of nodes on longitudinal edge of plate (left), transverse displacement of nodes on longitudinal edge on stiffened plate's buckling step (right)

4.2 One-span Hull Model

The model is a simplification of the model of 58m width and 32m height VLCC's hull described on chapter 4.1. In the longitudinal direction, the one span model consists only of one bay of 5.12 m length (L).

As on the previous three span model of chapter 4.1, the investigation will concentrate on the horizontal stiffened plate in the middle of the deck, as hull is sagging.

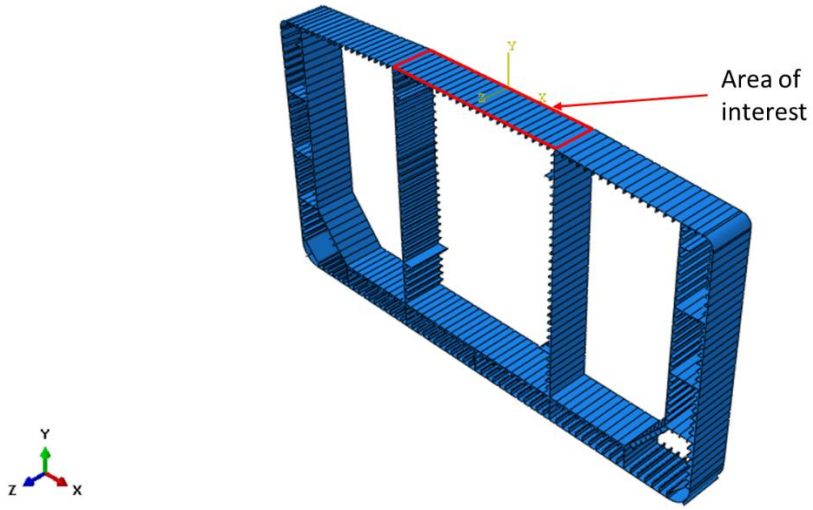

FIGURE 4.19 Final assembly of model and Area of interest

4.2.1 Model Geometry, Mesh and Material Properties

Model Geometry

Bay designed accurately according to the dimensions of the same VLCC as on Chapter 4.1. There are three stiffener types in the construction (tee-stiffeners, angular stiffeners, tee-stiffeners with angular stiffeners to stiffen webs). Principal stiffener dimensions vary and not all plates of the construction have the same thickness.

Area of interest on deck consists of a 5.12 m long stiffened plate with 23 tee-stiffeners. Span between stiffeners is 910mm. Plates thickness is 17.5 mm. Web's height and thickness is 400mm and 13mm respectively and flange has a width of 165mm and a thickness of 18mm.

Stiffened plate geometry (deck, area of interest)	
s (mm)	910
L (mm)	5120
t_p (mm)	17,5
h_w (mm)	400
t_w (mm)	13
b_f (mm)	130
t_f (mm)	18

TABLE 4.4 Stiffened plate geometry (deck, area of interest)

Mesh

Although considering size of one span model a denser mesh than this used for the analysis of three span model could be used, shell elements S4R of 250 mm length is proposed. Using the same elements on both simulations makes sure that any differences on the results of the analysis are products of the assumptions made to simplify the three-span to one-span model, since mesh used on both simulations leads to equally accurate estimations of stresses and displacements

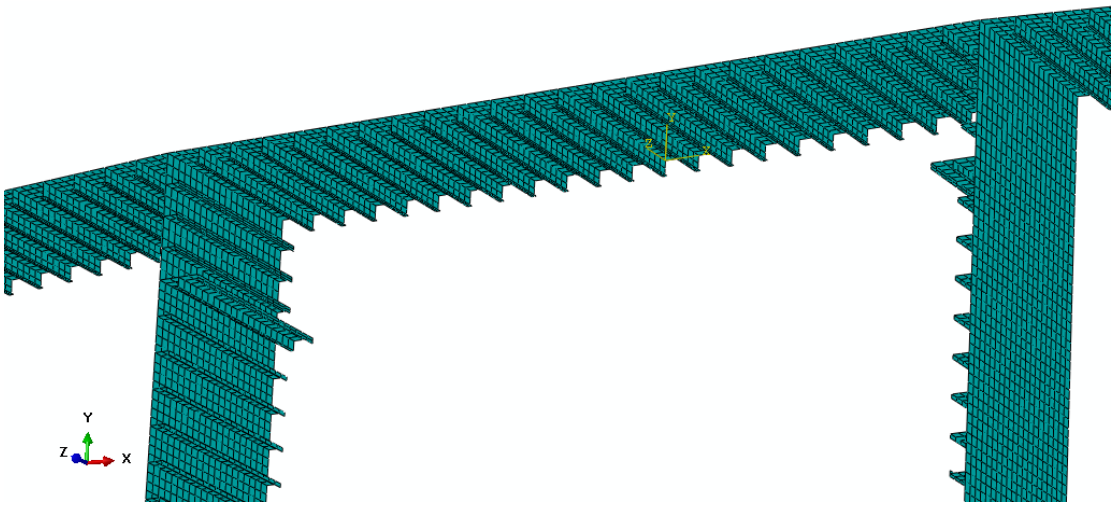

FIGURE 4.20 Mesh of one-span model

Material properties

Material used is AH32. AH32 steel is a structural high tensile strength marine steel mainly used for making the hull of ship building and ship repairing, offshore oil drilling platforms, the platform pipe joints and other components. It is an isotropic material that has Young's modulus/modulus of elasticity (E) of 206 GPa, Poisson's ratio (v) of 0.3 and Yield strength (σ_y) of 315 MPa.

AH32 steel	
Young's modulus E (GPa)	206
Poisson's ratio v	0.3
Yield strength σ_y (MPa)	315

TABLE 4.5 Material properties of hull

4.2.2 Boundary Conditions

Boundary conditions are applied so that hull is subjected to pure longitudinal bending. To maintain symmetry, at each transverse section of the model, one Reference Point (RP) is placed at the center of surface of each edge cross section. One RP is clamped and the other is free to move in vertical and longitudinal directions and rotate around transverse axis. Nodes of each cross section are controlled by RPs through kinematic coupling constraint. Kinematic constraints are imposed by eliminating the chosen degrees of freedom at the coupling nodes. Constrained edge nodes follow RP's motion as rigid body for the constrained degrees of freedom. Considering pure longitudinal bending, cross-sections must remain plane as hull bends, so longitudinal translation, rotation around transverse axis, rotation around vertical axis and rotation around longitudinal axis should be constrained by kinematic coupling. Taking into account results from the analysis of three span model (chapter 4.1.4), it is assumed that transverse's edge local vertical dimensions remain constant. This is achieved coupling vertical translation of the cross-section nodes with RP motion and under the influence of aforementioned constraints. From three-span model analysis is not clear, whether transverse displacement of nodes on transverse edge should be considered negligible, therefore two sets of boundary conditions should be set. One considering transverse displacements significant and another considering them negligible, meaning transverse translation free and coupled with RP respectively.

x=transverse, y=vertical, z=longitudinal							
Location	Translation			Rotation			Constraints
	Ux	Uy	Uz	URx	URy	URz	
RP1	Suppressed	Free	Free	Free	Suppressed	Suppressed	Kinematic coupling with transversel edge nodes. Constrained degrees of freedom: Uy, Uz, URx, URy, Urz
RP2	Suppressed	Suppressed	Suppressed	Suppressed	Suppressed	Suppressed	Kinematic coupling with transverse edge nodes. Constrained degrees of freedom: Uy, Uz, URx, URy, Urz

TABLE 4.6 Boundary conditions considering nodes on transverse edge are free to move through transverse direction

x=transverse, y=vertical, z=longitudinal							
Location	Translation			Rotation			Constraints
	Ux	Uy	Uz	URx	URy	URz	
RP1	Suppressed	Free	Free	Free	Suppressed	Suppressed	Kinematic coupling with transverse edge nodes. Constrained degrees of freedom: Ux, Uy, Uz, URx, URy, Urz
RP2	Suppressed	Suppressed	Suppressed	Suppressed	Suppressed	Suppressed	Kinematic coupling with transverse edge nodes. Constrained degrees of freedom: Ux, Uy, Uz, URx, URy, Urz

TABLE 4.7 Boundary conditions considering nodes on transverse edge to move as rigid body through transverse direction

4.2.3 Analysis Considering Free Transverse Displacement for Transverse Section Nodes

4.2.3.1 Linear Analysis

The model is imposed to pure longitudinal bending by subjecting rotation about transverse axis to the free to move/rotate RP.

The first eigenmode located to the deck arises at the horizontal stiffened plate at the middle of the deck. The eigenmode is similar to the one arises from linear analysis of three-span model. Z-axis and X-axis are antisymmetry axis. Six half waves are being formed and plate buckling seems to be dominant. Deformation of the plate and stiffeners is higher at the middle and is decreasing as edges of the plate are approached. Stiffeners' webs seem to buckle locally. The same collapse mode predicted from linear analysis of three-span model.

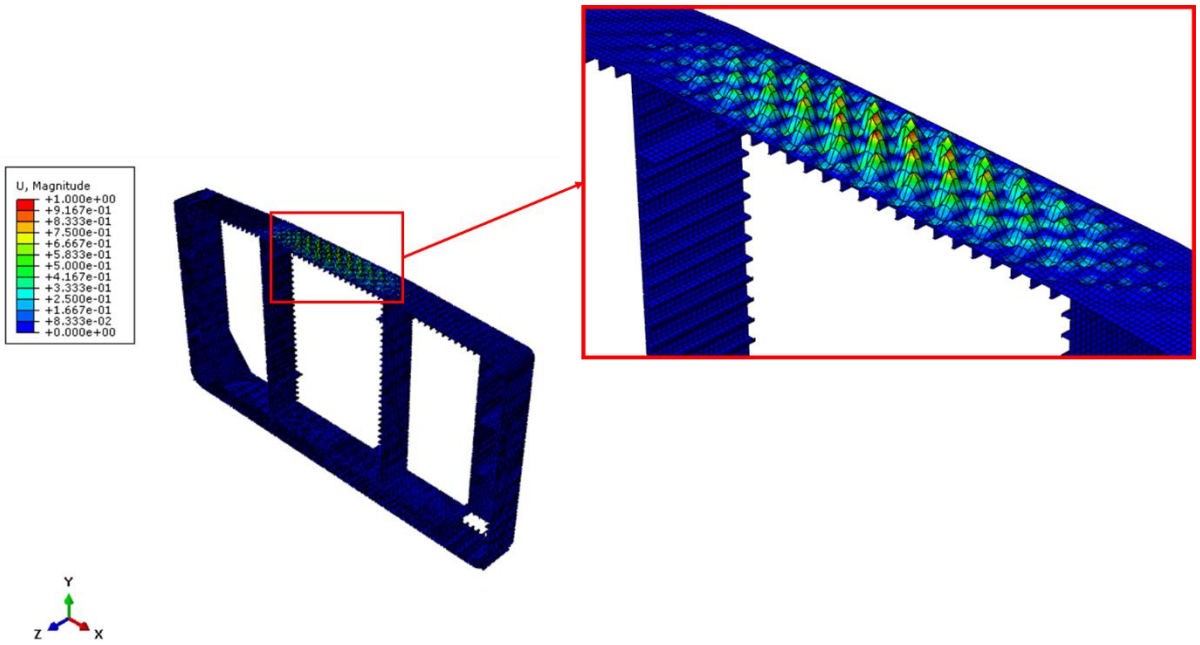

FIGURE 4.21 First antisymmetric buckling mode that forms on deck

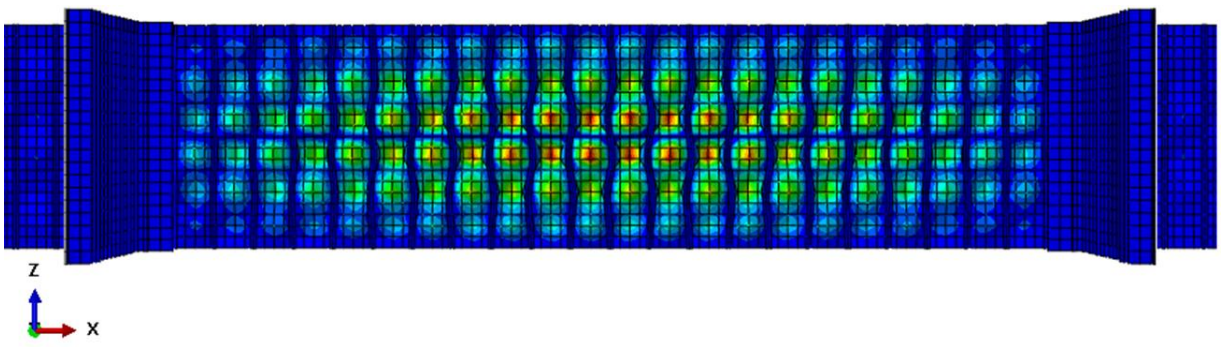

FIGURE 4.22 First symmetric/antisymmetric buckling mode that forms on deck (Z-X plane)

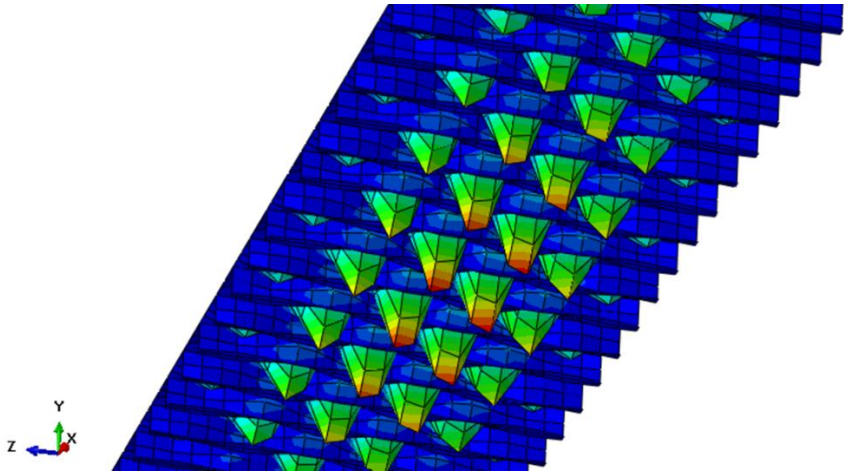

FIGURE 4.23 First symmetric/antisymmetric buckling mode that forms on deck (stiffeners view)

4.2.3.2 Nonlinear Analysis

The aforementioned eigenmode would be utilized as initial geometrical imperfections of the model, applied with the proposed tolerance level. Since plate buckling is the dominating source of buckling, maximum amplitude of 4.55 mm (s/200) is applied.

The model is imposed to pure longitudinal bending by subjecting rotation about transverse axis to the free to move/rotate RP.

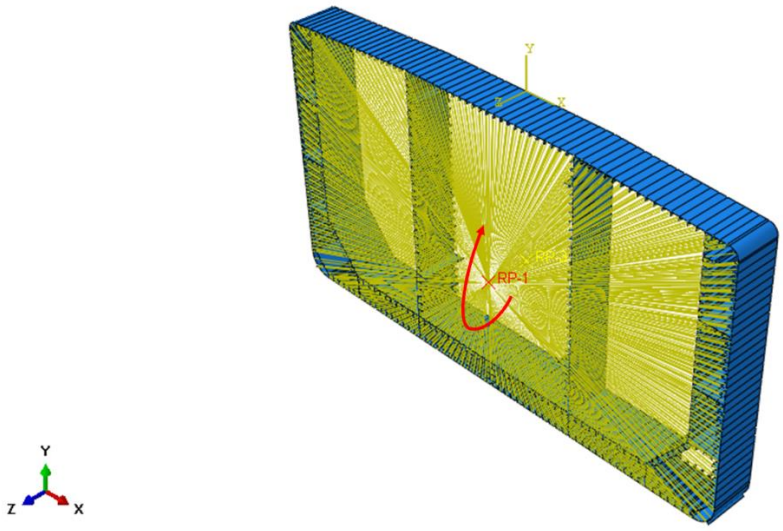

FIGURE 4.24 Rotation of RP

Simulation run using dynamic implicit solver of quasi static type. RP rotates with a radial velocity of 0,0015 rad/s. During the analysis Kinetic Energy remains under 5% of Internal Energy of the model, so could be regarded negligible and the consideration of quasi static loads is true.

For this analysis Hourglass Energy values remain under 10% of Internal Energy of model. Values under 5% of Internal Energy are noticed for the first 5 s of the analysis. It should be noted that critical values of the analysis such as maximum reaction moment of Hull or maximum axial stress of the Horizontal Stiffened Plate are reached while Hourglass energy is under the 5% limit.

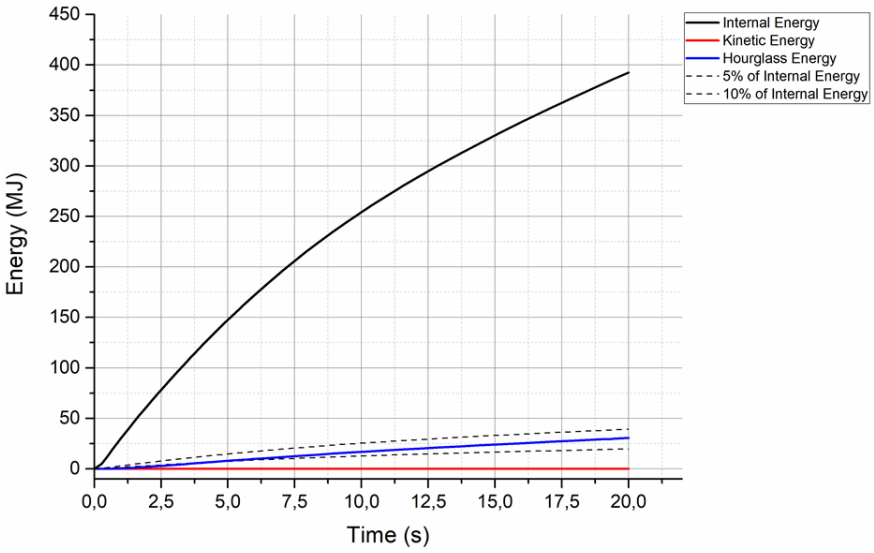

FIGURE 4.25 Internal, kinetic and hourglass energy comparison

Reaction Moment-RP rotation curve for Hull reaches its peak with linear trend. After reaching peak, Reaction Moment remains constant while RP rotates and drops slowly after 0,001 rotation angle. Stress-RP rotation curve reaches its peak with linear trend and drops quickly. (FIGURE 4.26)

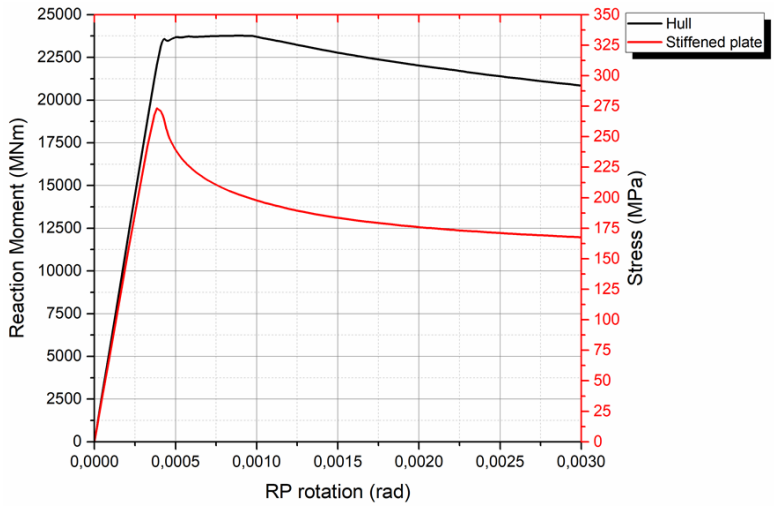

FIGURE 4.26 Reaction moment-RP rotation curve and Stress-RP rotation curve for hull and horizontal stiffened plate on deck respectively

Maximum Reaction Moment of Hull and maximum stress of Stiffened plate do not achieve for the same rotation of reference point. The same behavior noted analyzing the three-span model (Chapter 4.1.4) As mentioned before, the reason for this behavior is that geometrical imperfections are applied only on the horizontal stiffened plate of deck while the other components of structure are geometrically perfect. Any loss of stability due to imperfect plate collapse, is overcome by geometrically perfect elements of Hull.

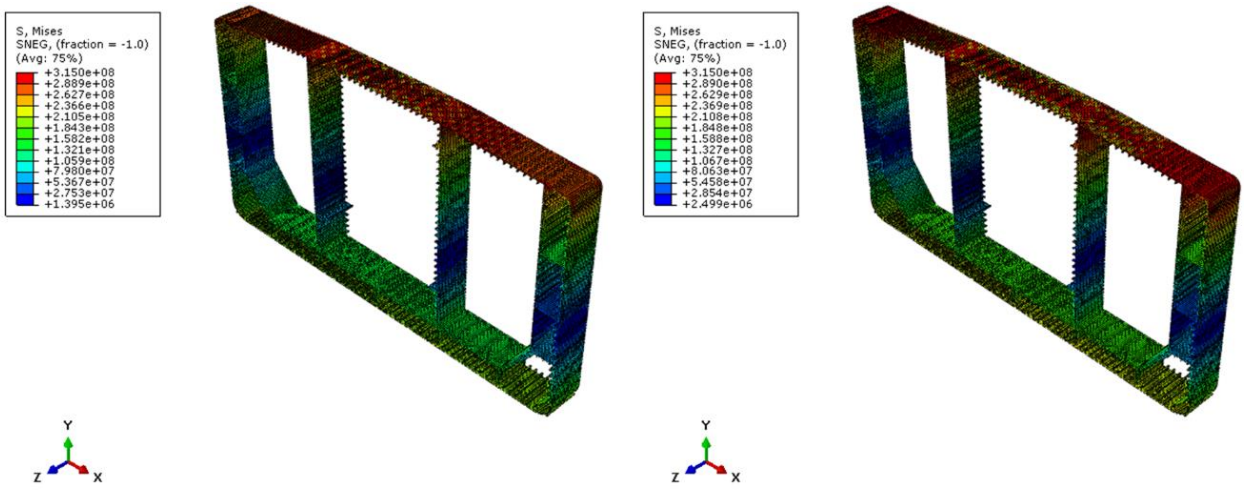

FIGURE 4.27 Von Misses stress on stiffened plate's collapse step (left), maximum reaction moment of hull step

As shown in FIGURE 4.28 local plate buckling is dominating when stiffened plate collapses. At the same time stiffeners' webs buckle locally. Through linear analysis of the model the same collapse mode is predicted. The stiffened plate on the three-span model collapses under the same mode.

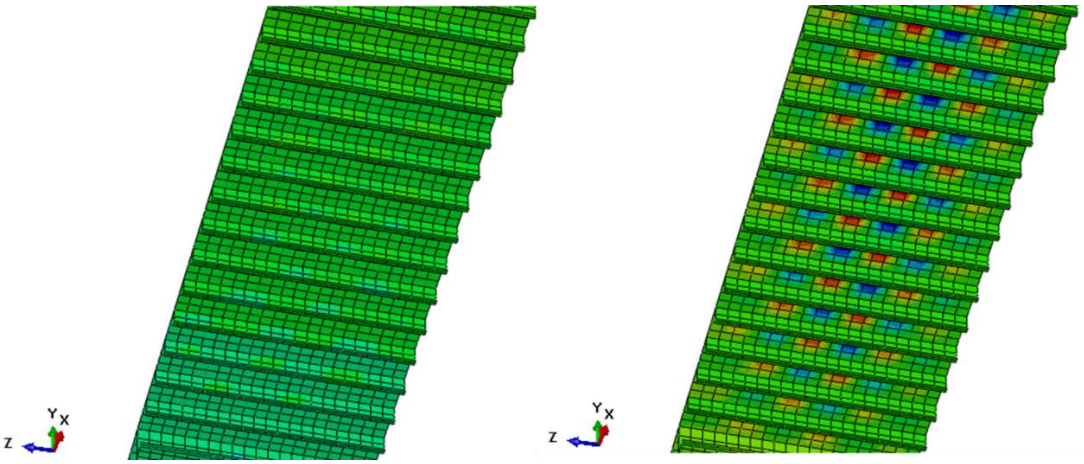

FIGURE 4.28 Transverse (left) and vertical (right) displacement of stiffened plate when it collapses

One span model does not contain any transverse frame. Since frames would be right on the transverse sections of the one span model, comparing the change in vertical and transverse length between the cross section of one span model and frame of the three-span model, would help to draw conclusions about the impact that makes the absence of frame. As shown in FIGURE 4.29, boundary conditions set to the transverse cross-section of the model seem to make hull more stiff vertically and less stiff transversely.

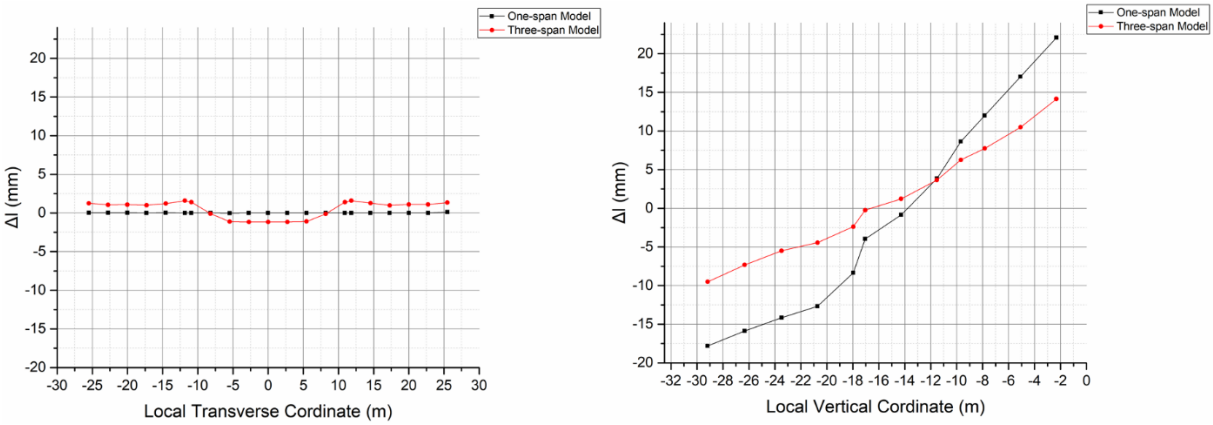

FIGURE 4.29 Change in vertical and transverse length of transverse cross section when horizontal stiffened plate collapses

As Hull sags deck is imposed to compression, leading its structural elements to buckle. The "imperfect" Horizontal Stiffened Plate in the middle of the deck, reaches critical buckling stress of 273 MPa for a strain of 0,00144. Critical buckling stress of the stiffened plate which is part of one-span model is a little lower compared to the equivalent resulting from three-span model. At the same time shortening strain before instability occurs, falls too from 0,00152 for the three-span model to 0,00144 for the one span model.

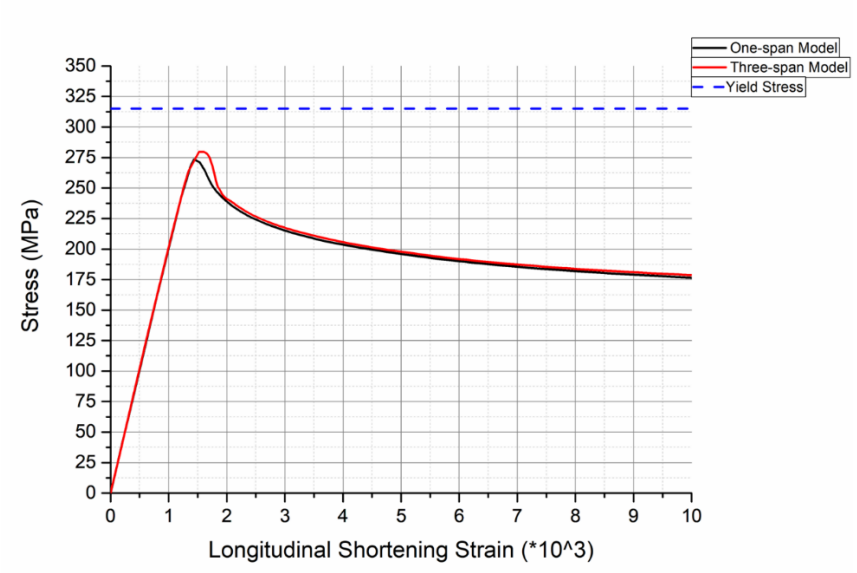

FIGURE 4.30 Stress-strain curve for horizontal stiffened plate on deck

Taking advantage of symmetry, conditions on the boundaries of plate, as Hull is imposed to pure bending, can be examined using two edges of the plate, one transverse edge and one longitudinal.

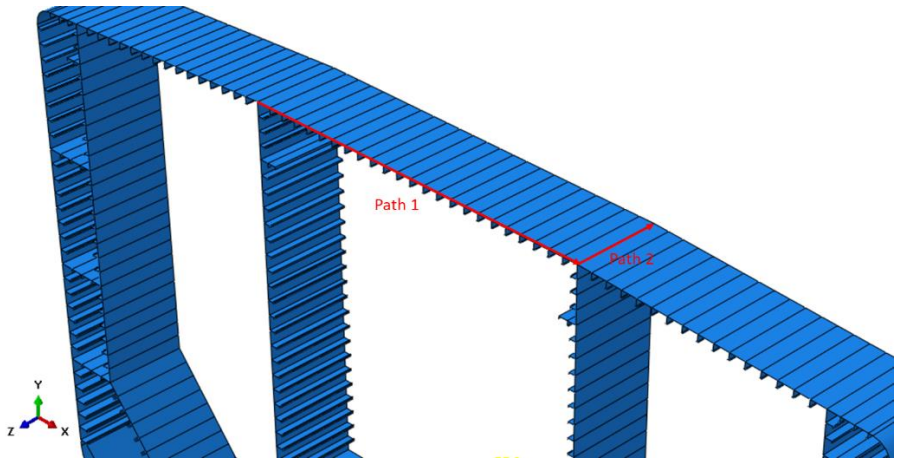

FIGURE 4.31 Edges of stiffened plate used to examine boundary conditions

Conditions on the boundaries of the plate are similar to those of three-span model analysis. As shown in FIGURE 4.32 as plate shortens, the node on the middle of the Transverse edge remains motionless. Nodes lying on the left and right of the motionless middle point, move away from it antisymmetricaly. Each node's Transverse Displacement-Strain curve separetely, reaches its peak with almost linear trend. For each curve separetely, when buckling occurs peak is reached. Post buckling all nodes' displacement reduces. The further away from the motionless middle node a node is, the greater its displacement is. When plate buckles, Transverse Displacement of nodes on Transverse edge of stiffened plate, changes equivalently with three-span model. Maximum difference in displacement values between two cases is about 0,25 mm.

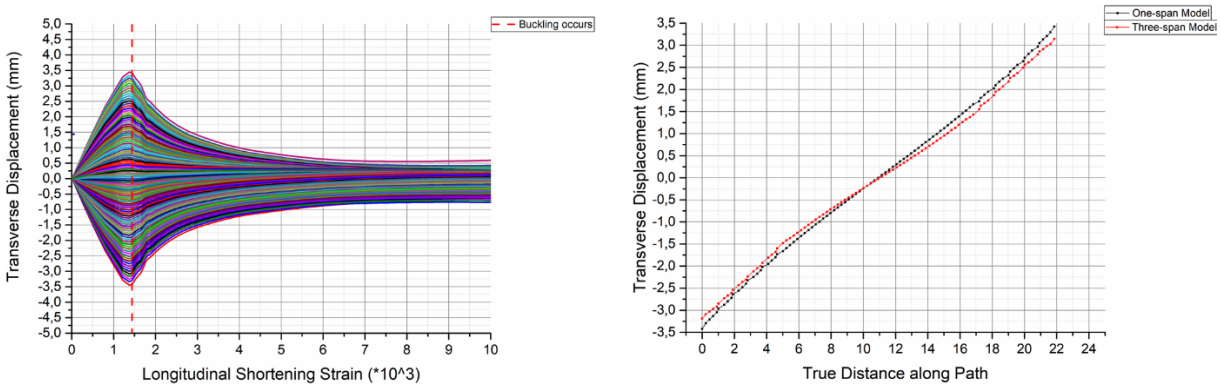

FIGURE 4.32 Transverse displacement-Strain curve of nodes on transverse edge of Plate (left), Transverse Displacement of nodes on Transverse edge on stiffened plate's buckling step (right)

It is observed (FIGURE 4.33) that nodes on longitudinal edge of the plate have common displacement through transverse direction. This behavior remains post buckling, but changes after a while. Post buckling all nodes displacement reduces. The same behavior noticed for nodes on longitudinal edge for three-span model. Comparing displacement values when buckling of plate occurs, maximum difference between three-span and one-span model analysis is about 0,325 mm.

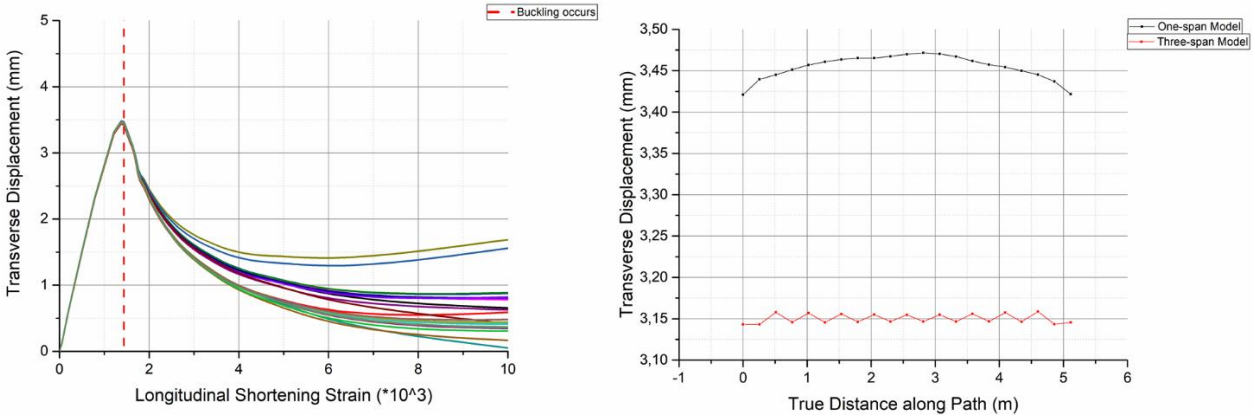

FIGURE 4.33 Transverse displacement-Strain curve of nodes on longitudinal edge of plate (left), transverse displacement of nodes on longitudinal edge on stiffened plate's buckling step (right)

4.2.4 Analysis Considering Suppressed Transverse Displacement for Transverse Section Nodes

4.2.4.1 Linear Analysis

The model is imposed to pure longitudinal bending by subjecting moment about transverse axis to the free to move/rotate RP.

The first eigenmode located to the deck arises at the horizontal stiffened plate at the middle of the deck. Applied moment results to completely different buckling formulations from what has been encountered on three-span model. Z-axis is symmetry axis and X-axis is antisymmetry axis. One half wave is being formed on the plate between stiffeners. Deformation of stiffeners and plate is equivalent significant. Critical part is considered in the middle where deformation of both stiffeners and plate are higher than closer to the edge of stiffened plate. The eigenmode acquired differs from this resulting from linear buckling analysis of three-span model.

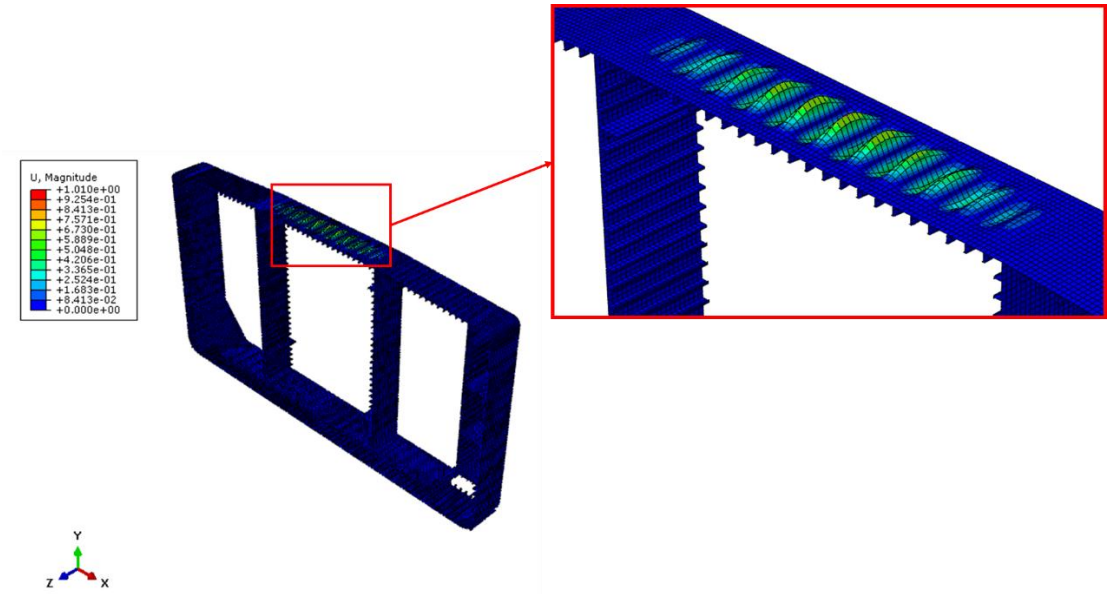

FIGURE 4.34 First symmetric/antisymmetric buckling mode that forms on deck

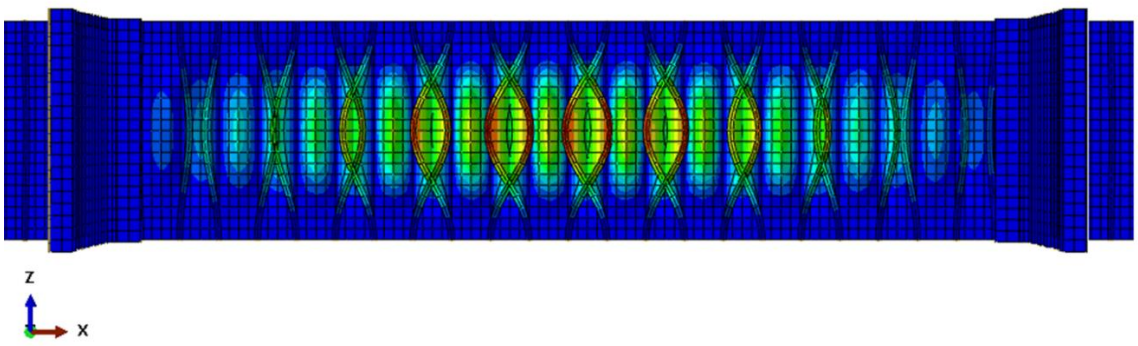

FIGURE 4.35 First symmetric/antisymmetric buckling mode that forms on deck (Z-X plane)

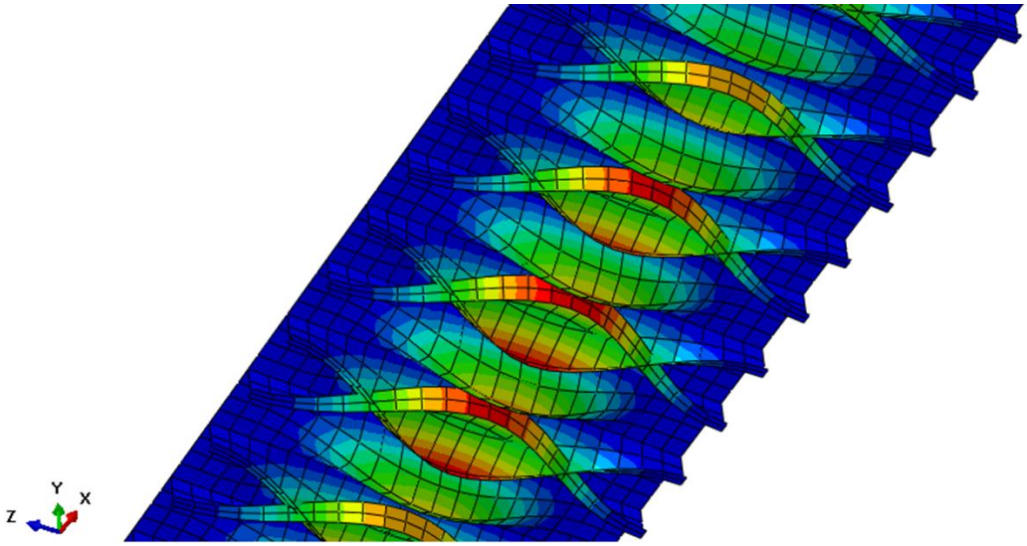

FIGURE 4.36 First symmetric/antisymmetric buckling mode that forms on deck (stiffeners view)

4.2.4.2 Nonlinear Analysis

The aforementioned eigenmode would be utilized as initial geometrical imperfections of the model, applied with the proposed tolerance level. Since stiffeners deformation is slightly higher than this of plate, maximum amplitude of 5,12 mm (L/1000) is applied.

The model is imposed to pure longitudinal bending by subjecting rotation about transverse axis to the free to move/rotate RP.

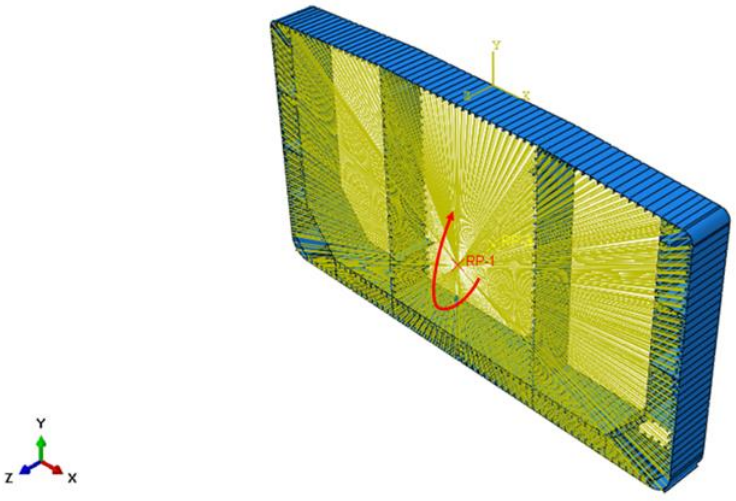

FIGURE 4.37 Rotation of RP

As on previous simulations, dynamic implicit solver of quasi static type used. RP rotates with a radial velocity of 0,0015 rad/s. During the analysis Kinetic Energy remains under 5% of Internal Energy of the model, so could be regarded negligible and the consideration of quasi static loads is true.

For this analysis Hourglass Energy values remain under 10% of Internal Energy of model. Values under 5% of Internal Energy are noticed for the first 5 s of the analysis.

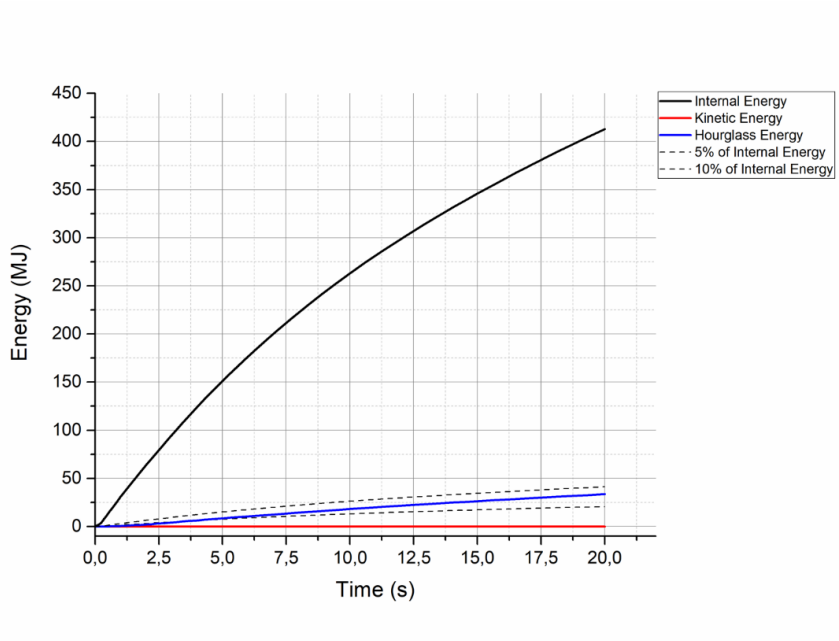

FIGURE 4.38 Internal, kinetic and hourglass energy comparison

Reaction Moment-RP rotation curve for Hull reaches its peak with linear trend. After reaching peak, Reaction Moment remains constant while RP rotates and drops slowly after about 0,0008 rotation angle of RP. Stress-RP rotation curve reaches its peak with linear trend and drops quickly. (FIGURE 4.39)

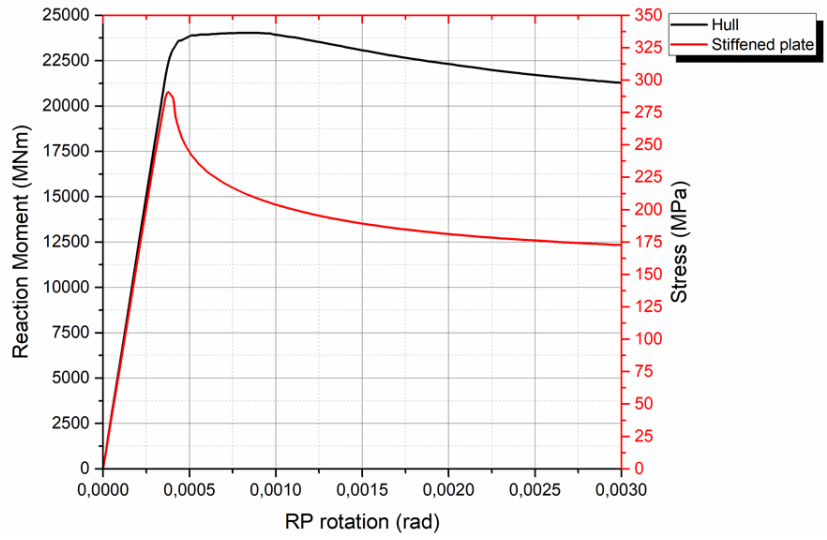

FIGURE 4.39 Reaction moment-RP rotation curve and Stress-RP rotation curve for hull and horizontal stiffened plate on deck respectively

Maximum Reaction Moment of Hull and maximum stress of Stiffened plate do not achieve for the same rotation. The same behavior noted on previous models too (Chapter 4.1.4, Chapter 4.2.3.2) As mentioned before, the reason for this behavior is that geometrical imperfections are applied only on horizontal stiffened plate on deck and the other components of structure are geometrically perfect. Any loss of stability due to imperfect plate collapse, is overcome by geometrically perfect elements of Hull.

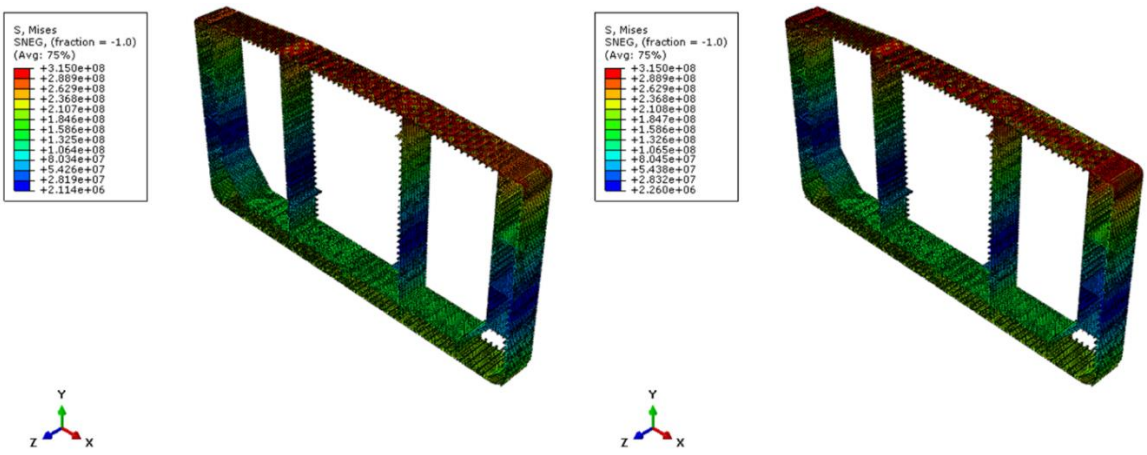

FIGURE 4.40 Von Misses stress on stiffened plate's buckling step (left), maximum reaction moment of hull step (right)

The stiffened plate on deck collapses under a combination of local plate buckling and stiffener tripping (FIGURE 4.41). Five halfwaves are being formed to the plating between stiffeners. Linear analysis of the model predicted a different collapse mode, with plating between stiffeners buckling overall. Collapse mode also differs from this predicted from the three-span analysis of the model.

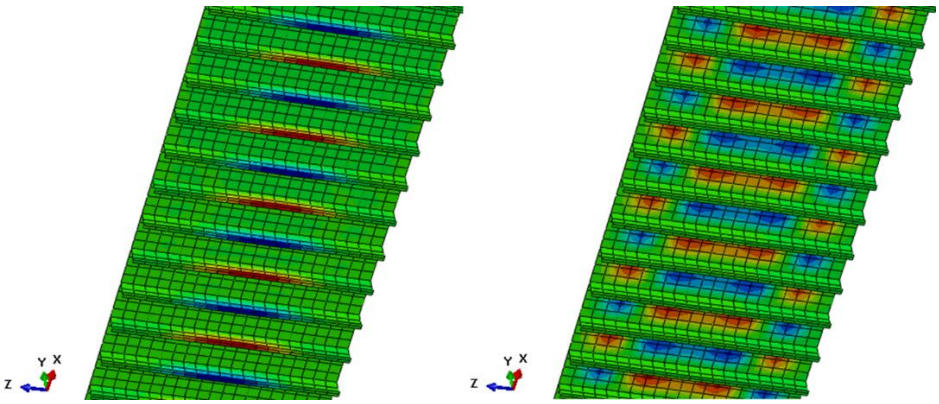

FIGURE 4.41 Transverse (left) and vertical (right) displacement of stiffened plate when it collapses

Transverse frame on three-span model is placed on the intersection between two bays. One-span model does not contain any transverse frame, however its effect on the transverse cross section of the bay modeled through boundary conditions. Nodes on transverse cross section of the model are assumed to move as rigid body through local transverse and

vertical direction. The aforementioned assumptions seem to make Hull more stiff transversely and vertically, since frame's impact is overestimated.

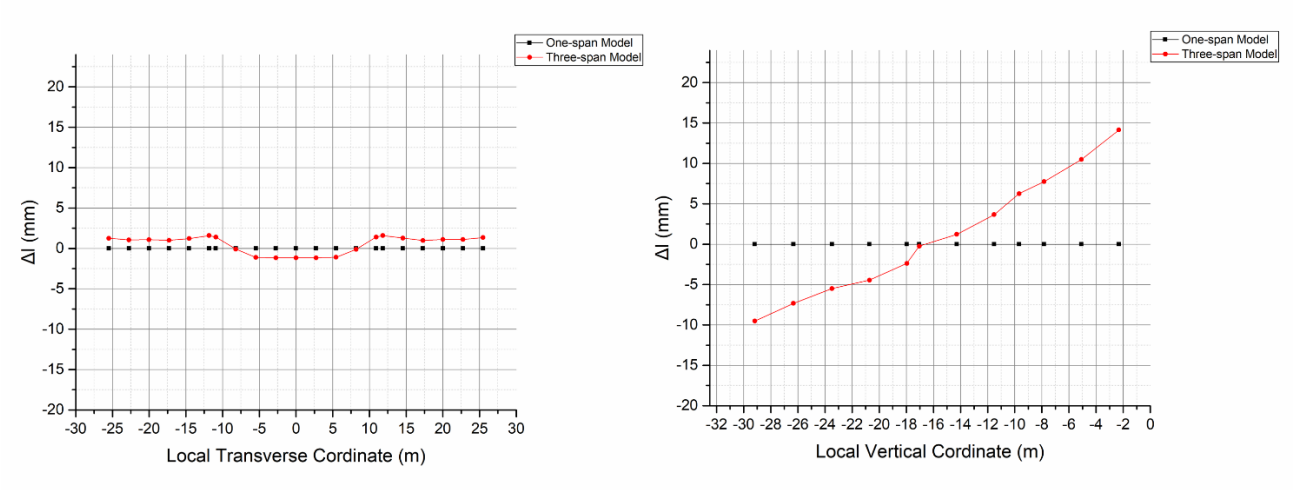

FIGURE 4.42 Change in vertical and transverse length of transverse cross section when horizontal stiffened plate buckles

As Hull sags and structural elements buckle, the "imperfect" Horizontal Stiffened Plate in the middle of the deck, reaches critical buckling stress of 291 MPa for a strain of 0,00142. Critical buckling stress of the stiffened plate which is part of one-span model is a little higher compared to the equivalent resulting from three-span model. At the same time shortening strain before instability occurs, falls too.

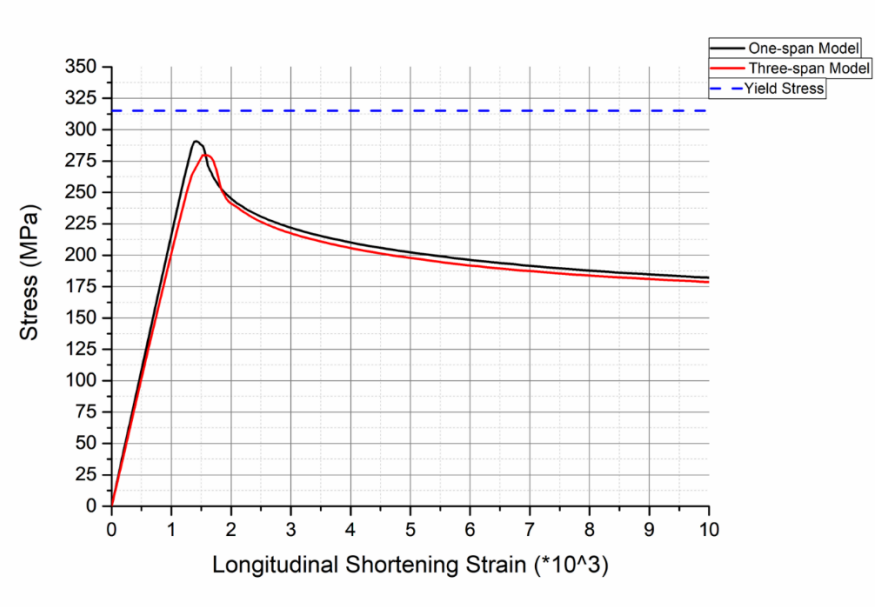

FIGURE 4.43 Stress-strain curve for Horizontal stiffened plate on deck

Taking advantage of symmetry, conditions on the boundaries of plate, as hull is imposed to pure bending, can be examined using two edges of the plate, one transverse edge and one longitudinal.

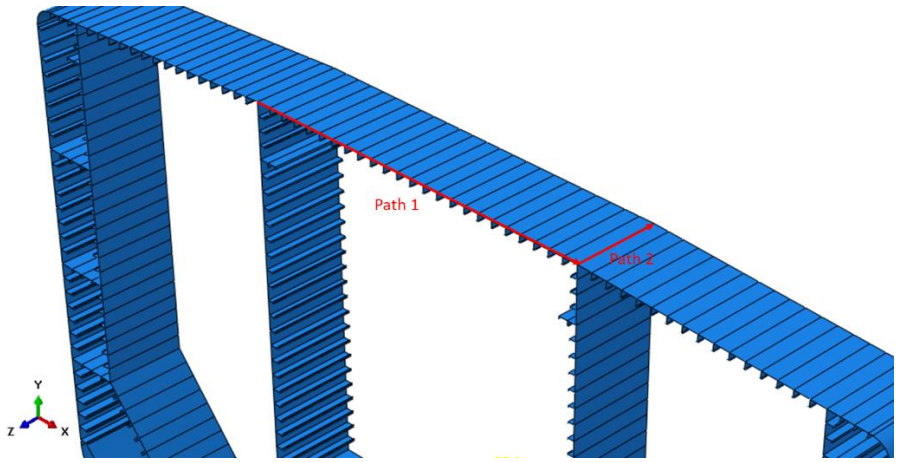

FIGURE 4.44 Edges of plate used to examine boundary conditions

Conditions on the boundaries of the plate do not have similarities compared to those of three-span Hull model analysis. As plate shortens, the nodes on of the transverse edge remains motionless pre-buckling and post-buckling, as expected due to boundary conditions.

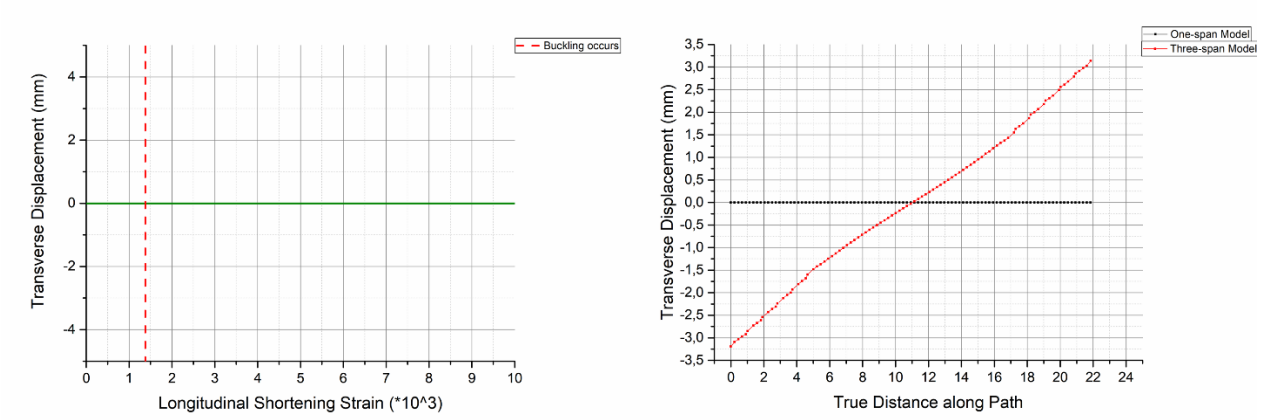

FIGURE 4.45 Transverse displacement-Strain curve of nodes on transverse edge of stiffened plate (left), transverse displacement of nodes on transverse edge on stiffened plate's buckling step (right)

Nodes on Longitudinal Edge of the plate have zero displacement in transverse direction. This behavior does not match with the expected, according to the analysis of three-span model. Considering that no boundary conditions set for the longitudinal edges of the plate, it can be concluded that boundary conditions on the transverse edge have great influence in the behavior of nodes on the plate's longitudinal edges.

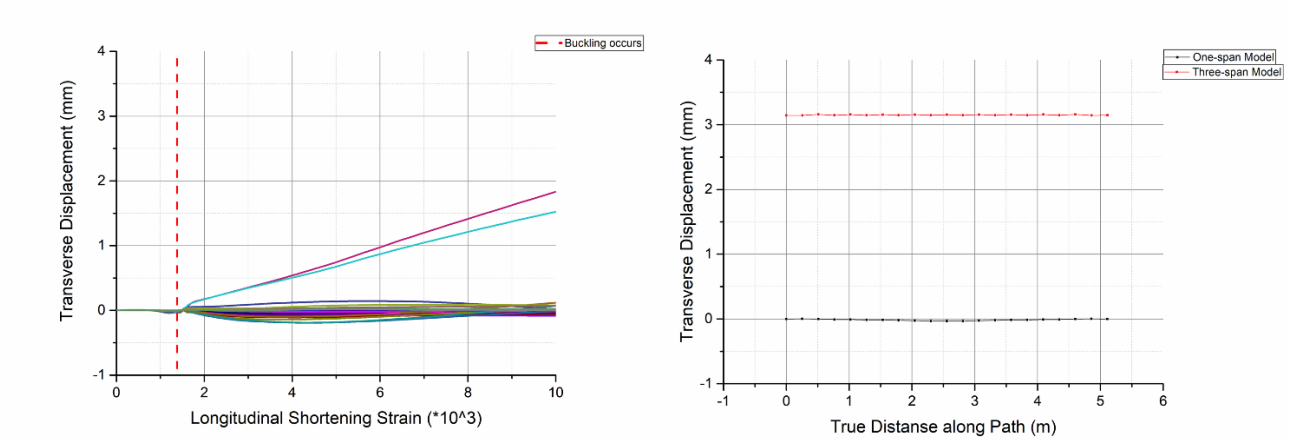

FIGURE 4.46 Transverse displacement-Strain curve of nodes on longitudinal edge of stiffened plate (left), transverse displacement of nodes on longitudinal edge on stiffened plate's buckling step (right)

4.3 One-span Deck's Stiffened Plate Model

The behavior of a stiffened plate on a ships deck as hull is sagging, can be studied through a model of an isolated stiffened plate under uniaxial compression, using the appropriate boundary conditions. In chapter 4.2 showed that for a hull subjected to sagging, different considerations about stiffness of transverse frame alters significantly the conditions a stiffened plate on deck encounters, affecting also the conditions on the longitudinal edges of the plate and leading to different collapse modes. Specifically, showed that underestimating stiffness of the transverse frame assuming that nodes on the transverse cross-section of a one span model of a hull are free to move in transverse direction, followed from common transverse displacement of nodes on longitudinal edges of the plate. On the other hand, overestimating stiffness of transverse frame by assuming translation of nodes on the transverse section of hull is suppressed, followed from zero displacement of nodes on longitudinal edges of the plate. Collapse mode is governed by local plate buckling of plate between stiffeners for the first case and by stiffener tripping for the second. This chapter aims to investigate whether an isolated stiffened plate follows the same behavior under the aforementioned assumptions and whether setting those boundary conditions on an isolated stiffened plate describe appropriately its behavior as part of a construction. This will be fulfilled by comparing ultimate strength and collapse mode of the isolated plate with those acquired for an identical stiffened plate, through the analysis of three-span and one-span hull model subjected to bending.

4.3.1 Model Geometry, Mesh and Material Properties

Model geometry

One-span model of a plate 5.12 m long stiffened plate with 23 tee-stiffeners has been used. Span between stiffeners is 910mm. Plates thickness is 17.5 mm. Web's height and thickness is 400mm and 13mm respectively and flange has a width of 165mm and a thickness of 18mm.

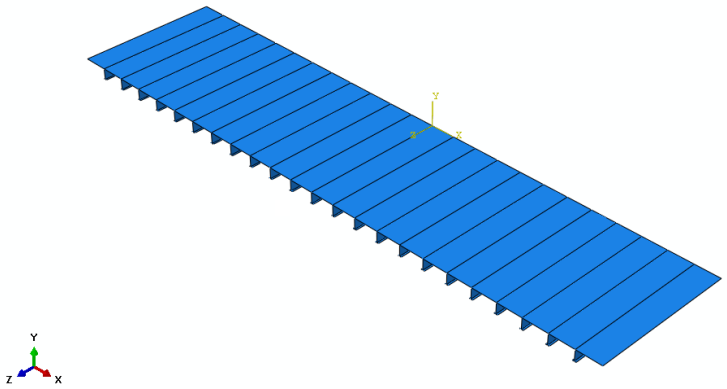

FIGURE 4.47 Isolated stiffened plate with 24 stiffeners model

Stiffened plate geometry	
s (mm)	910
L (mm)	5120
t_p (mm)	17,5
h_w (mm)	400
t_w (mm)	13
b_f (mm)	130
t_f (mm)	18

TABLE 4.8 Stiffened plate geometry

Mesh

Size of model allows much denser mesh than previous analysis to be used. However, it is proposed that the same mesh as previous models should be used, shell elements S4R of 250 mm length. Using the same elements in simulations, makes sure that any differences on the results of the analysis are products of the assumptions made to simplify models, since mesh used on simulations leads to equally accurate estimations of stresses and displacements

Material Properties

Material used is AH32. AH32 steel is a structural high tensile strength marine steel mainly used for making the hull of ship building and ship repairing, offshore oil drilling platforms, the platform pipe joints and other components. It is an isotropic material that has Young's modulus/modulus of elasticity (E) of 206 GPa, Poisson's ratio (v) of 0.3 and Yield strength (σ_y) of 315 MPa.

AH32 steel	
Young's modulus E (GPa)	206
Poisson's ratio v	0.3
Yield strength σ_y (MPa)	315

TABLE 4.9 Material properties of stiffened plate

4.3.2 Boundary Conditions

The successful approach of real conditions encountered on ship's deck's structures depends on the accurate simulation of the model's boundaries. Boundary conditions shall be such that the structural element can be checked for its buckling capacity as Hull sags and deck compresses.

Taking into account conclusions from previous analysis, two different sets of boundary conditions were introduced corresponding to the model edges.

One transverse edge should be free to move in longitudinal direction imposing to compressive loads. Thence an equation has been set between plate's and stiffeners' edge nodes and a Reference point. Keeping the relative displacement between Reference point and edge nodes constant any load acting on the reference point is forcing edge nodes to move as rigid body in axial direction. Both the plate and the stiffeners shall not translate in any plane, also vertical displacement should be suppressed. As on previous models, regarding transverse movement of edge nodes, two cases shall be examined one considering free movement and one considering nodes don't move in transverse direction.

On the opposite transverse side, model shall comply with the same boundary conditions, with an additional restriction in longitudinal direction to resist force acting on loaded edge.

Concerning longitudinal edges, all rotations shall be suppressed, along with vertical displacements. As ascertained on previous analysis, whether nodes on transverse edge move in transverse direction or not, has a great impact in the transverse displacement of nodes on longitudinal edge, hence assuming free transverse movement of nodes on transverse edge results common transverse displacement of nodes on longitudinal edge and suppressed transverse movement of nodes on transverse edge results nodes on longitudinal edge not to move in transverse direction.

x=transverse, y=vertical, z=longitudinal							
Location	Translation			Rotation			Constraints
	Ux	Uy	Uz	URx	URy	URz	
Transverse Edge 1	Free	Suppressed	Free	Suppressed	Suppressed	Suppressed	Equation, Uz=common. Relative displacement between RP and edge's nodes is constant
Transverse edge 2	Free	Suppressed	Suppressed	Suppressed	Suppressed	Suppressed	
Longitudinal Edges	Free	Suppressed	Free	Suppressed	Suppressed	Suppressed	Equation, Ux=common
RP	Suppressed	Suppressed	Free	Suppressed	Suppressed	Suppressed	

TABLE 4.10 Boundary conditions considering transverse edge nodes are free to move in transverse direction and longitudinal edges nodes have common transverse displacement

x=transverse, y=vertical, z=longitudinal							
Location	Translation			Rotation			Constraints
	Ux	Uy	Uz	URx	URy	URz	
Transverse Edge 1	Suppressed	Suppressed	Free	Suppressed	Suppressed	Suppressed	Equation, Uz=common. Relative displacement between RP and edge's nodes is constant
Transverse edge 2	Suppressed	Suppressed	Suppressed	Suppressed	Suppressed	Suppressed	
Longitudinal Edges	Suppressed	Suppressed	Free	Suppressed	Suppressed	Suppressed	
RP	Suppressed	Suppressed	Free	Suppressed	Suppressed	Suppressed	

TABLE 4.11 Boundary conditions considering transverse edge and longitudinal edge nodes have zero transverse displacement

4.3.3 Transverse Edge Nodes are Free to Move in Transverse Direction, Longitudinal Edge Nodes have Common Transverse Displacement

4.3.3.1 Linear Analysis

The model is imposed to pure uniaxial compression by subjecting force through longitudinal axis to the free to move RP.

Six half waves are being formed and plate buckling seems to be dominant. Deformation of the plate and stiffeners is higher at the middle and is decreasing as edges of the plate are approached. Stiffeners seem to buckle locally at the webs. Collapse mode predicted from linear eigenvalue analysis is similar with collapse mode acquired from the analysis of three-span and one-span model with equivalent boundary conditions.

The buckling load is 203,931 MN, which is equivalent to a critical buckling stress of 367 MPa.

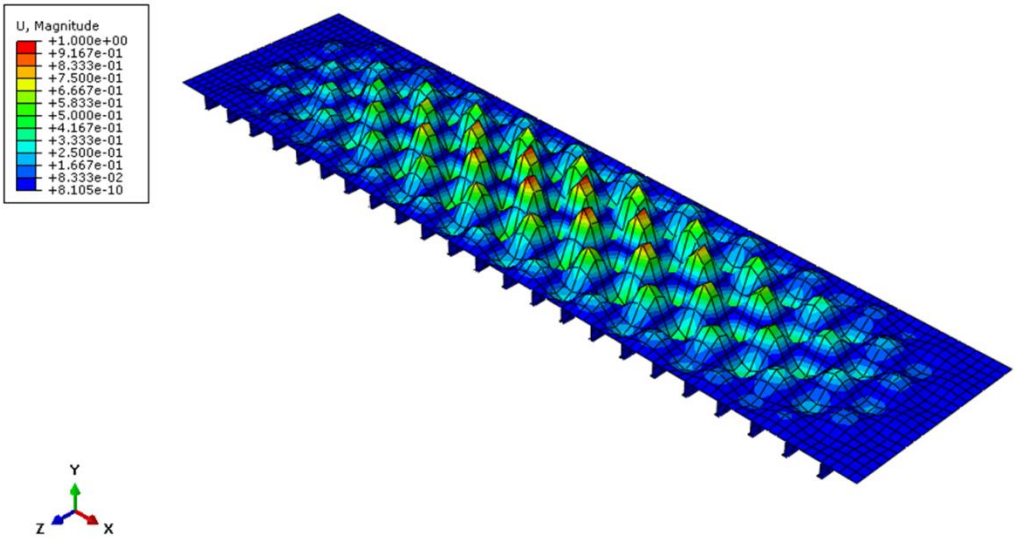

FIGURE 4.48 First symmetric/antisymmetric buckling mode that forms on Stiffened Plate

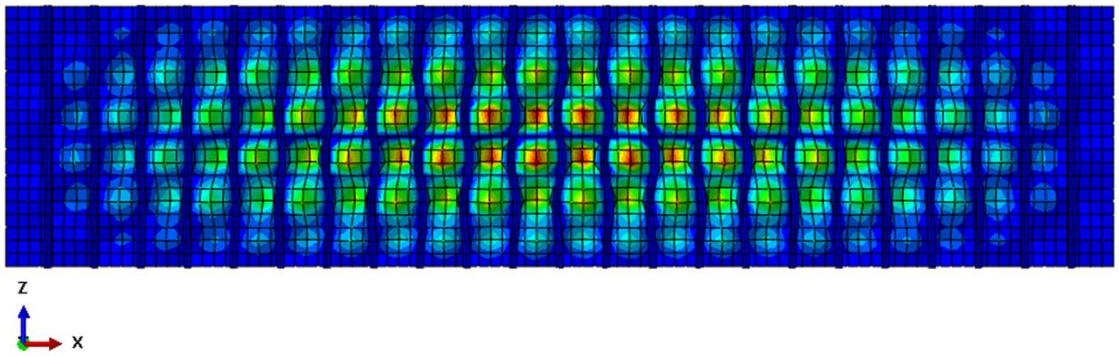

FIGURE 4.49 First symmetric/antisymmetric buckling mode that forms on Stiffened Plate (Z-X plane)

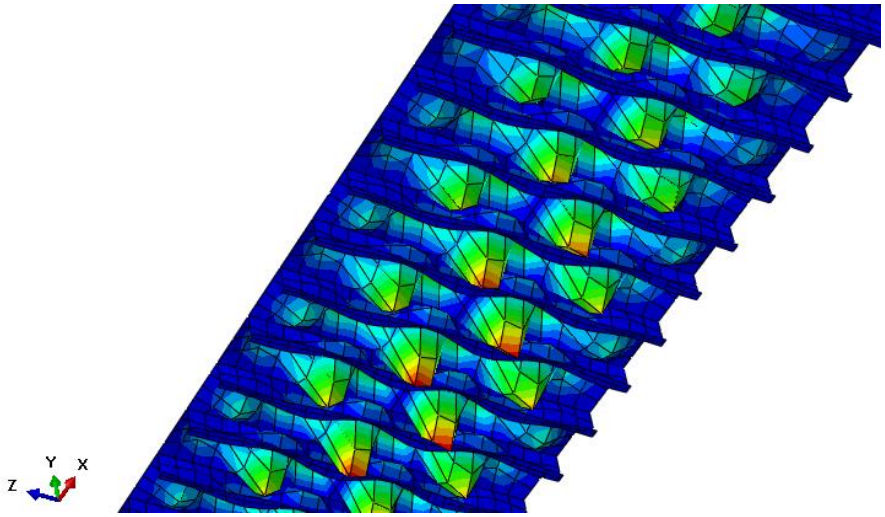

FIGURE 4.50 First symmetric/antisymmetric buckling mode that forms on Stiffened Plate (stiffeners view)

4.3.3.2 Nonlinear Analysis

The aforementioned eigenmode would be utilized as initial geometrical imperfections of the model, applied with the proposed tolerance level. Since plate buckling is the dominant source of buckling, maximum amplitude of 4,55 mm (s/200) is applied.

The model is imposed to pure uniaxial compression by subjecting displacement in longitudinal axis to the free to move RP.

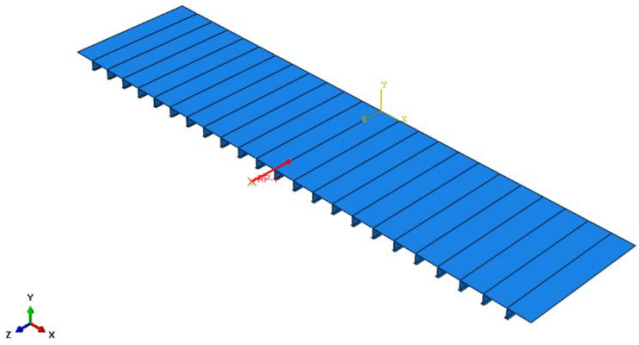

FIGURE 4.51 RP movement

As on previous simulations, dynamic implicit solver of quasi static type used. RP moves with a velocity of 1 mm/s. During the analysis Kinetic Energy remains under 5% of Internal Energy of the model, so could be regarded negligible and the consideration of quasi static loads is true.

For this analysis Hourglass Energy values remain under 5% of Internal Energy of model.

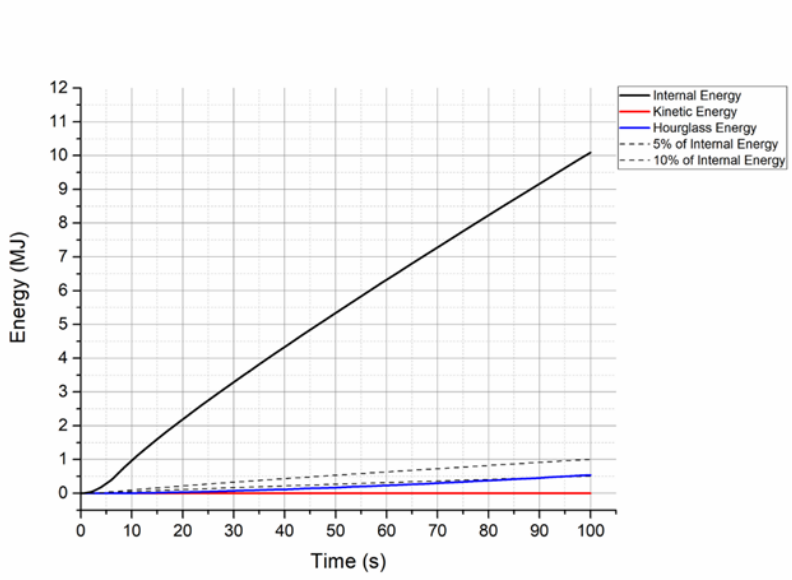

FIGURE 4.52 Internal, Kinetic and Hourglass Energy comparison

Results from eigenvalue analysis conclude that plate is not expected to collapse before material yielding. However, maximum stress of 269 MPa is reached for a strain of 0,00149. The stiffened plate is expected to not achieve its theoretical buckling strength predicted from linear analysis, due to nonlinearities and inserted imperfections. Stress-Strain curve of the stiffened plate is almost identical with the equivalent curve acquired from the one-span hull model analysis. Compared with the Stress-strain curve of stiffened plate acquired from three-span model analysis, maximum Stress value is slightly lower and is reached for lower strain.

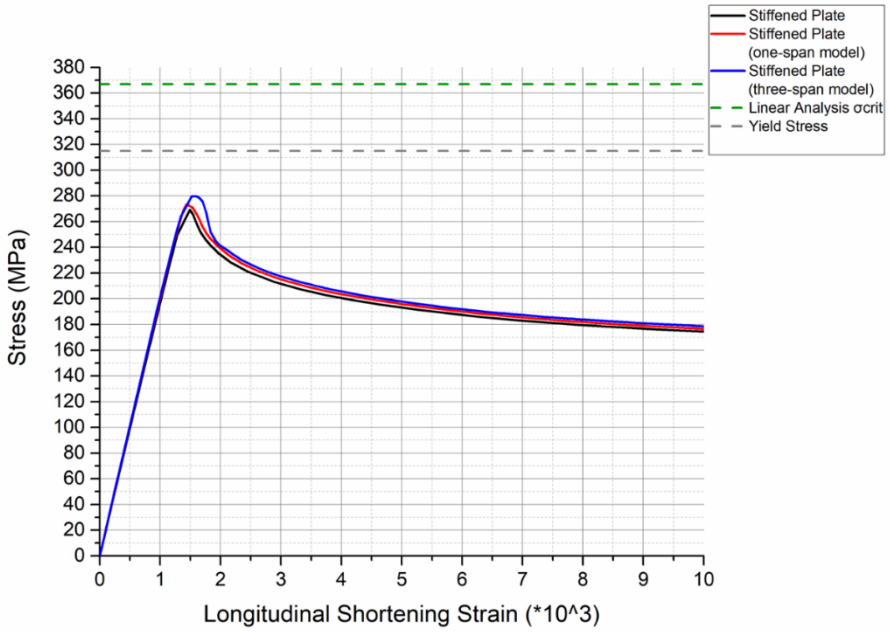

FIGURE 4.53 Stress-strain curve for stiffened plate

Stiffened plate collapses under the collapse mode predicted from linear analysis. Maximum displacements when instability occurs shows a compilation of local plate buckling with six half waves and local stiffener web buckling with a slight torsion of the stiffeners locally. Stiffeners' deformation seems to maximize close to the longitudinal edge, while plating seems to have greater displacement near the middle. The same collapse mode is observed for the stiffened plate on the equivalent one-span hull model analysis. When buckling occurs almost the whole structure yields. (FIGURE 4.54)

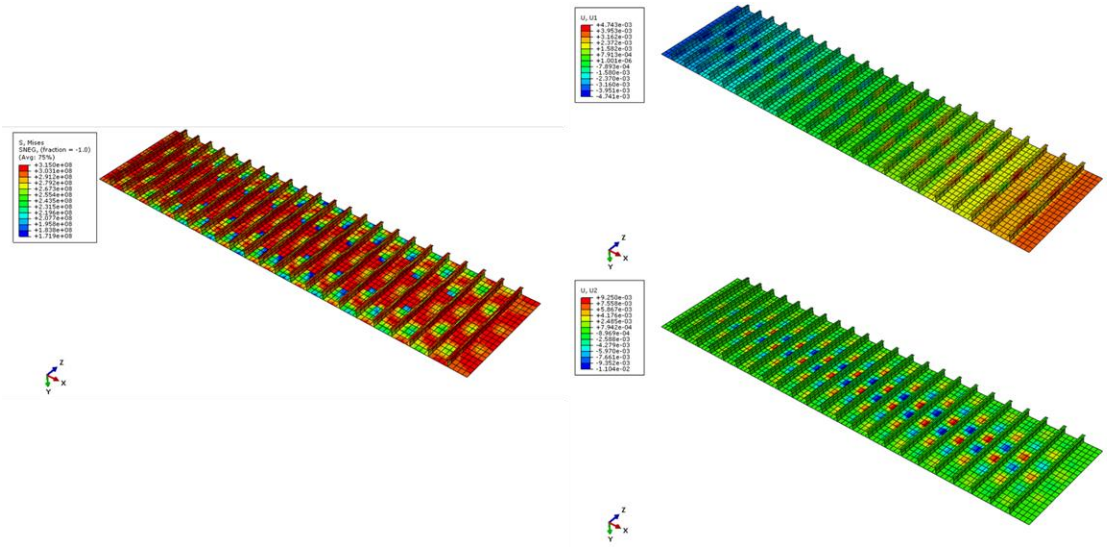

FIGURE 4.54 Von Misses stresses (left), transverse displacement (top right), vertical displacement (bottom right) when buckling occurs

Conditions on the boundaries of the plate are similar to those of three-span and one-span Hull model analysis. As plate shortens, the node on the middle of the Transverse edge remains motionless. Nodes lying on the left and right of the motionless middle point, move away from it antisymmetrically. Each node's Transverse Displacement-Strain curve separately, reaches its peak with almost linear trend. For each curve separately, when buckling occurs peak is reached. Post buckling all nodes' displacement reduces. The further away from the motionless middle node a node is, the greater its displacement is.

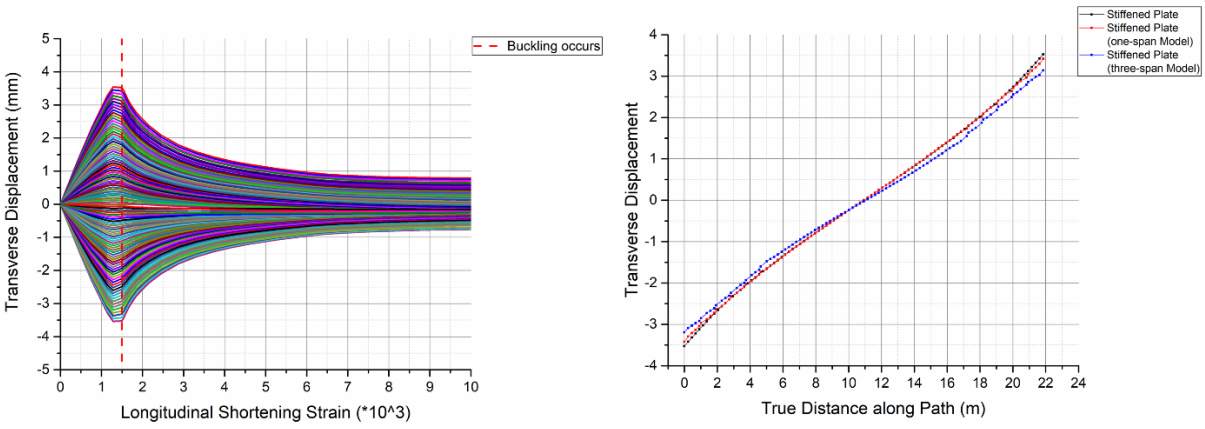

FIGURE 4.55 Transverse displacement-Strain curve of nodes on transverse edge of stiffened plate (left), transverse displacement of nodes on transverse edge on stiffened plate's buckling step (right)

Boundary conditions used, force nodes on longitudinal edge of the stiffened plate to have common displacement through transverse direction. Post buckling all nodes displacement reduces. Transverse displacement values of nodes when construction reaches maximum load capacity are very close to those acquired from the one-span hull analysis.

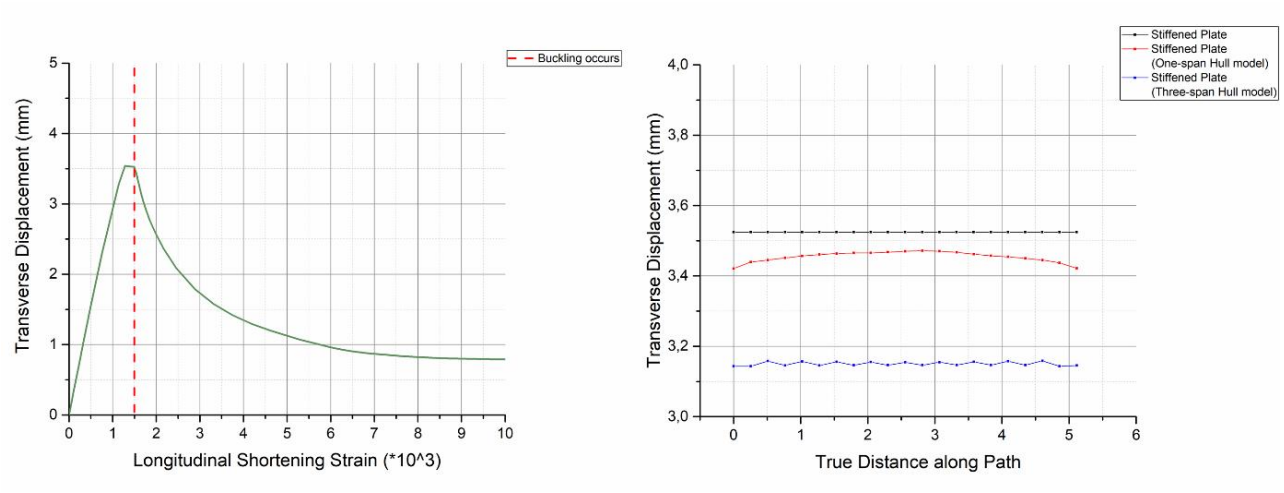

FIGURE 4.56 Transverse displacement-Strain curve of nodes on longitudinal edge of stiffened plate (left), transverse displacement of nodes on longitudinal edge on stiffened plate's buckling step (right)

4.3.4 Transverse Edge and Longitudinal Edge Nodes have zero Transverse Displacement

4.3.4.1 Linear Analysis

The model is imposed to pure uniaxial compression by subjecting force through longitudinal axis to the free to move RP.

Plate between stiffeners buckles overall. Deformation of stiffeners and plate is equivalent significant, but stiffeners deformation is slightly higher. Critical part is considered in the middle where deformation of both stiffeners and plate are higher. Collapse mode predicted from linear eigenvalue analysis is similar with collapse mode acquired from the analysis of one-span model with equivalent boundary conditions, but doesn't match with collapse mode predicted from three-span hull model analysis.

The buckling load is 135,113 MN, which is equivalent to a critical buckling stress of 243 MPa

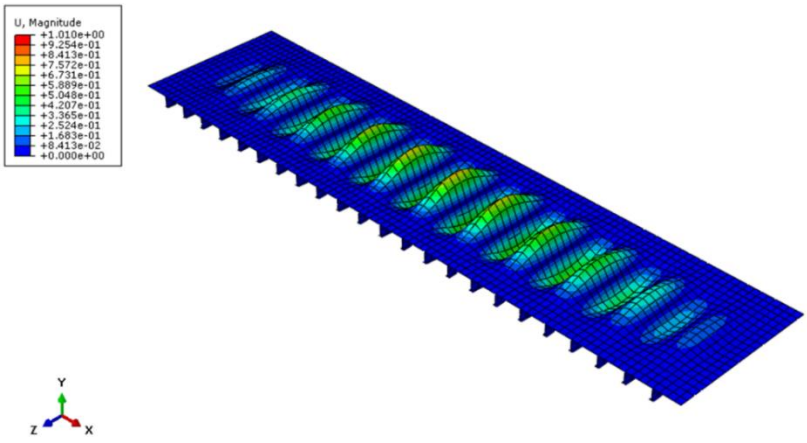

FIGURE 4.57 First symmetric/antisymmetric buckling mode that forms on stiffened plate

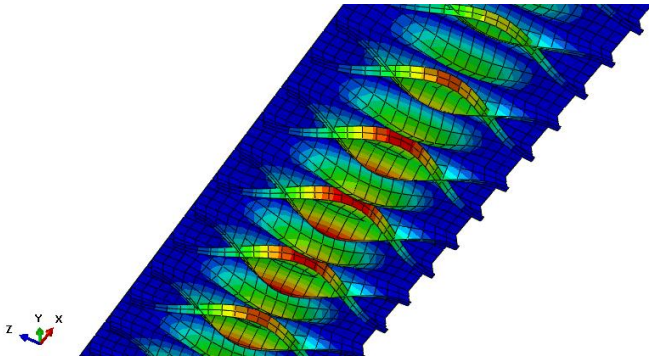

FIGURE 4.58 First symmetric/antisymmetric buckling mode that forms on stiffened plate (Stiffeners view)

4.3.4.2 Nonlinear Analysis

The model is imposed to pure uniaxial compression by subjecting displacement through longitudinal axis to the free to move RP.

The aforementioned eigenmode would be utilized as initial geometrical imperfections of the model, applied with the proposed tolerance level. Since stiffeners deformation amplitude is slightly higher than this of plate, maximum amplitude of 5,12 mm (L/1000) is applied.

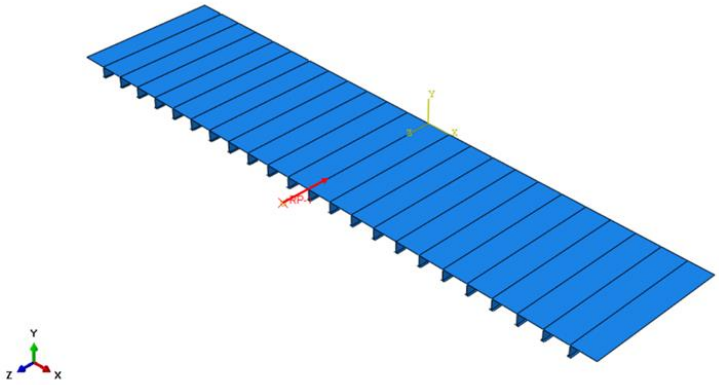

FIGURE 4.59 RP movement

As on previous simulations, dynamic implicit solver of quasi static type used. RP moves with a velocity of 1 mm/s. During the analysis Kinetic Energy remains under 5% of Internal Energy of the model, so could be regarded negligible and the consideration of quasi static loads is true.

For this analysis Hourglass Energy values remain under 5% of Internal Energy of model.

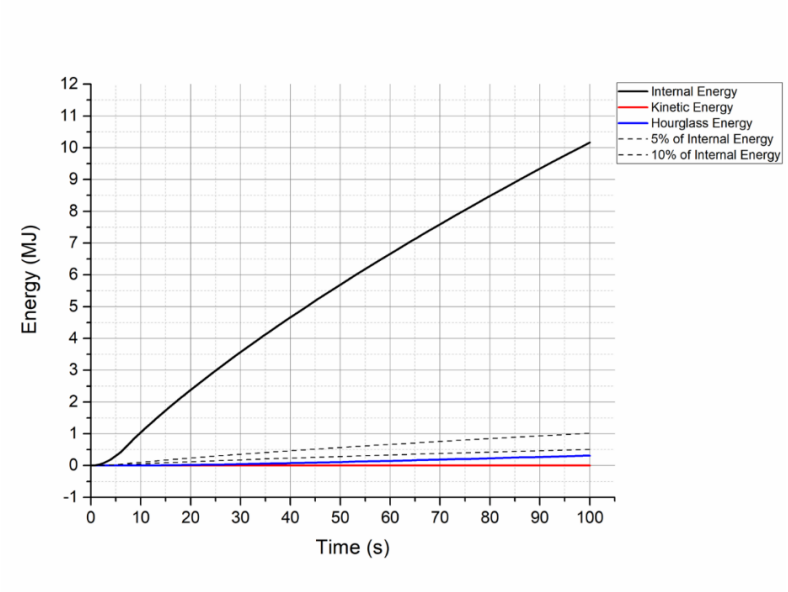

FIGURE 4.60 Internal, kinetic and hourglass energy comparison

Results from eigenvalue analysis conclude that Stiffened Plate expected to collapse under 243 MPa compressive axial stress. However, maximum axial stress of 285 MPa is reached for a strain of 0,00143 before construction collapses. This behavior is unexpected, since nonlinearities and inserted imperfections are expected to decrease construction's buckling capacity. Stress-Strain curve of the stiffened plate is almost identical with the equivalent curve acquired from the one-span Hull model analysis. Compared with the Stress-strain curve of stiffened plate acquired from three span Hull model analysis, maximum Stress value is slightly higher and is reached for lower strain and with a completely different collapse mode.

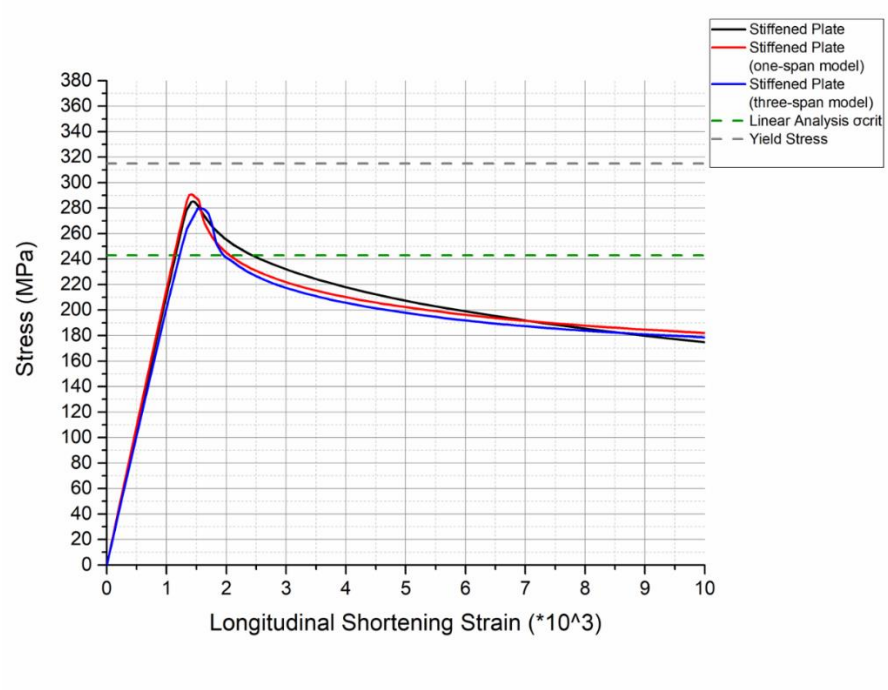

FIGURE 4.61 Stress-strain curve for stiffened plate

When structure loses stability almost the whole of the construction yields. Maximum displacements when instability occurs shows that stiffeners collapse under tripping. Stiffeners' deformation seems to maximize in the middle of each stiffener and gets more significant approaching the middle of the construction. Buckling mode of plating between stiffeners differs from this predicted from linear eigenvalue analysis. According to linear analysis plating is expected to buckle overall, however it seems to buckle forming five halfwaves. It must be noted that for the equivalent one-span hull model, stiffened plate collapses under the same mode.

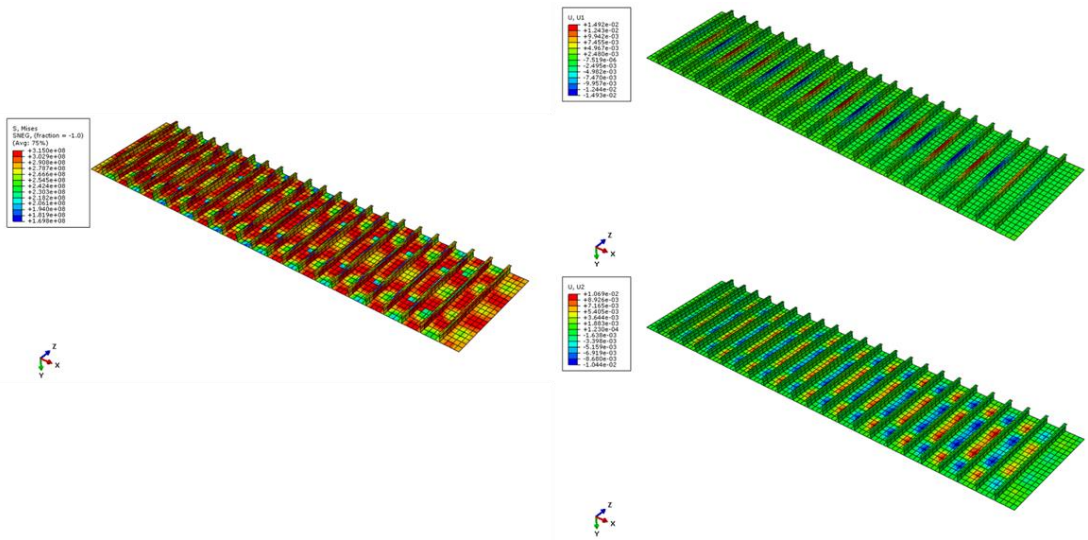

FIGURE 4.62 Von Misses stresses (left), transverse displacement (top right), vertical displacement (bottom right) when buckling occurs

Conditions on the boundaries of the plate do not have similarities compared to those of three-span hull model analysis but are identical with those from one-span hull model with equivelent boundary conditions. As plate shortens, the nodes on of the transverse and longitudinal edges remain motionless pre-buckling and post-buckling, as expected due to boundary conditions.

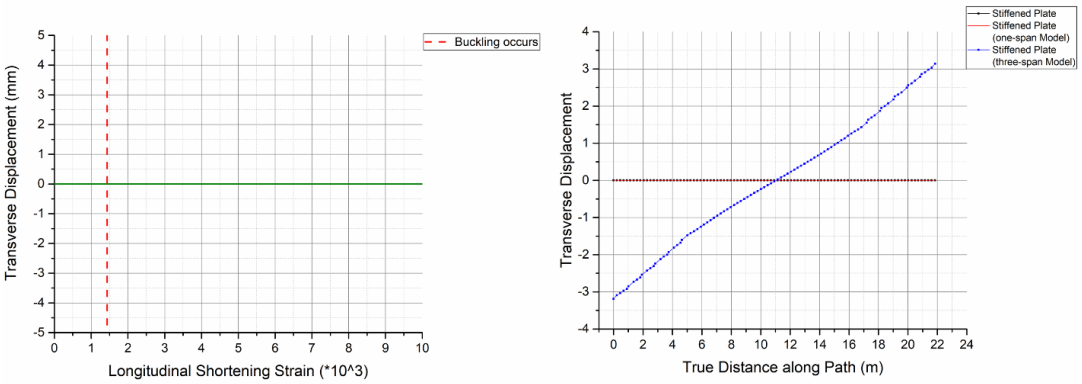

FIGURE 4.63 Transverse displacement-Strain curve of nodes on Transverse edge of stiffened late (left), transverse displacement of nodes on transverse edge on stiffened plate's buckling step (right)

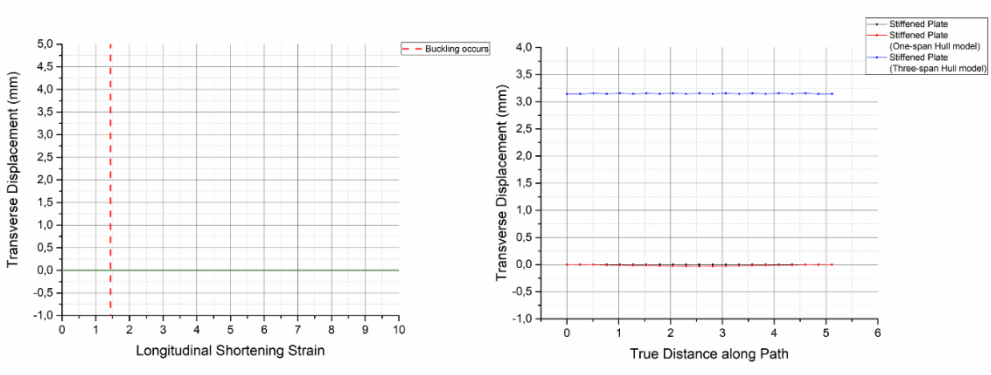

FIGURE 4.64 Transverse displacement-Strain curve of nodes on longitudinal edge of stiffened plate (left), transverse displacement of nodes on longitudinal edge of stiffened plate on buckling step (right)

5 One-span Stiffened Plate with 6 Stiffeners Model

Analysis results from chapter 4 lead to useful conclusions about the conditions a stiffened plate encounters as structural element of a ship's deck, as hull is sagging. Boundary conditions obtained from previous procedure could be used to simulate the behavior of any stiffened plate on deck of a ship. Typically, stiffened plates consisting of 5 to 10 stiffeners are often used in marine structures. Hence, a stiffened plate within this range regarding number of stiffeners will be studied.

This chapter aims to accurately investigate the behavior (collapse mode, ultimate strength) of a stiffened plate with 6 stiffeners and its elements under compressive loads. Displacement of nodes in the boundaries of stiffened plate's elements will be monitored, to obtain the appropriate boundary conditions that represent realistically the behavior of an isolated stiffened plate's element.

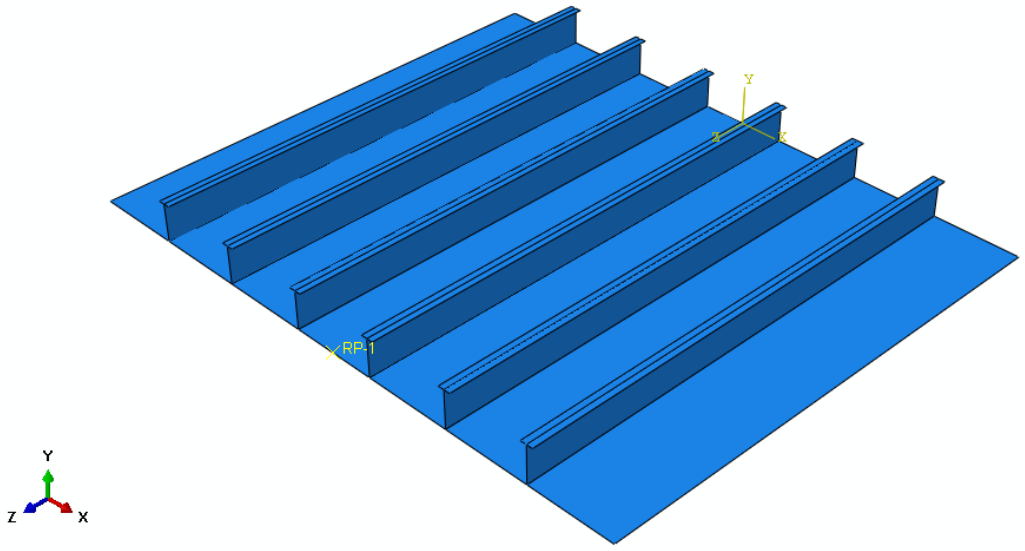

FIGURE 5.1 Stiffened plate with 6 stiffeners model

5.1 Model mesh, Geometry and Material Properties

Model Geometry

One-span model of a 5.12 m long stiffened plate with 6 tee-stiffeners has been used. Span between stiffeners is 910mm. Plates thickness is 17.5 mm. Web's height and thickness is 400mm and 13mm respectively and flange has a width of 165mm and a thickness of 18mm.

Stiffened plate geometry	
s (mm)	910
L (mm)	5120
t_p (mm)	17,5
h_w (mm)	400
t_w (mm)	13
b_f (mm)	130
t_f (mm)	18

TABLE 5.1 Stiffened Plate geometry

Mesh

The use of S4R type elements of 50 mm it is proposed. The discretization of model with elements of this size leads to highly accurate estimations of stresses and displacements with sufficient processing time. A converge study has been made as shown in FIGURE 5.2 for both of the sets of boundary conditions used. Using denser mesh than the proposed of 50m elements increases greatly the computational cost while the increase in accuracy is insignificant.

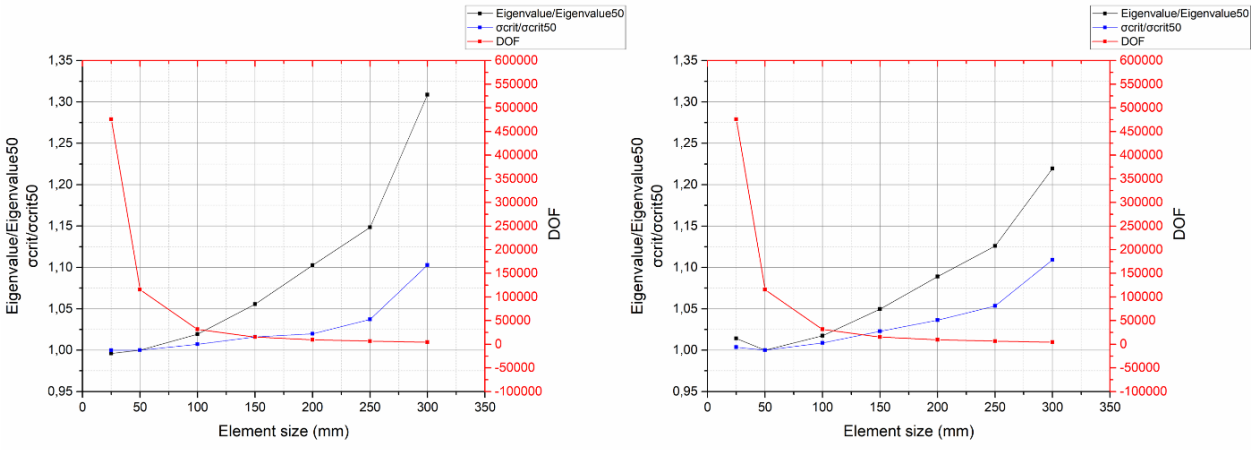

FIGURE 5.2 Mesh convergence study, transverse edge nodes are free to move in transverse direction and longitudinal edges nodes have common transverse displacement (left) transverse edge and longitudinal edge nodes have zero transverse displacement (right)

Material properties

Material used is AH32. AH32 steel is a structural high tensile strength marine steel mainly used for making the hull of ship building and ship repairing, offshore oil drilling platforms, the platform pipe joints and other components. It is an isotropic material that has Young's modulus/modulus of elasticity (E) of 206 GPa, Poisson's ratio (v) of 0.3 and Yield strength (σ_y) of 315 MPa.

AH32 steel	
Young's modulus E (GPa)	206
Poisson's ratio v	0.3
Yield strength σ_y (MPa)	315

TABLE 5.2 Material properties of stiffened plate

5.2 Boundary Conditions

Boundary conditions described in chapter 4.3.2 approach realistically the conditions encountered by a stiffened plate as structural element of a ship's deck.

One transverse edge should be free to move in longitudinal direction imposing to compressive axial loads. Thence an equation has been set between plate's and stiffeners' edge nodes and a Reference point. Keeping the relative displacement between Reference point and edge nodes constant any load acting on the reference point is forcing edge nodes to move as rigid body in axial direction. Both the plate and the stiffeners shall not translate in any plane, also vertical displacement should be suppressed. As on previous models, regarding transverse movement of transverse edge nodes, two cases shall be examined one considering free movement and one considering nodes don't move in transverse direction.

On the opposite transverse side, model shall comply with the same boundary conditions, with an additional restriction in longitudinal direction to resist force acting on loaded edge.

Concerning longitudinal edges, all rotations shall be suppressed, along with vertical displacements. As ascertained on previous analysis, whether nodes on transverse edge move in transverse direction or not, has a great impact in the transverse displacement of nodes on longitudinal edge, hence assuming free transverse movement of nodes on transverse edge results common transverse displacement of nodes on longitudinal edge and suppressed transverse movement of nodes on transverse edge results nodes on longitudinal edge not to move in transverse direction.

x=transverse, y=vertical, z=longitudinal							
Location	Translation			Rotation			Constraints
	Ux	Uy	Uz	URx	URy	URz	
Transverse Edge 1	Free	Suppressed	Free	Suppressed	Suppressed	Suppressed	Equation, Uz=common. Relative displacement between RP and edge's nodes is constant
Transverse edge 2	Free	Suppressed	Suppressed	Suppressed	Suppressed	Suppressed	
Longitudinal Edges	Free	Suppressed	Free	Suppressed	Suppressed	Suppressed	Equation, Ux=common
RP	Suppressed	Suppressed	Free	Suppressed	Suppressed	Suppressed	

TABLE 5.3 Boundary conditions considering transverse edge nodes are free to move in transverse direction and longitudinal edges nodes have common transverse displacement

x=transverse, y=vertical, z=longitudinal							
Location	Translation			Rotation			Constraints
	Ux	Uy	Uz	URx	URy	URz	
Transverse Edge 1	Suppressed	Suppressed	Free	Suppressed	Suppressed	Suppressed	Equation, Uz=common. Relative displacement between RP and edge's nodes is constant
Transverse edge 2	Suppressed	Suppressed	Suppressed	Suppressed	Suppressed	Suppressed	
Longitudinal Edges	Suppressed	Suppressed	Free	Suppressed	Suppressed	Suppressed	
RP	Suppressed	Suppressed	Free	Suppressed	Suppressed	Suppressed	

TABLE 5.4 Boundary conditions considering transverse edge and longitudinal edge nodes have zero transverse displacement

5.3 Transverse Edge Nodes are Free to move in Transverse Direction, Longitudinal Edge Nodes have Common Transverse Displacement

5.3.1 Linear Analysis

The model is imposed to pure uniaxial compression by subjecting force in longitudinal direction to the free to move RP.

Six half waves are being formed and plate buckling seems to be dominant. Deformation of the plate and stiffeners is higher at the middle and is decreasing as edges of the plate are approached. Stiffeners seem to buckle locally at the web.

The buckling load is 51,12750 MN, which is equivalent to a critical buckling stress of 326 MPa

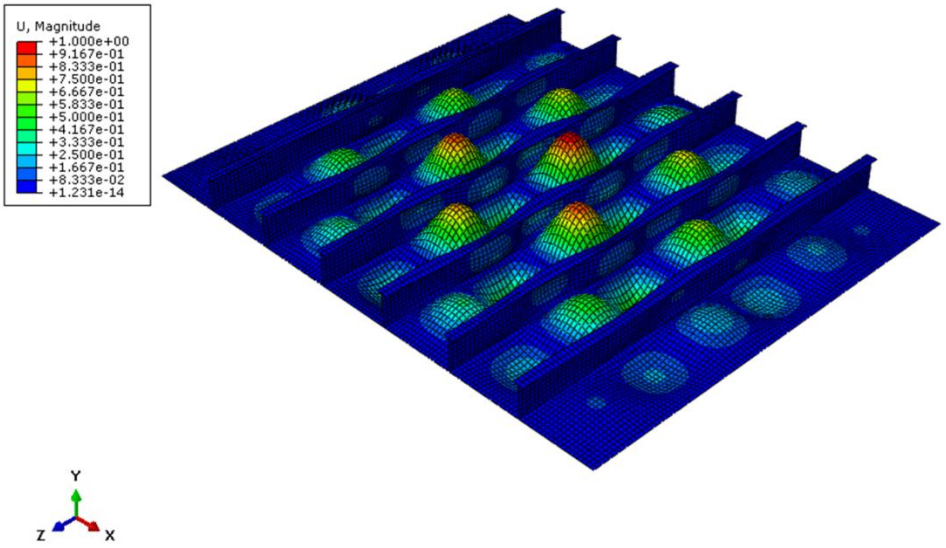

FIGURE 5.3 First buckling mode

5.3.2 Nonlinear Analysis

The aforementioned eigenmode would be utilized as initial geometrical imperfections of the model, applied with the proposed tolerance level. Since plate buckling is the dominant source of buckling, maximum amplitude of 4,55 mm (s/200) is applied.

The model is subjected to pure uniaxial compression by subjecting displacement in longitudinal axis to the free to move RP. Simulation run using Rik's Method.

As shown in FIGURE 5.4 hourglass energy is under the proposed tolerance level of 5% of internal energy.

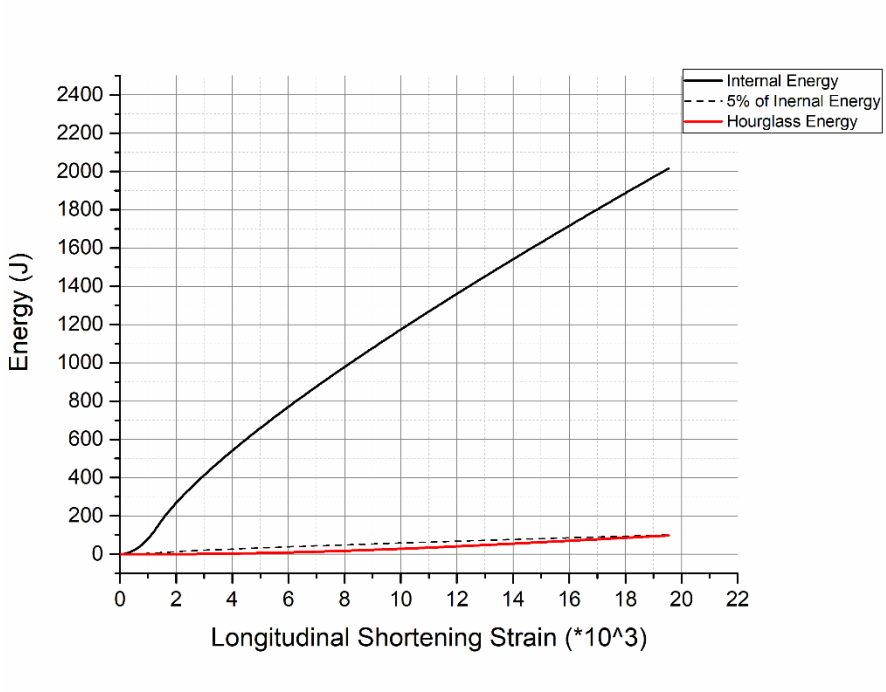

FIGURE 5.4 Internal and hourglass energy comparison

Linear Eigenvalue buckling analysis estimates a buckling load of 51,2750 MN, which is equivalent to a critical buckling stress of 326 MPa. Material yielding occurs at 315 MPa. Structure loses its stability after reaching peak value of 270 MPa for 0,00144 shortening strain. Curve reaches peak value on linear trend and drops quickly afterwards. It's reasonable that due to inserted initial imperfections value of maximum stress before instability occurs drops compared to this predicted from linear analysis.

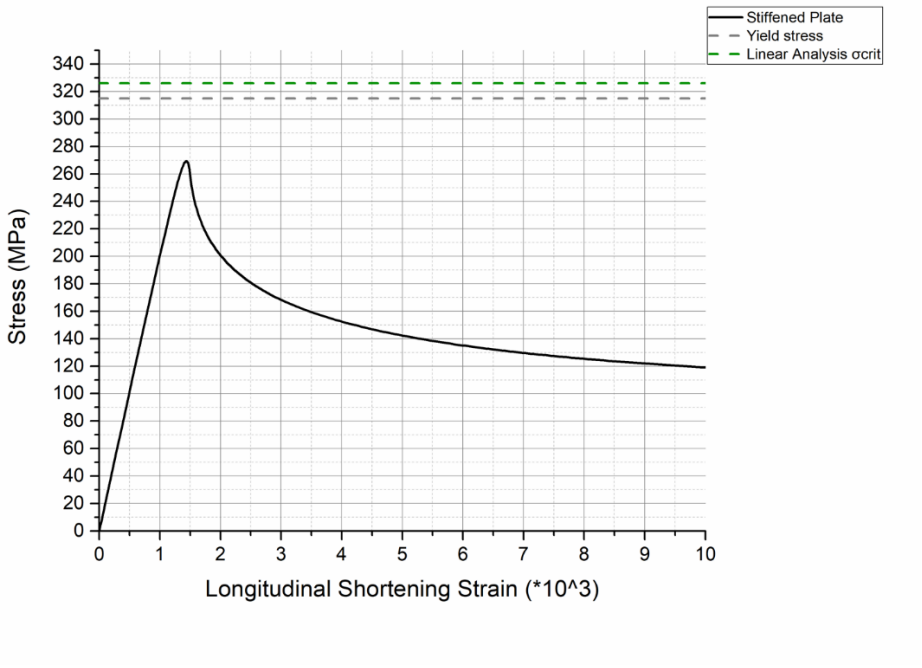

FIGURE 5.5 Stress-strain curve for stiffened plate

When structure loses stability almost the whole of the construction yields. Maximum displacements when instability occurs shows a compilation of local plate buckling with six half waves as linear eigenvalue analysis predicts and local stiffener web buckling with a slight torsion of the stiffeners locally.

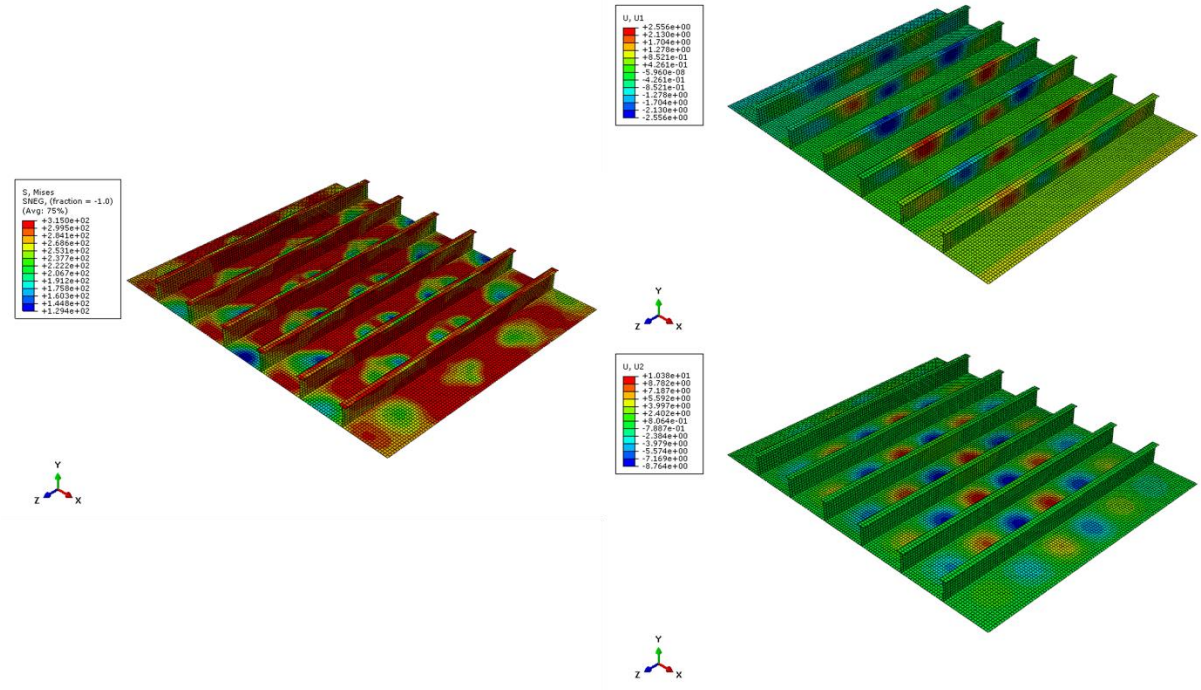

FIGURE 5.6 Von Misses stress (right), transverse displacement (top left), vertical displacement (bottom left) when buckling occurs.

It is observed that stiffened plate's elements behave similarly under the applied load. All curves in FIGURE 5.7 reach peak value for the same shortening strain, the same strain construction loses stability for. However not all element's ultimate buckling strength is the same. Elements closer to the center of the construction are more vulnerable and collapse after reaching a load value of 261 MPa. Elements closer to the longitudinal edges collapse under 277 MPa load.

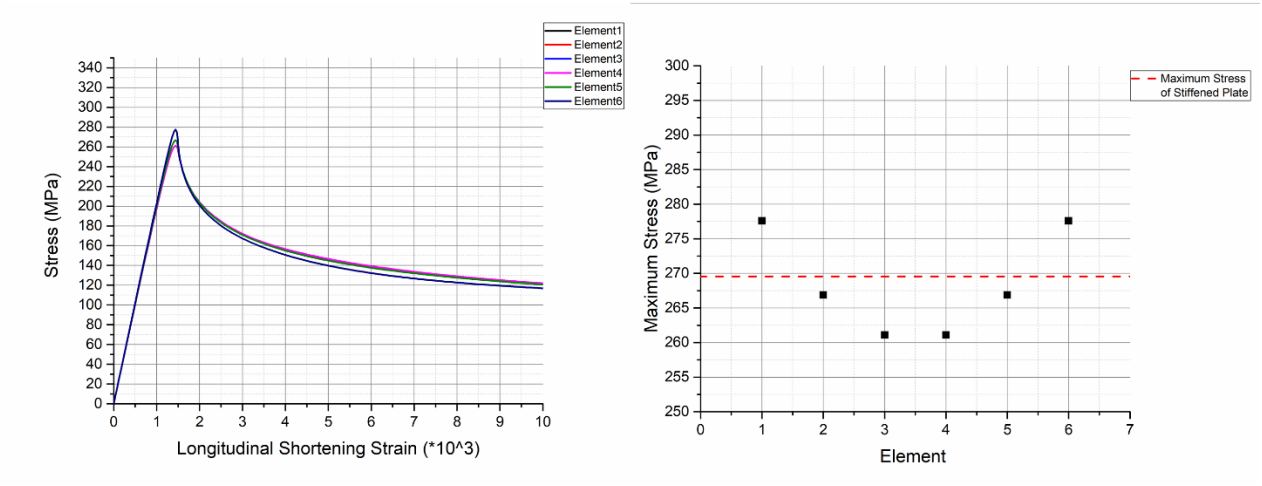

FIGURE 5.7 Stress-strain curve for each element of stiffened plate (left) and maximum stress of each element(right)

Taking advantage of symmetry, investigating first three, from right to left, stiffener's nodes displacements, accurate conclusions about the shape construction collapses under can be made. For each stiffener three paths investigated. Path 1 contains nodes on the intersection between web and flange, Path 2 contains nodes on the intersection between web and plate and Path 3 contains nodes on the long axis of the web.

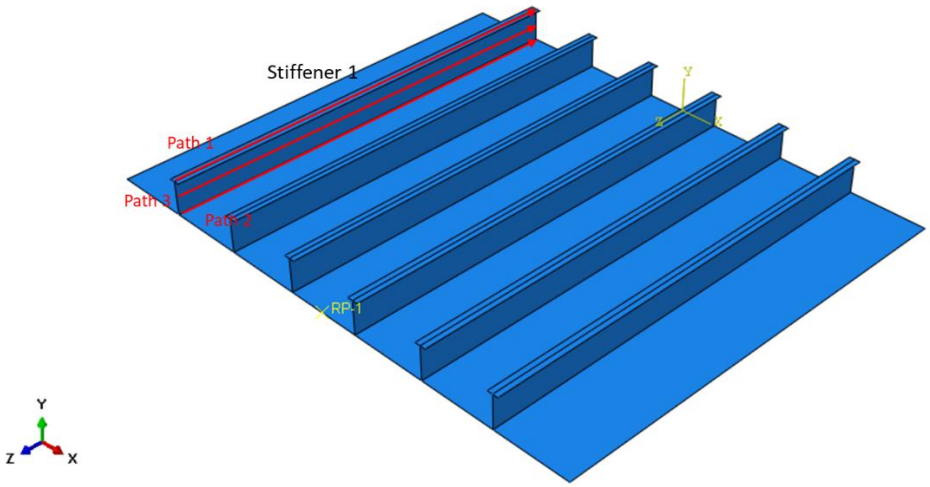

FIGURE 5.8 Paths on stiffeners

Deflection follows the same pattern in all stiffeners (FIGURE 5.9). Vertical displacement of nodes on Path 1 is greater than this of nodes on Path 2 in all three stiffeners. Deflection of nodes on Path 3 is greater than this of nodes on Path 1. Peaks and troughs of Displacement-Distance along Path curves are reached for almost the same distance for Path 1 and Path 3. Considering those it can be conclude that when construction collapses stiffeners webs

buckle locally but at the same time contributes to the local torsion of the stiffener. Amplitude of deflection gets lower approaching stiffened plates longitudinal edges.

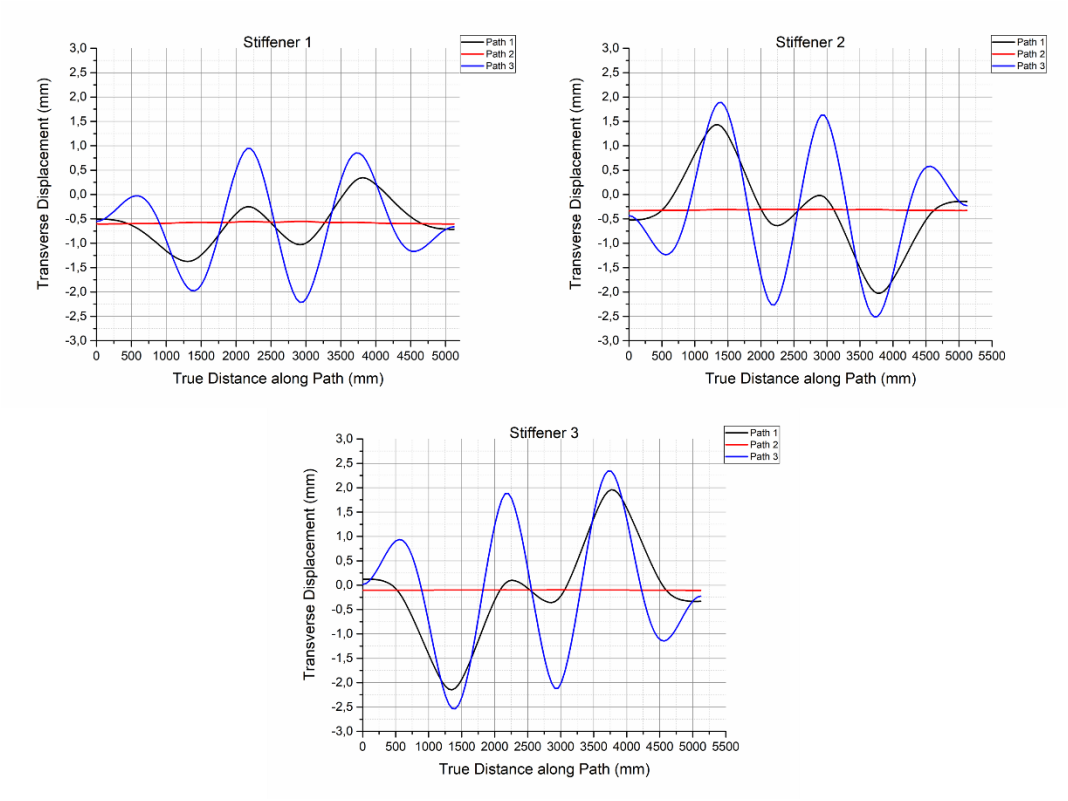

FIGURE 5.9 Transverse displacement on stiffeners' paths when structure collapses

Again, taking advantage of symmetry and investigating vertical displacement of nodes on paths between stiffeners, conclusions about the shape of plate when structure collapses can be made.

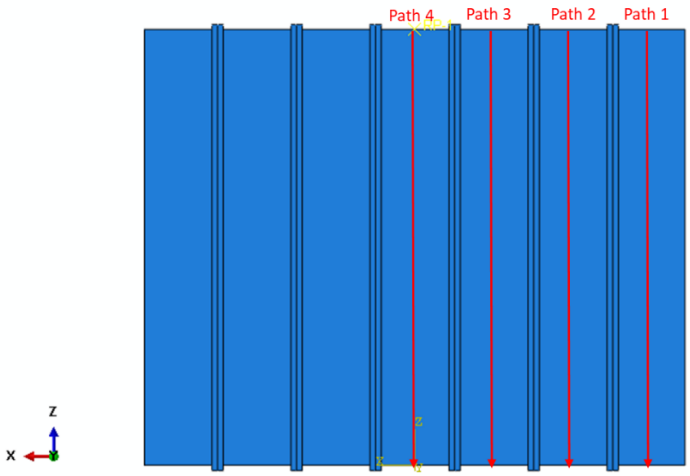

FIGURE 5.10 Paths on plate between stiffeners

When structure collapses, plate between stiffeners loses its stability and buckles locally. As linear eigenvalue buckling analysis estimates six halfwaves are formed. Amplitude of halfwaves gets higher closer to the center of the Stiffened Plate. Plate's deformation is significantly higher that this of stiffeners.

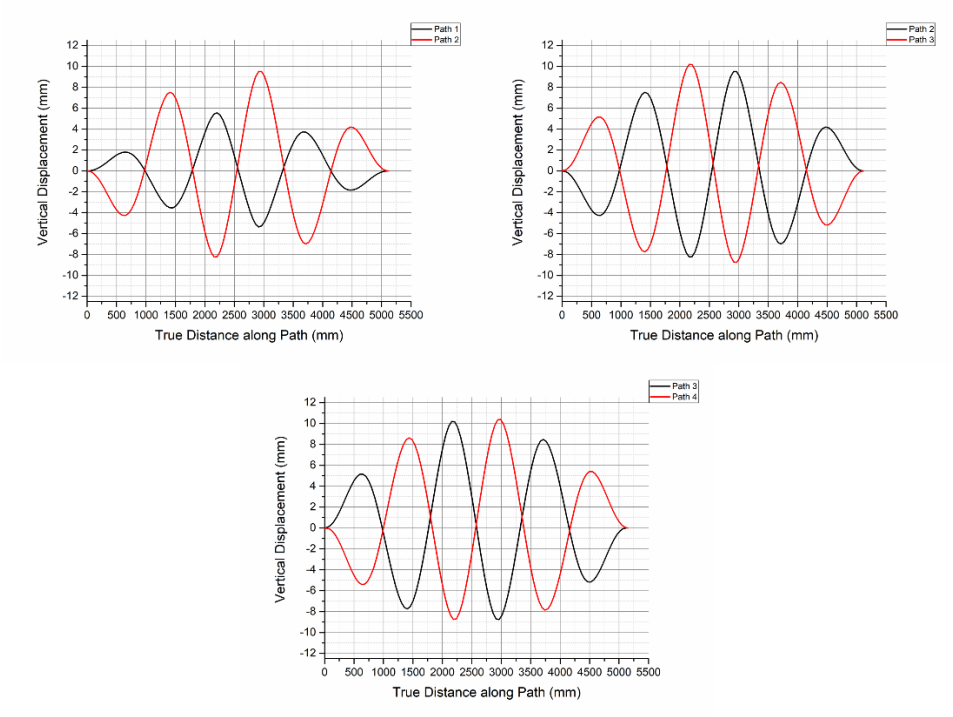

FIGURE 5.11 Vertical displacement on paths between stiffeners when structure collapses

The key to approach the conditions each element of the stiffened plate encounters on its longitudinal edges, is the relative transverse displacement between stiffener and element's longitudinal edges. Stiffener transverse displacement is measured through Path 2 of FIGURE 5.8 and elements' boundaries are the paths showed in FIGURE 5.10. As shown in FIGURE 5.12 and FIGURE 5.13, each of the construction's elements experience same pattern conditions on its longitudinal boundaries. Nodes of each longitudinal edge of each element move almost together in transverse direction, moving away from the stiffener. Post-buckling the distance between stiffener and longitudinal edges of each elements reduces. After the collapse of construction, halfwaves formed locally on the stiffener's web, spread and their amplitude gets higher affecting the intersection between stiffener's web and plating. Hence, it is observed that for nodes on the intersection with the same longitudinal coordinate as the web's halfwaves, relative transverse displacement with longitudinal edges increases or decreases rapidly.

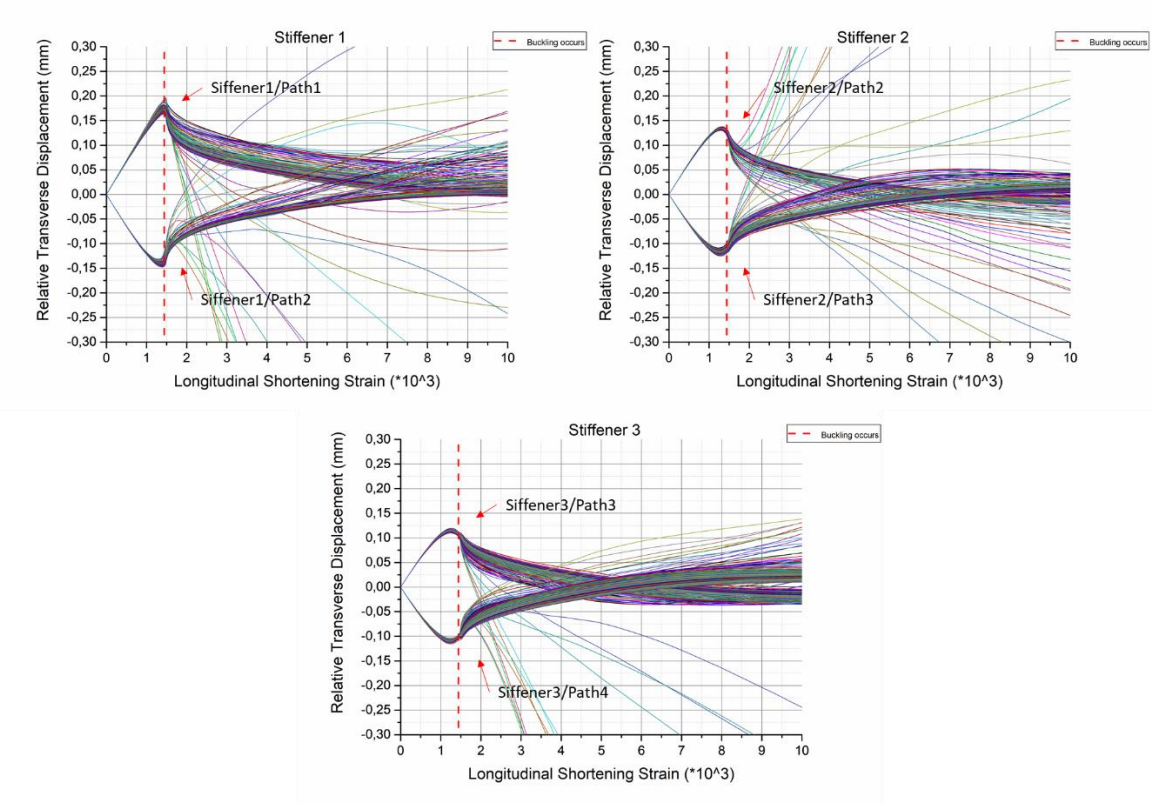

FIGURE 5.12 Relative transverse displacement of stiffeners and neighboring paths (each node separately)

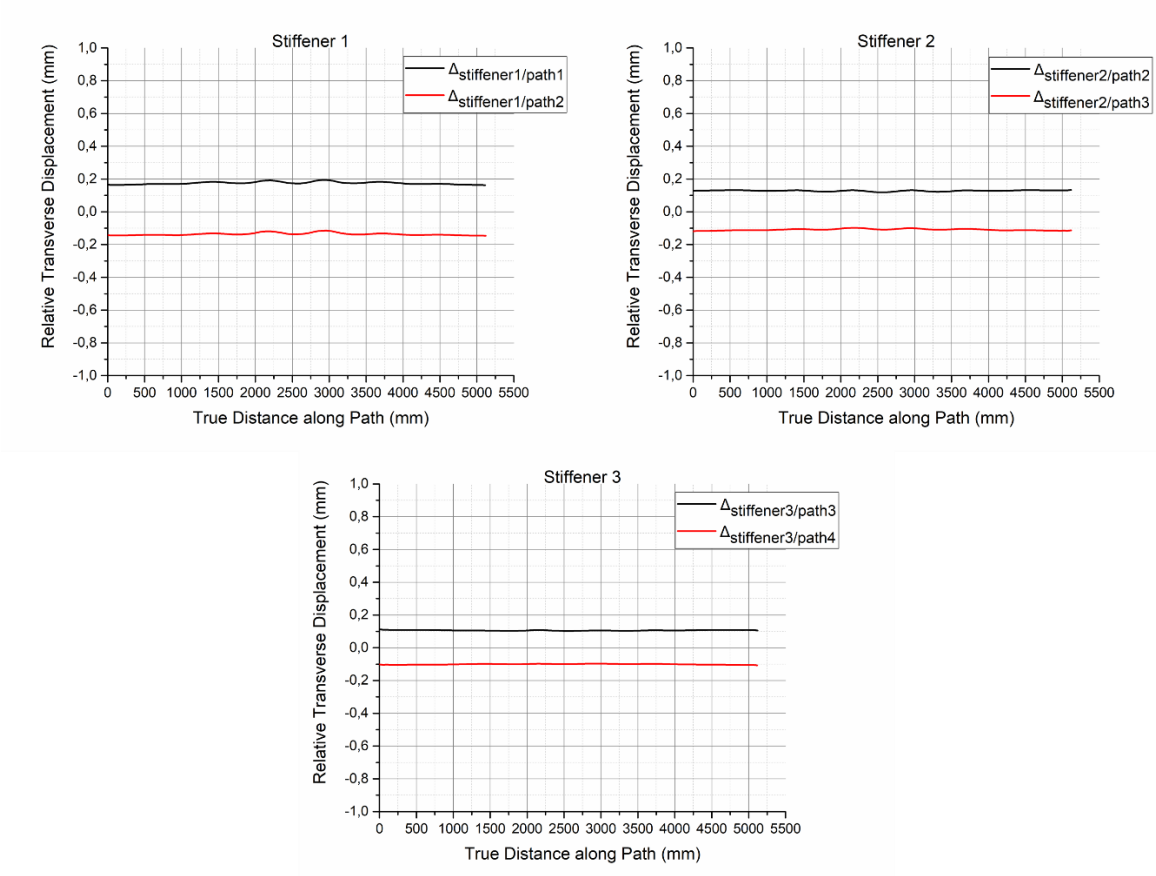

FIGURE 5.13 Relative transverse displacement of stiffeners and neighboring paths when structure collapses

5.4 Transverse Edge and Longitudinal Edge Nodes have Zero Transverse Displacement

5.4.1 Linear Analysis

The model is subjected to pure uniaxial compression by subjecting force through longitudinal axis to the free to move RP.

Plate between stiffeners buckles overall. Deformation of stiffeners and plate is equivalent significant. Critical part is considered in the middle where deformation of both stiffeners and plate are higher than closer to the edge of stiffened plate

The buckling load is 36,4867 MN, which is equivalent to a critical buckling stress of 233 MPa

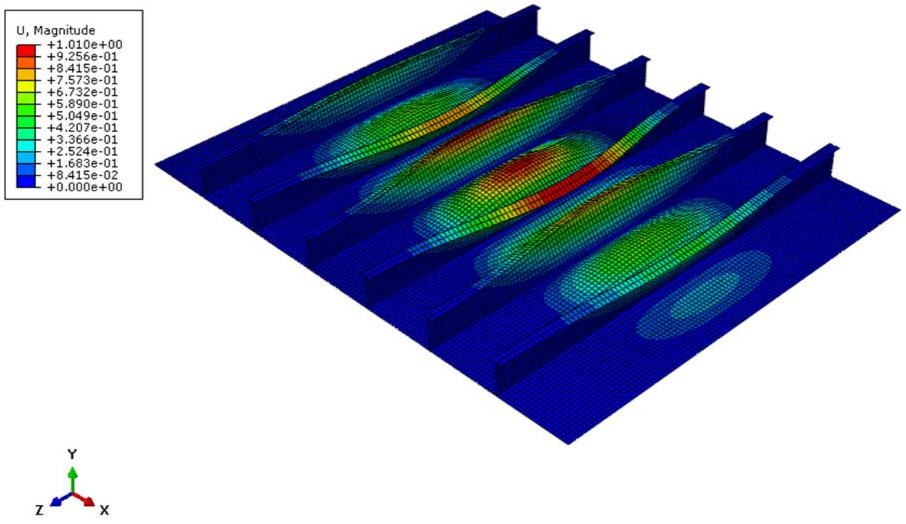

FIGURE 5.14 First buckling mode

5.4.2 Nonlinear Analysis

The aforementioned eigenmode would be utilized as initial geometrical imperfections of the model, applied with the proposed tolerance level. Since stiffeners deformation is slightly higher than this of plate, maximum amplitude of 5,12 mm (L/200) is applied.

The model is imposed to pure uniaxial compression by subjecting displacement in longitudinal axis to the free to move RP. Simulation run using Rik's Method.

As shown in FIGURE 5.15 hourglass energy is under the proposed tolerance level of 5% of internal energy.

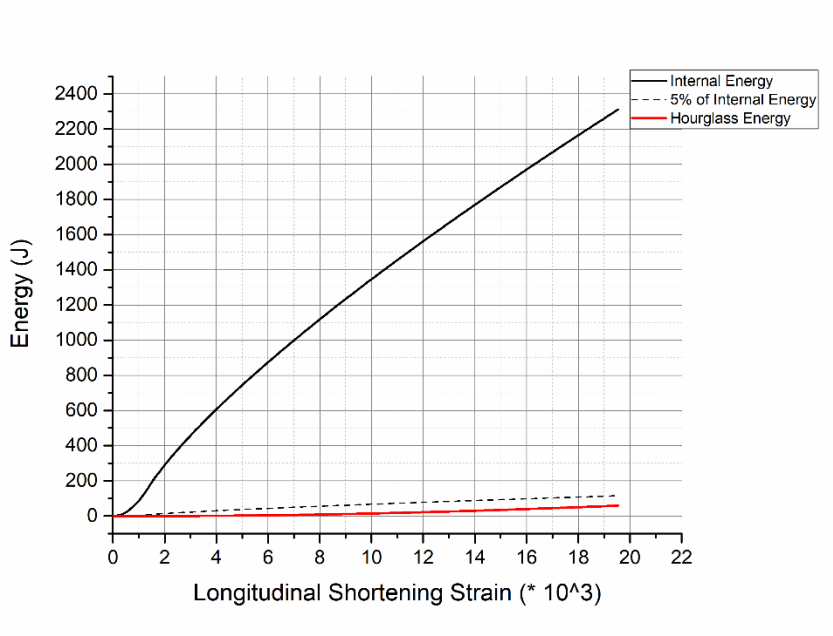

FIGURE 5.15 Internal and hourglass energy comparison

Linear Eigenvalue buckling analysis estimates a buckling load of 36,4867 MN, which is equivalent to a critical buckling stress of 233 MPa. Material yielding occurs at 315 MPa. Structure loses its stability after reaching peak value of 282 MPa for 0,00139 shortening strain. It must be noted that maximum load before structure collapses is higher than this estimated from linear buckling analysis. Considering that inserting initial imperfections should lead to reduced strength of the construction, this behavior must be explained.

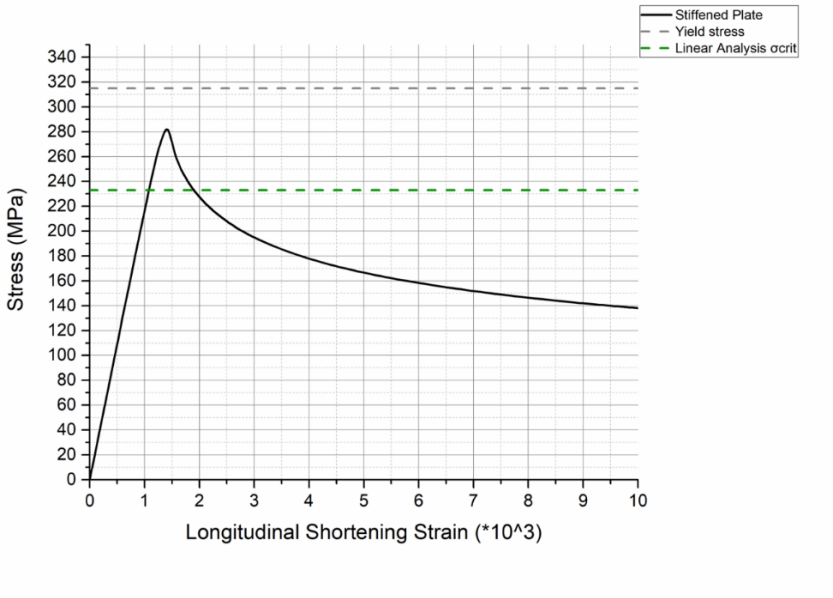

FIGURE 5.16 Stress-strain curve for Stiffened Plate

When structure loses stability almost the whole of the construction yields. Maximum displacements when instability occurs shows a compilation of stiffener tripping with a slight local buckling of the webs near the longitudinal ends of the stiffeners. Stiffeners' deformation seems to maximize in the middle of each stiffener and gets more significant approaching the middle of the construction. Buckling mode of plating between stiffeners differs from this predicted from linear eigenvalue analysis. According to linear analysis plating is expected to buckle overall, however it seems to buckle forming five halfwaves.

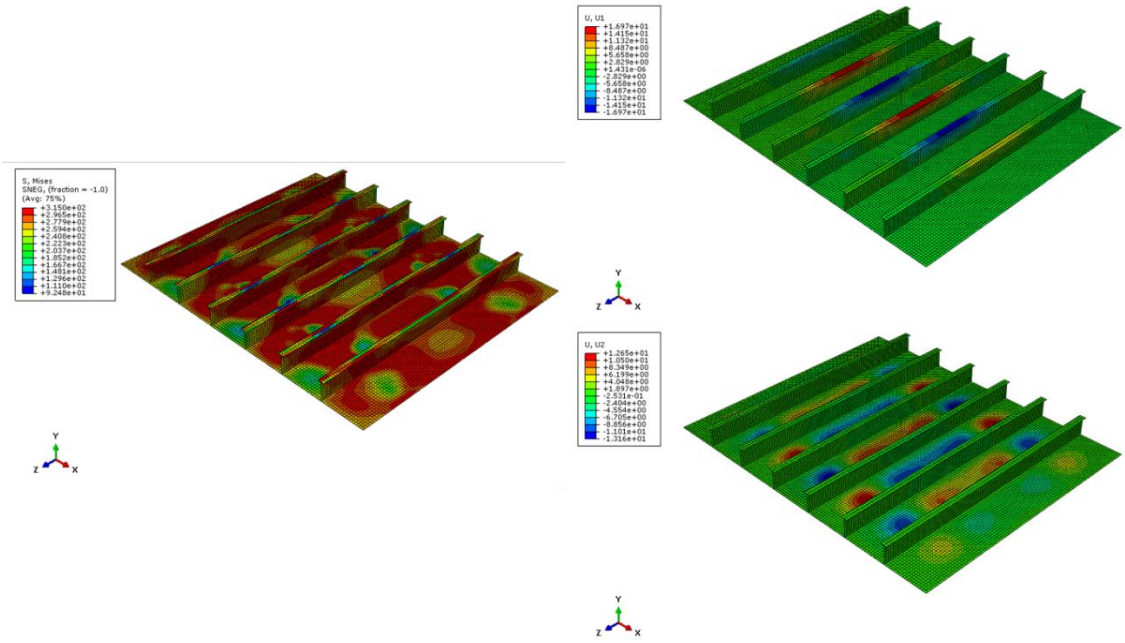

FIGURE 5.17 Von Misses stress (right), transverse displacement (top left), vertical displacement (bottom left) when buckling occurs.

Stiffened Plate's elements behave similarly under the applied load. All curves reach peak value for the same shortening strain, the same strain construction loses stability for. However not all element's ultimate buckling strength is the same. Elements closer to the center of the construction are more vulnerable and collapse after reaching a load value of 276 MPa. Elements closer to the longitudinal edges collapse under 289 MPa load.

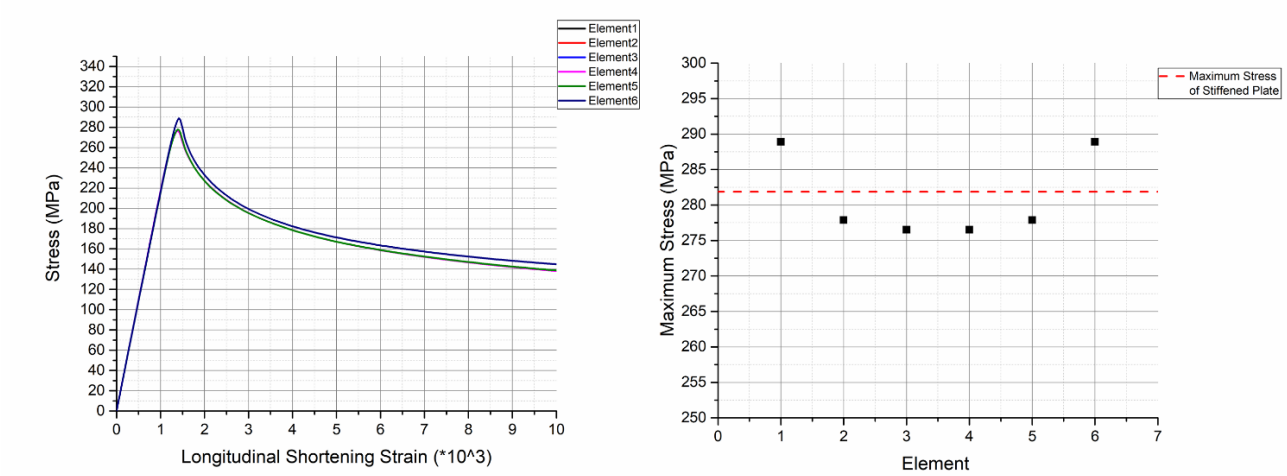

FIGURE 5.18 Stress-strain curve for each element of stiffened plate (left) and maximum stress of each element(right)

Taking advantage of symmetry, investigating first three, from right to left, stiffener's nodes displacements, accurate conclusions about the shape construction collapses under can be made. For each stiffener three paths investigated. Path 1 which contains nodes on the intersection between web and flange, Path 2 wick contains nodes on the intersection between web and plate and Path 3, which contains nodes on the long axis of the web.

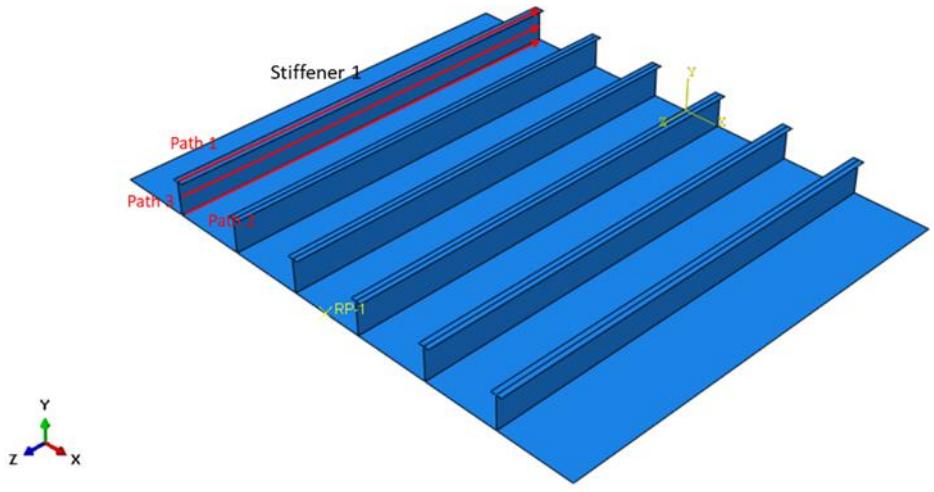

FIGURE 5.19 Paths on stiffeners

Deflection follows the same pattern in all stiffeners. Close to the ends of the stiffeners, transverse displacement of nodes on Path 3 is higher than this of nodes on Path 1 and path 2, there stiffener's web buckles locally which also contributes to local torsion of the stiffener. Approaching middle of stiffener translation of nodes on Path 1 is higher than this of nodes on Path 2 and Path 3, so it can be concluded that in this position stiffener is

governed by tripping. It must be noted that this is not the expected collapse mode of stiffeners according to linear buckling eigenmode analysis.

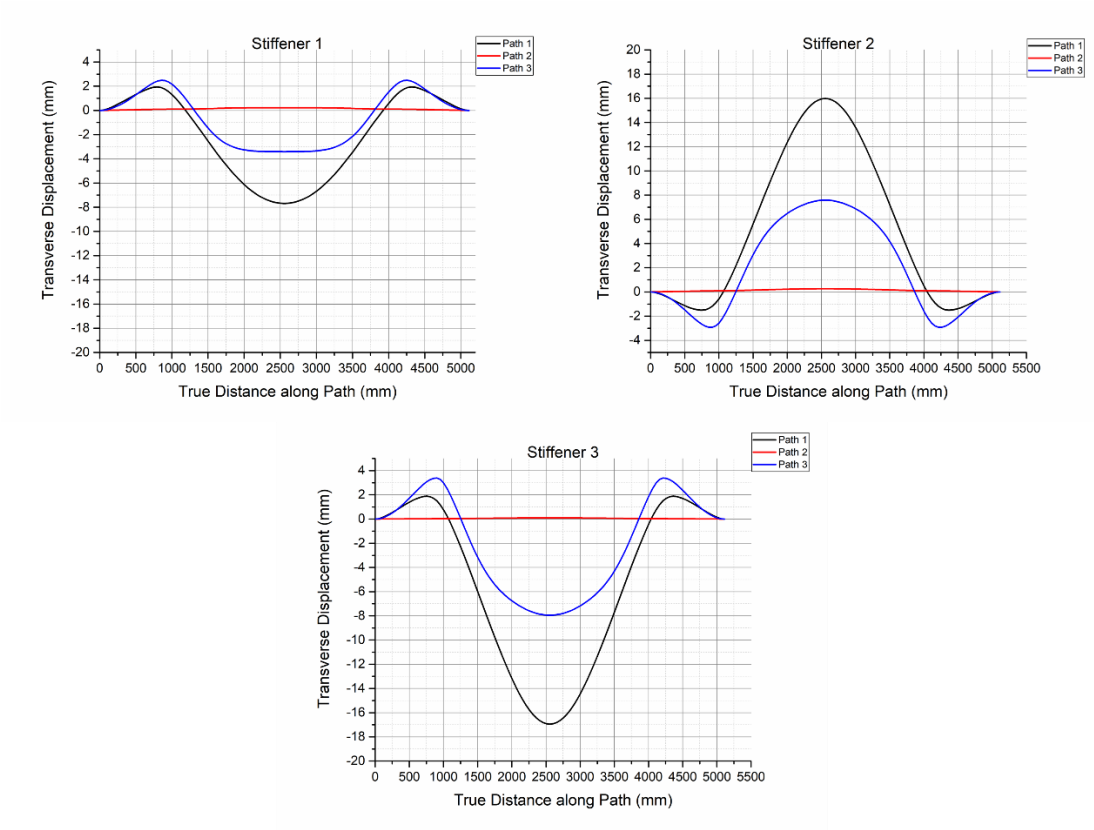

FIGURE 5.20 Transverse displacement on stiffeners' paths when structure collapses

Again, taking advantage of symmetry and investigating vertical displacement of nodes on paths between stiffeners, conclusions about the shape of plate when structure collapses can be made.

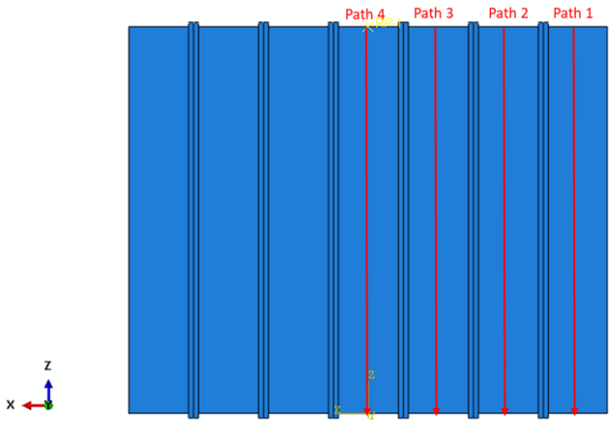

FIGURE 5.21 Vertical displacement on paths between stiffeners when structure collapses

According to linear buckling eigenmode analysis, when structure reaches its maximum buckling capacity plate between stiffeners is expected to buckle overall. However, this is not the actual response of the plate. Plate collapses forming five halfwaves. For each plate separately, deformation is higher close to the longitudinal ends.

Collapse mode of both the plate and the stiffeners differs from this predicted from linear buckling eigenmode analysis. This different mode shape seems that can carry further load than this predicted from linear analysis

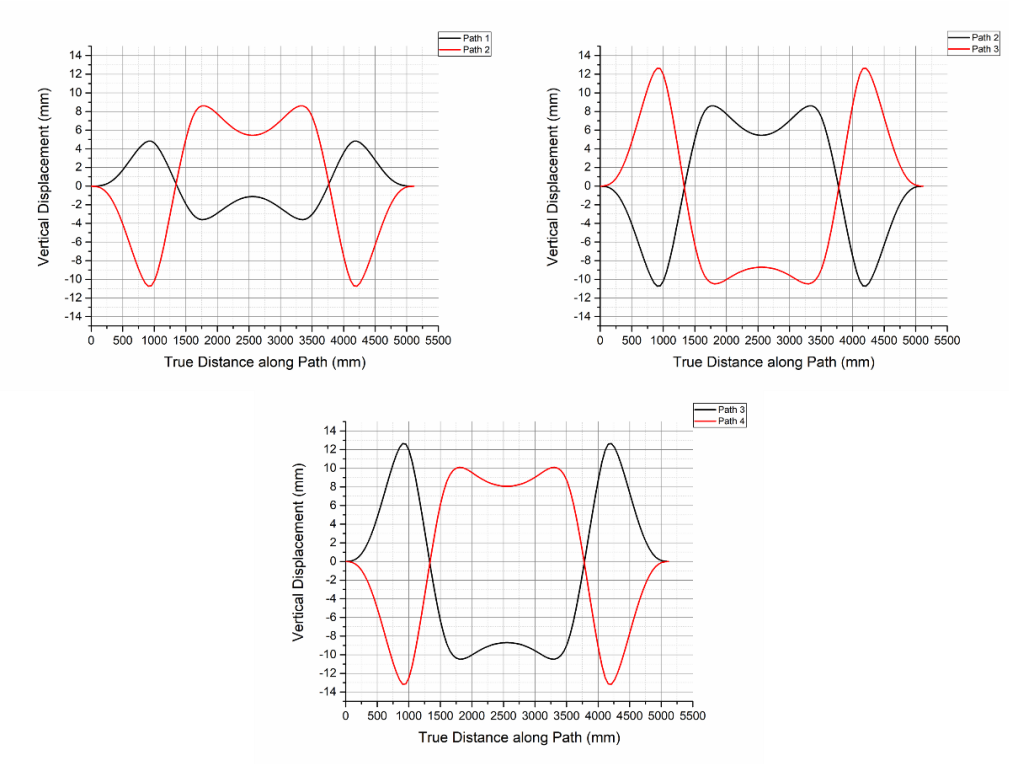

FIGURE 5.22 Vertical displacement on paths between stiffeners when structure collapses

As a plate is axially compressed tends to deform transversely too. However, boundary conditions force nodes on the longitudinal edges of the stiffened plate to not move in transverse direction. Hence, a force is acting on the nodes of longitudinal edge nodes preventing them from translating transversely (FIGURE 5.23). A loading condition equivalent to biaxial compression is generated. Ratio of load acting on transverse and longitudinal edges is not constant as plate shortens longitudinally (FIGURE 5.24). Different ratio of loads acting on edges, leads to different collapse modes. As shown in FIGURE 5.25, a stiffened plate subjected to biaxial load with $\sigma_z/\sigma_x=6$ is expected to collapse under a collapse mode of overall plate buckling for the plate between stiffeners and stiffener tripping. For a load ratio $\sigma_z/\sigma_x=8,5$ the collapse mode is expected to be local plate buckling and local web buckling. As the stiffened plate studied in this chapter shortens, experiences different load ratios, therefore a collapse mode affected by all different load ratios is formed. This could explain that nonlinear predicts higher buckling capacity and different collapse mode than this expected from linear analysis.

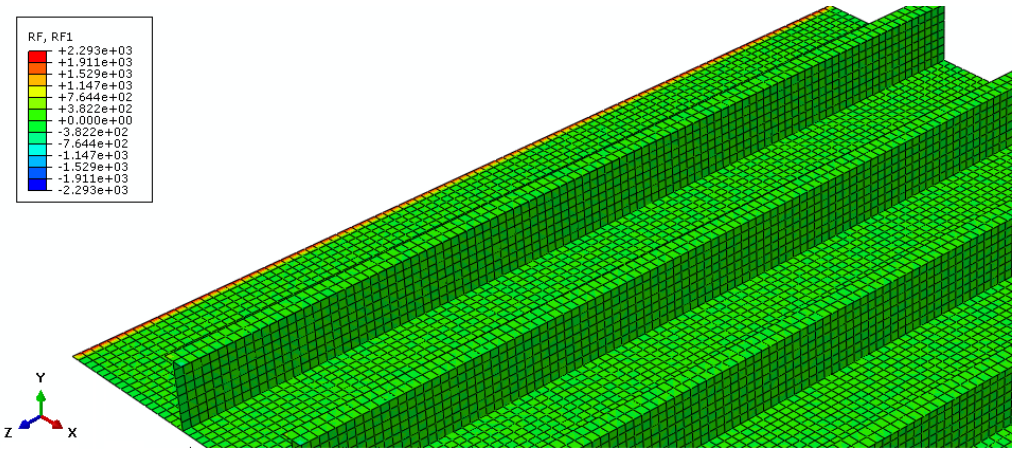

FIGURE 5.23 Reaction force on longitudinal edge of the stiffened plate

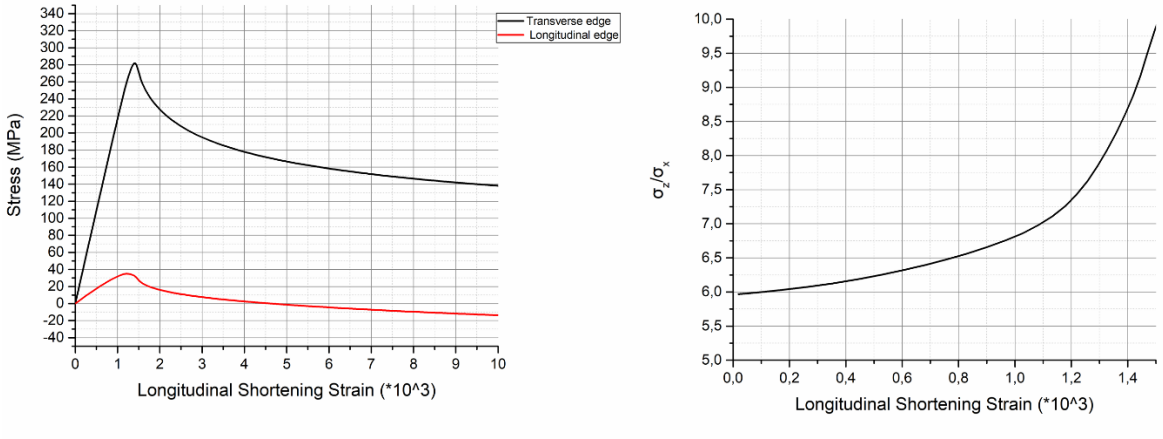

FIGURE 5.24 Stresses acting on stiffened plate's edges(left) and ratio of stresses(right)

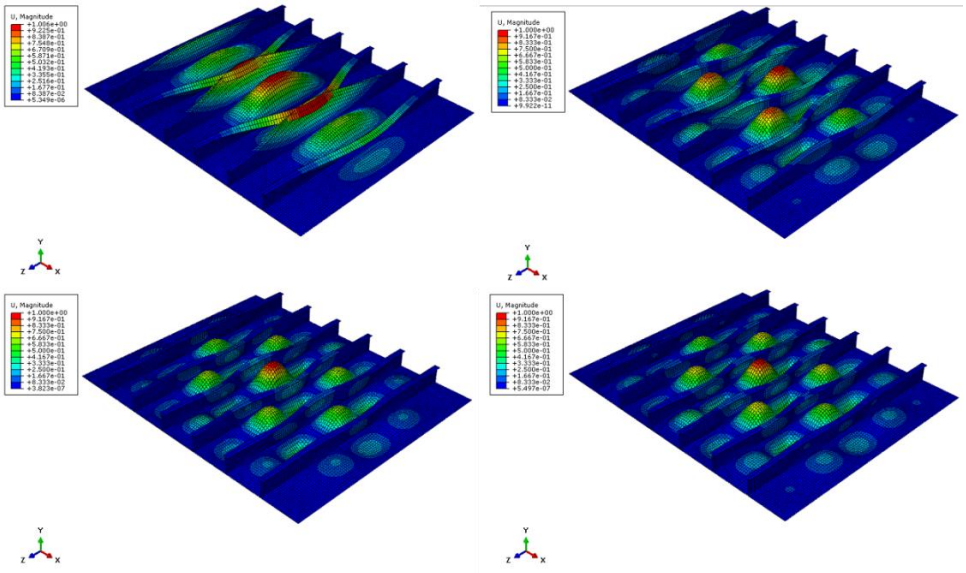

FIGURE 5.25 First eigenmode for biaxial compression σ_z/σ_x=6 (top left), σ_z/σ_x=6,5 (top right), σ_z/σ_x=7,5 (bottom left), σ_z/σ_x=8,5 (bottom right),

Transverse displacement of Path 2 in FIGURE 5.19 defines transverse displacement of stiffener. Paths in FIGURE 5.21 coincide with the stiffened plate's elements longitudinal edges. Relative transverse displacement of an element's stiffener and elements longitudinal edges, defines the transverse displacement the longitudinal edges of an isolated stiffened plate's element experience. As shown in FIGURE 5.26, 5.27 each of the construction's elements experience equivalent conditions on its longitudinal boundaries. Nodes of each longitudinal edge of each element barely move in transverse direction. Since displacement values are quite low could be considered insignificant. When structure collapses stiffeners are tripping in the middle and web buckles locally near the ends of the stiffeners. Post-buckling halfwaves formed on the stiffener's webs spread, affecting the intersection between web and plating. As a result, post-buckling, relative transverse displacement of nodes near the aforementioned halfwaves and nodes on the element's longitudinal boundaries increases or decreases rapidly.

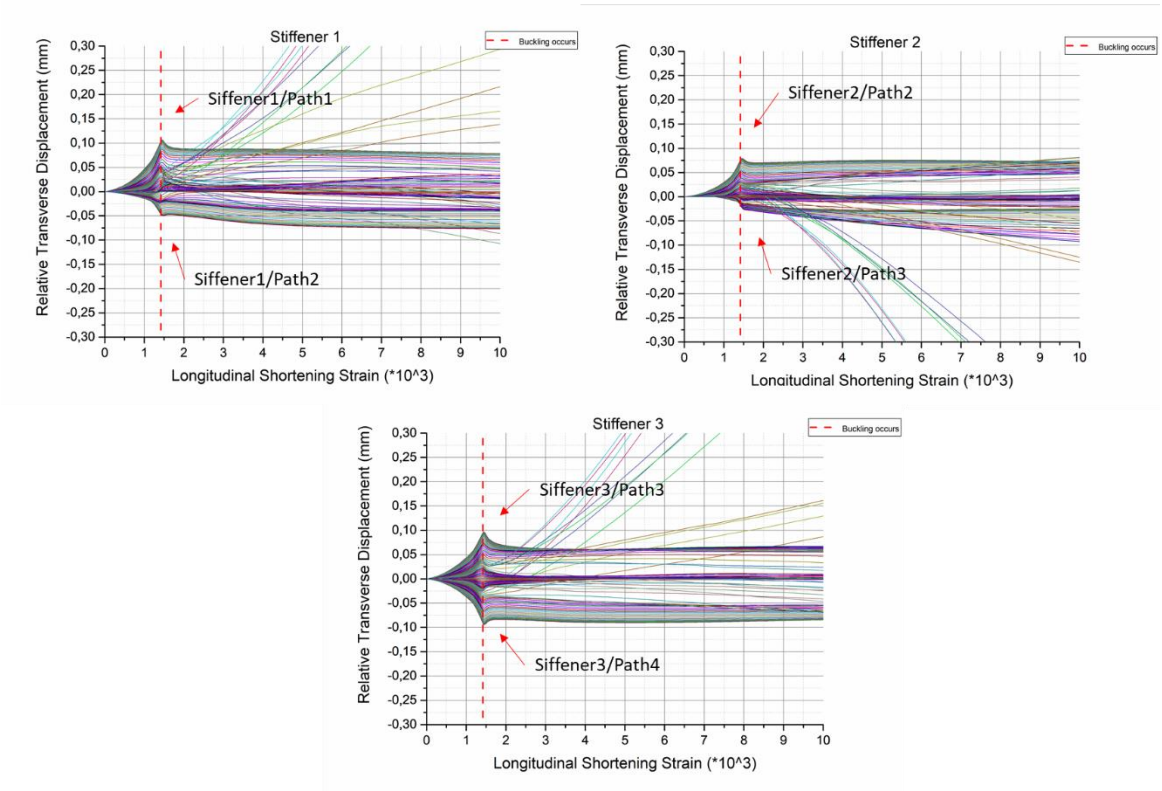

FIGURE 5.26 Relative transverse displacement stiffeners and neighboring paths (each node separately)

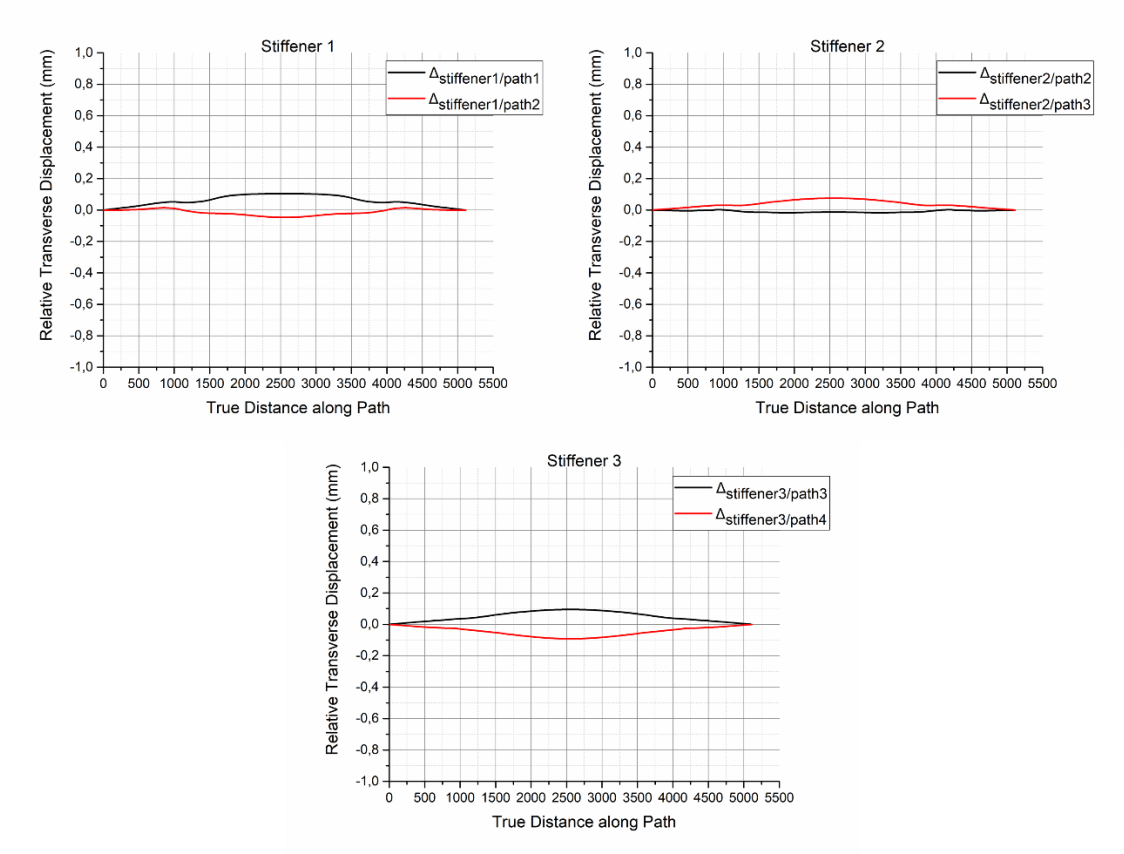

FIGURE 5.27 Relative transverse displacement of stiffeners and neighboring paths when structure collapses

6 Isolated Stiffened Plate's Element Model

This chapter aims to investigate the behavior (collapse mode, ultimate strength) of an isolated stiffened plate's element under compressive loads. Observing how the isolated element responds under compressive loads and comparing its behavior with this of a stiffened plate, it could be evaluated whether a plate could be studied analyzing just one of its elements (stiffener and attached plating). Realistic boundary conditions approached using conclusions extracted from chapter 5. For the study, models with both shell and cubic elements used. Hence, it is possible to compare the performance of shell and cubic elements

.

6.1 Model Geometry, Mesh, and Material Properties

Model geometry

Two identical models of a stiffened plate's elements created, one considering element's components (flange, web, effective width of plate) are homogeneous shells and one considering them homogeneous solids.

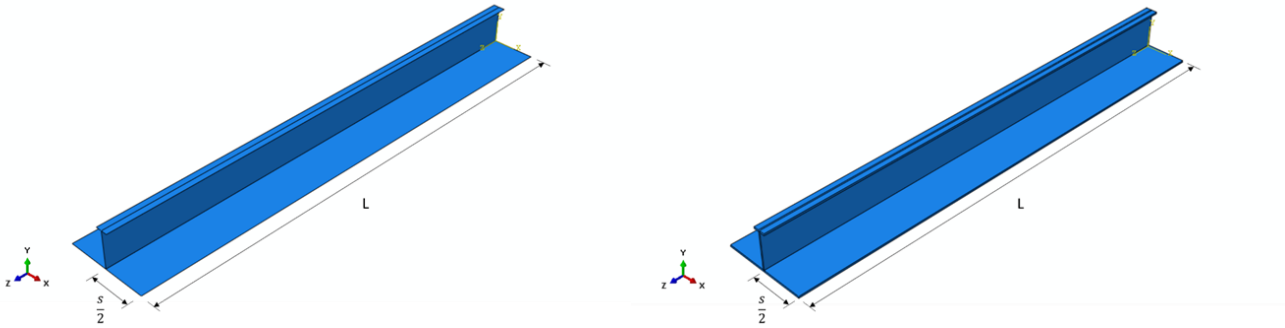

FIGURE 6.1 Shell model (left) and solid model(right)

Element geometry	
s (mm)	910
L (mm)	5120
t_p (mm)	17,5
h_w (mm)	400
t_w (mm)	13
b_f (mm)	130
t_f (mm)	18

TABLE 6.1 Element geometry

Mesh

Homogenous shell model was discretized by S4R type elements of 50 mm size. Homogeneous solid model was discretized by C3D8R type elements of 20 mm length, 20 mm width and 4 mm height. On the intersection between web and flange/plate elements of 20 mm length, 4 mm width and 4 mm height used. Finally, on web elements of 20 mm length, 4 mm width and 20 mm height used.

For the shell elements a mesh convergence study occurred, as shown in FIGURE 6.3. On the other hand, size of solid elements procced from limitations due to computational cost and needs for an accurate analysis. The number of elements should be the lowest possible and at the same time shells composing the element should discretized using at least 4 to 5 finite elements across the thickness. Additionally, the ratio of smallest to largest element's dimension should keep low. Considering all of the above the aforementioned proposed size for the mesh used.

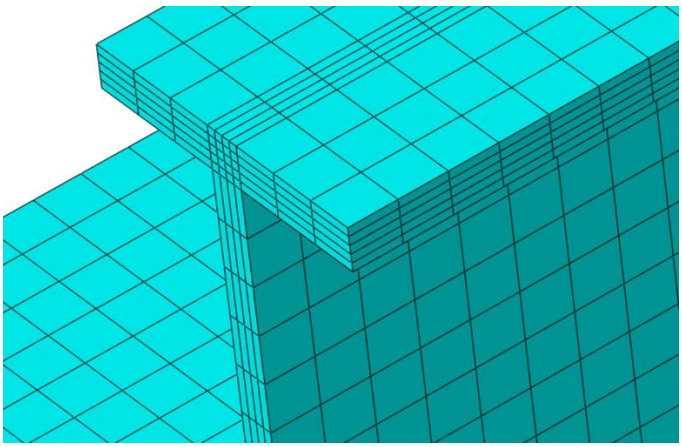

FIGURE 6.2 Discretized solid model using cubic elements

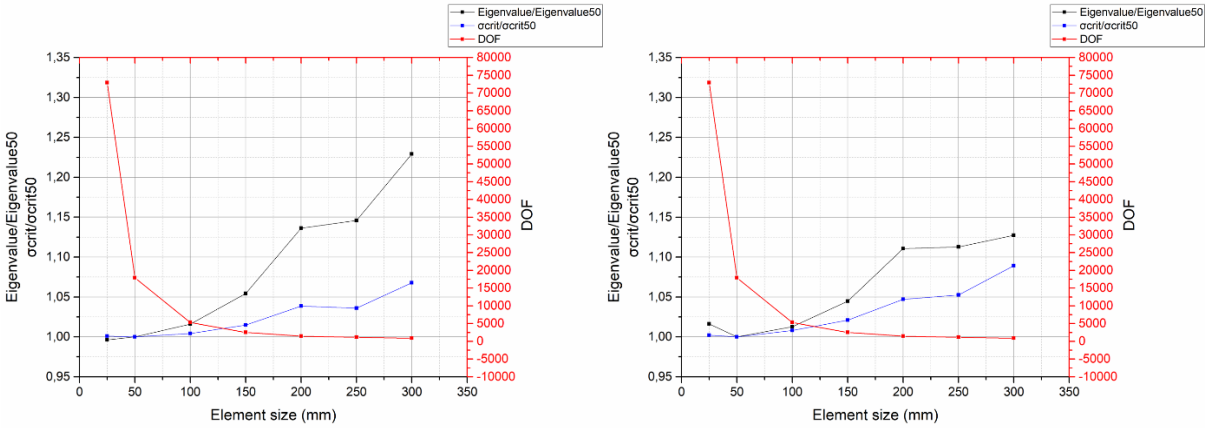

FIGURE 6.3 Mesh convergence study, transverse edge nodes are free to move in transverse direction and longitudinal edges nodes have common transverse displacement (left) transverse edge and longitudinal edge nodes have zero transverse displacement (right)

Material properties

Material used is AH32. AH32 steel is a structural high tensile strength marine steel mainly used for making the hull of ship building and ship repairing, offshore oil drilling platforms, the platform pipe joints and other components. It is an isotropic material that has Young's modulus/modulus of elasticity (E) of 206 GPa, Poisson's ratio (v) of 0.3 and Yield strength (σ_y) of 315 MPa.

AH32 steel	
Young's modulus E (GPa)	206
Poisson's ratio v	0.3
Yield strength σ_y (MPa)	315

TABLE 6.2 Material properties of stiffened plate's element

6.2 Boundary Conditions

One transverse edge should be free to move in longitudinal direction imposing to compressive axial stress. Thence an equation has been set between plate's and stiffeners' edge nodes and a reference point. Keeping the relative displacement between reference point and edge nodes constant any load acting on the reference point is forcing edge nodes to move as rigid body in axial direction. Both the plate and the stiffeners shall not translate in any plane, also vertical displacement should be suppressed. As on previous models, regarding transverse movement of edge nodes, two cases shall be examined one considering free movement and one considering nodes don't move in transverse direction.

On the opposite transverse side, model shall comply with the same boundary conditions, with an additional restriction in longitudinal direction to resist force acting on loaded edge.

Concerning longitudinal edges, rotations around vertical and longitudinal axis shall be suppressed. As concluded on previous analysis (Chapter 5), assuming free transverse movement of nodes on transverse edge results in common transverse displacement of nodes on longitudinal edge and suppressed transverse movement of nodes on transverse edge results nodes on longitudinal edge not to move in transverse direction.

x=transverse, y=vertical, z=longitudinal							
Location	Translation			Rotation			Constraints
	Ux	Uy	Uz	URx	URy	URz	
Transverse Edge 1	Free	Suppressed	Free	Suppressed	Suppressed	Suppressed	Equation, Uz=common. Relative displacement between RP and edge's nodes is constant
Transverse edge 2	Free	Suppressed	Suppressed	Suppressed	Suppressed	Suppressed	
Longitudinal Edges	Free	Free	Free	Free	Suppressed	Suppressed	Equation, Ux=common
RP	Suppressed	Suppressed	Free	Suppressed	Suppressed	Suppressed	

TABLE 6.3 Boundary conditions considering transverse edge nodes are free to move in transverse direction and longitudinal edges nodes have common transverse displacement

x=transverse, y=vertical, z=longitudinal							
Location	Translation			Rotation			Constraints
	Ux	Uy	Uz	URx	URy	URz	
Transverse Edge 1	Suppressed	Suppressed	Free	Suppressed	Suppressed	Suppressed	Equation, Uz=common. Relative displacement between RP and edge's nodes is constant
Transverse edge 2	Suppressed	Suppressed	Suppressed	Suppressed	Suppressed	Suppressed	
Longitudinal Edges	Suppressed	Free	Free	Free	Suppressed	Suppressed	
RP	Suppressed	Suppressed	Free	Suppressed	Suppressed	Suppressed	

TABLE 6.4 Boundary conditions considering transverse edge and longitudinal edge nodes have zero transverse displacement

6.3 Transverse Edge Nodes are Free to move in Transverse Direction, Longitudinal Edge Nodes have Common Transverse Displacement

6.3.1 Linear Analysis

Both shell elements and cubic elements models are imposed to pure uniaxial compression by subjecting force in longitudinal direction to the free to move RP.

For both shell and cubic element models six half waves are being formed and plate buckling seems to be dominant. Deformation of the plate and stiffeners is higher at the middle and is decreasing as edges of the plate are approached. Stiffeners seem to buckle locally at the web.

The buckling load is 7,49975 MN, which is equivalent to a critical buckling stress of 320 MPa for shell model and 7,53567 MN or 321 MPa for solid model.

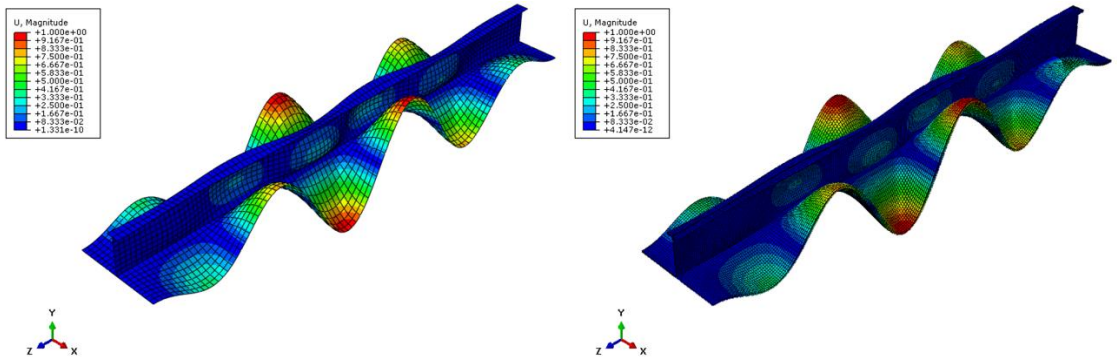

FIGURE 6.4 First buckling mode for shell (left) and solid (right) model

6.3.2 Nonlinear Analysis

Each of the aforementioned eigenmodes would be utilized as initial geometrical imperfections to the counterpart model, applied with the proposed tolerance level. Since plate buckling is the dominant source of buckling, maximum amplitude of 4,55 mm (s/200) is applied.

Each model is imposed to pure uniaxial compression by subjecting displacement in longitudinal axis to the free to move RP. Simulation run using Rik's Method.

As shown in FIGURE 6.5 and FIGURE 6.6 Hourglass Energy is under 5% of Internal Energy for shell elements model. When it comes to solid elements model, Hourglass Energy remains under 5% of Internal Energy for Longitudinal Shortening Strain of the stiffened plate's element of 0,005 and for strain up to 0,012 Hourglass Energy values range between 5% and

10% of Internal Energy. In solid elements model Hourglass Energy is higher than this of shell elements model, which is expected to result a stiffer behavior for solid element model.

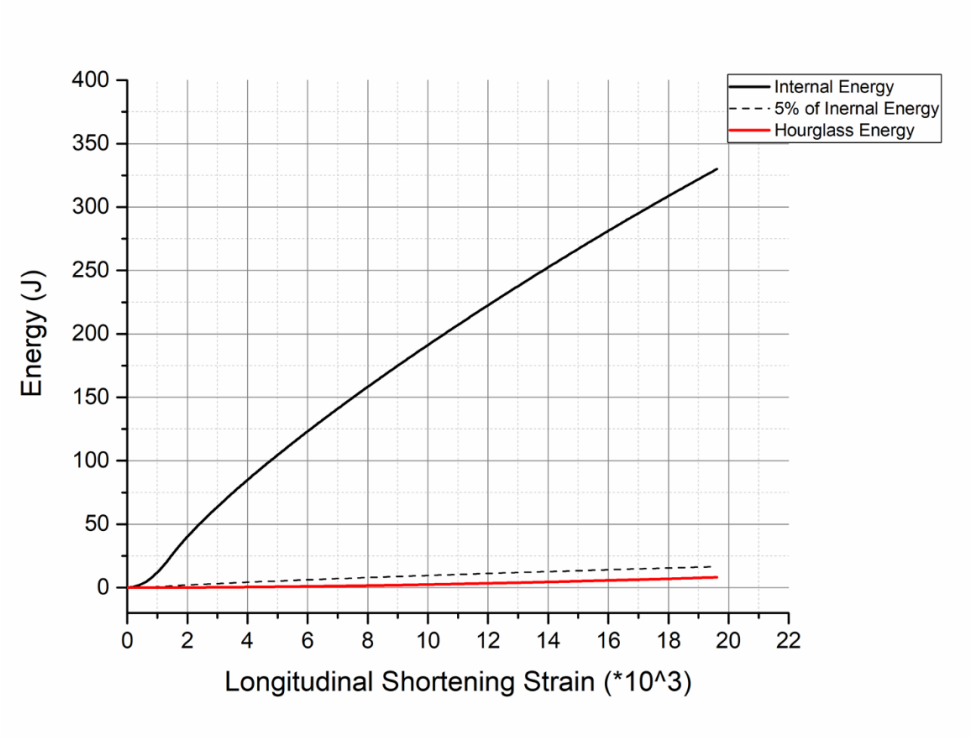

FIGURE 6.5 Internal and hourglass energy comparison for shell elements model

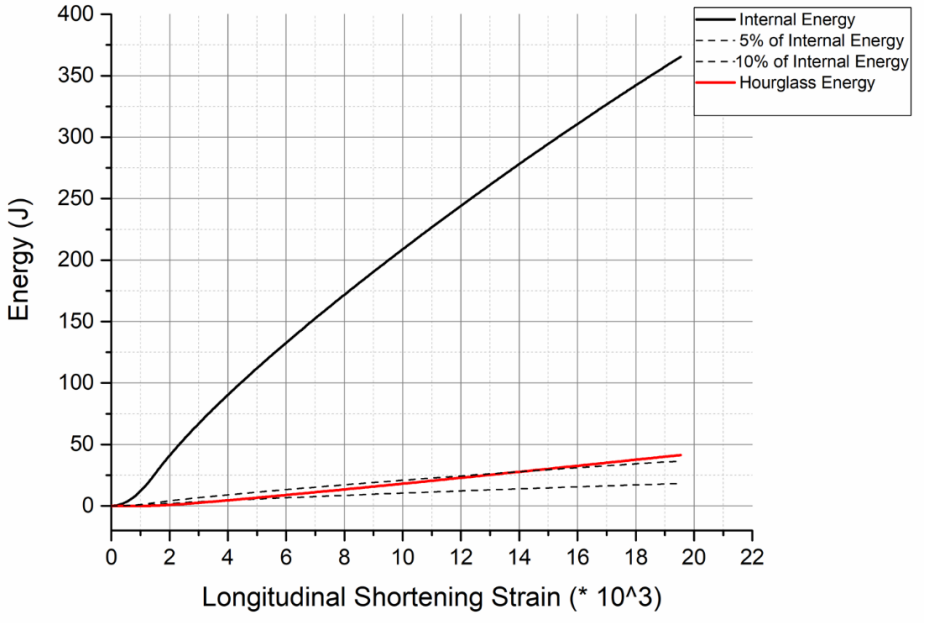

FIGURE 6.6 Internal and hourglass energy comparison for solid elements model

Linear Eigenvalue buckling analysis of shell elements model estimates a buckling load of 7,49975 MN, which is equivalent to a critical buckling stress of 320 MPa. The estimation for cubic elements model is 7,53567 MN or 321 MPa. As shown in FIGURE 6.7 The theoretical buckling load is not achieved neither for shell elements model nor for solid elements model. This behavior is expected, considering nonlinearities and assigned imperfections.

For both models is predicted that the stiffened plate element collapses under almost the same load and strain. For shell elements analysis, maximum compressive stress is equal to 258 MPa for a shortening strain of 0,00144 and for cubic elements analysis 260 MPa and 0,00147 respectively. Post buckling cubic element model is stiffer. According to Common Structural Rules (CSR) maximum compressive stress the element can carry is 258 MPa for a shortening strain of 0,00153, however collapse mode predicted from CSR is not equivalent with this acquired from FEM analysis, since CSR predicts that stiffeners buckle due to torsion.

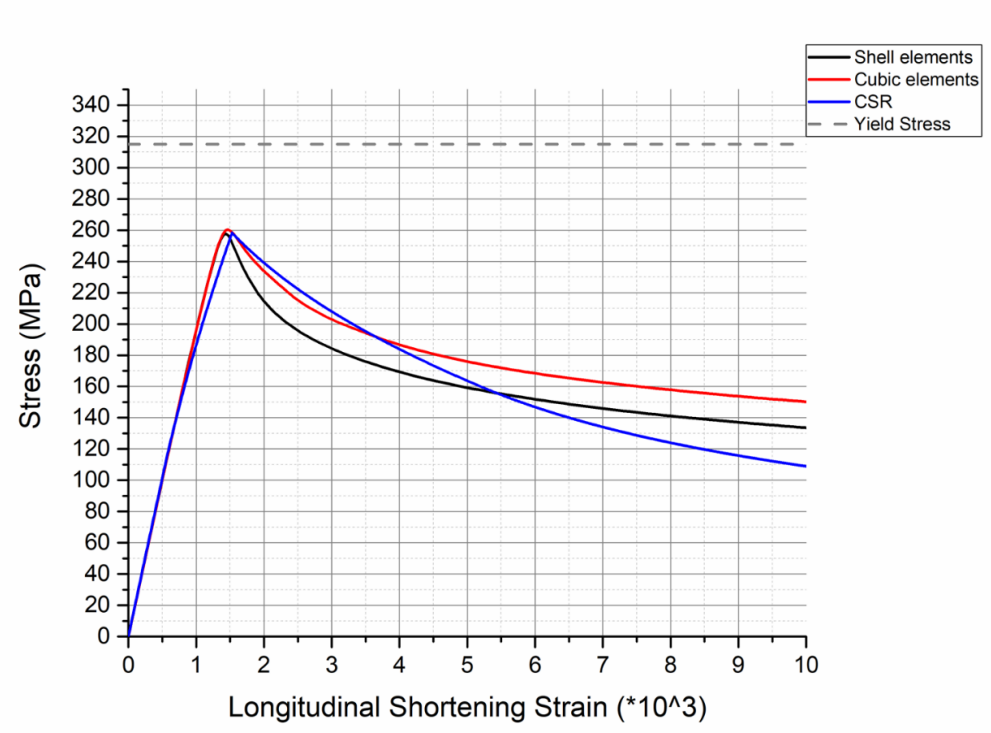

FIGURE 6.7 Stress-strain curves of single element

Both on the model of shell and solid elements, almost the whole of the element yields when instability occurs (FIGURE 6.8). Von Mises stresses are distributed antisymmertically on the plates to the left and right of the stiffener.

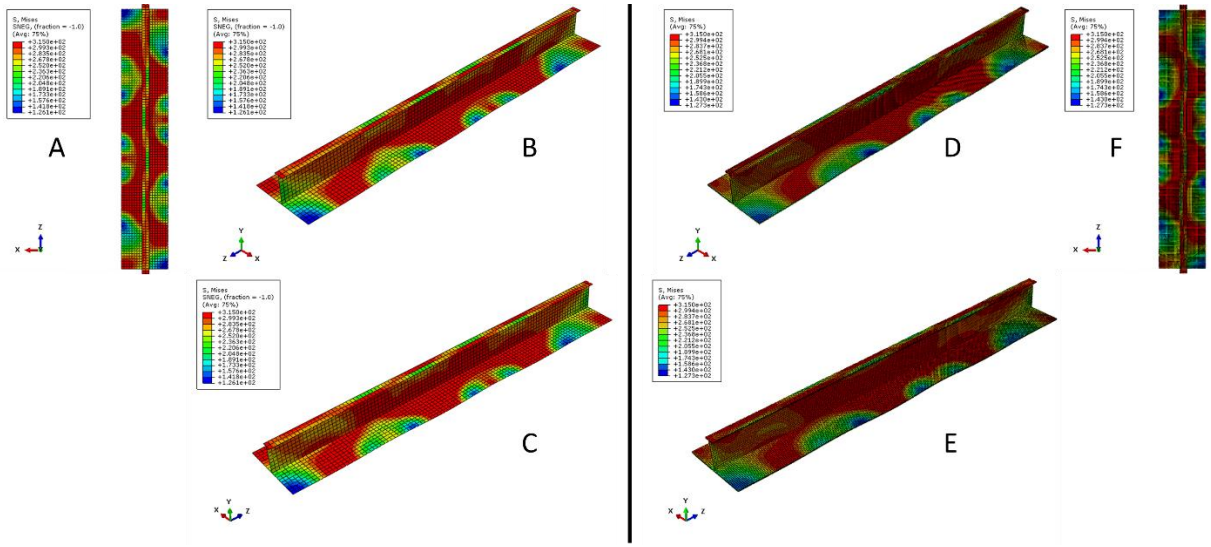

FIGURE 6.8 Von Misses Stress distribution for shell model (left), solid model (right) when element collapses

Maximum displacements when element collapses match with those acquired from the stiffened plate having equivalent boundary conditions. The element collapses under a compilation of local plate buckling with six half waves as linear eigenvalue analysis predicts and local stiffener web buckling and a slight torsion of the stiffeners locally. (FIGURE 6.9, 6.10)

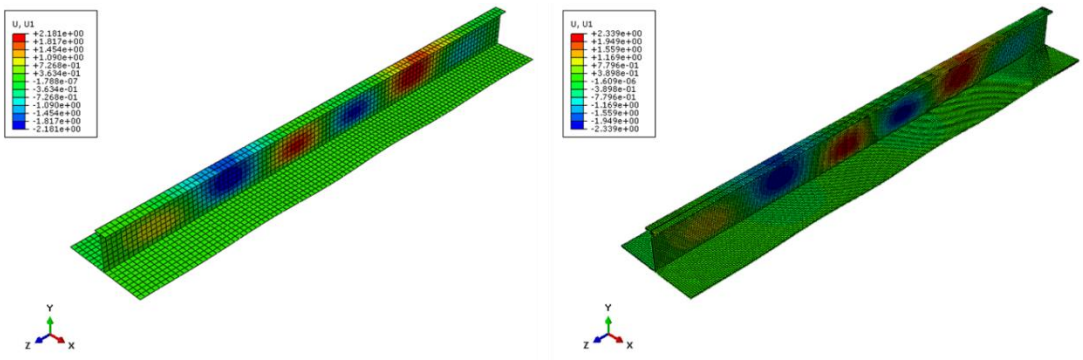

FIGURE 6.9 Transverse displacement for shell model (left), solid model (right) when element collapses

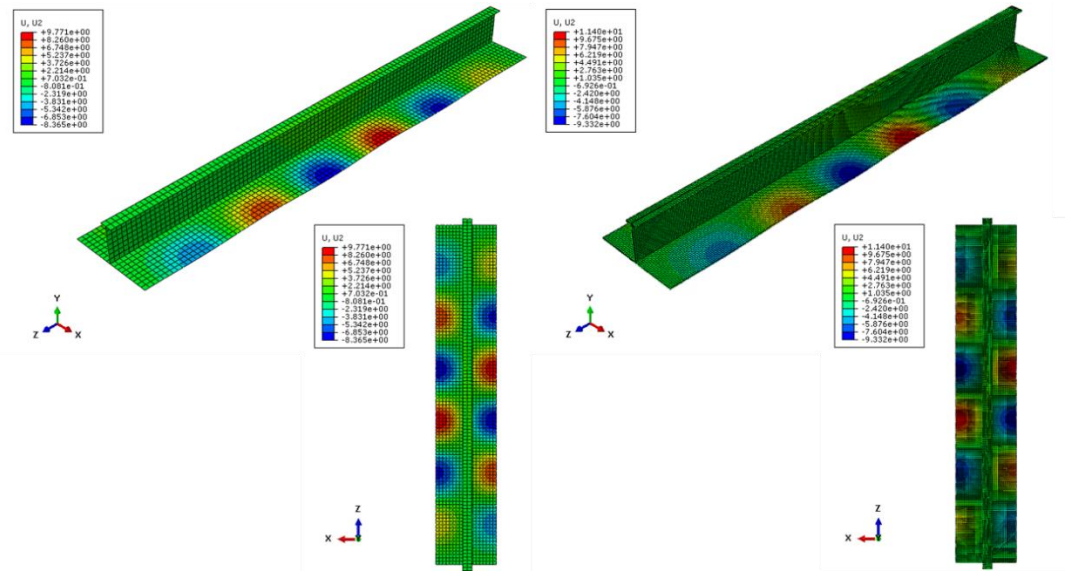

FIGURE 6.10 Vertical displacement for shell model (left), solid model (right) when element collapses

Results acquired from analysis of a single element of a stiffened plate seem to be a good estimation of a stiffened plate's buckling capacity. Buckling capacity of an element is 258/260 MPa for shell/cubic elements and this of a stiffened plate with 6 stiffeners is 270 MPa. Shortening strain before collapse of the element is 0,00144/0,00147 for shell/cubic finite elements and 0,00144 for stiffened plate using shell elements.

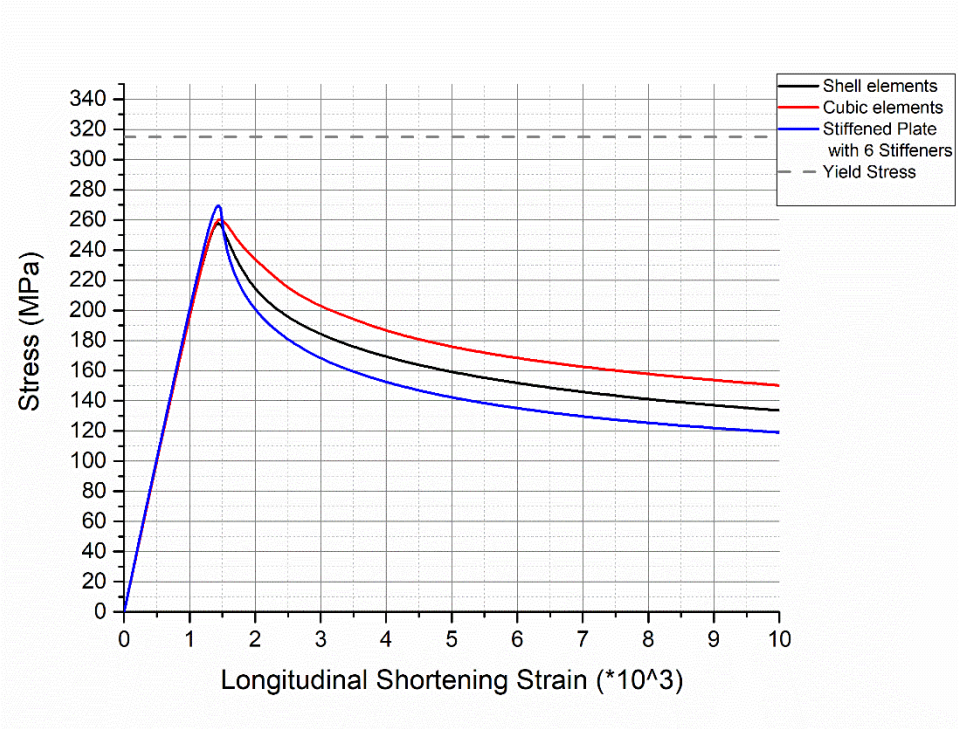

FIGURE 6.11 Single element and stiffened plate with 6 Stiffeners comparison

6.4 Transverse Edge and Longitudinal Edge Nodes have Zero Transverse Displacement

6.4.1 Linear Analysis

Both shell elements and cubic elements models are imposed to pure uniaxial compression by subjecting force in longitudinal direction to the free to move reference point.

Plate between stiffeners buckles overall. Deformation of stiffeners and plate is equivalent significant. Critical part is considered in the middle where deformation of both stiffeners and plate are higher than closer to the edge of stiffened plate

The buckling load is 5,08857 MN, which is equivalent to a critical buckling stress of 217 MPa for shell model and 5,01422 MN or 214 MPa for solid model.

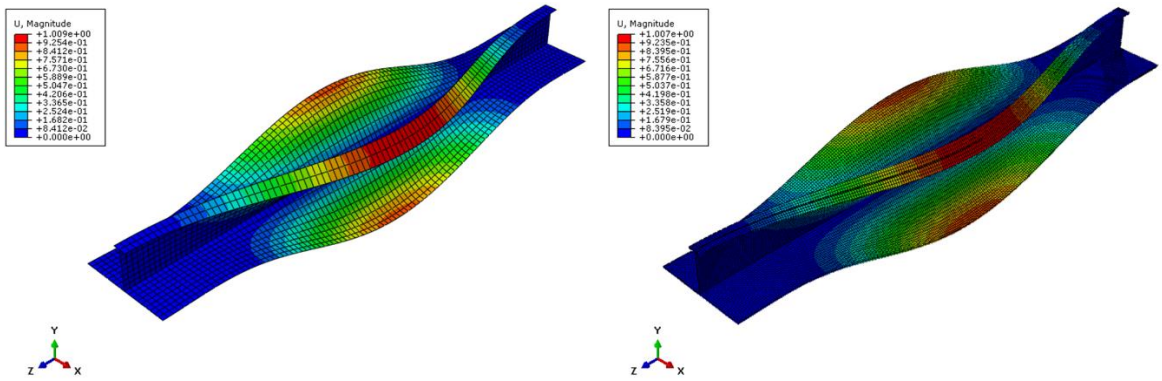

FIGURE 6.12 First buckling mode for shell (left) and solid (right) model

6.4.1.1 Nonlinear Analysis

The aforementioned eigenmode would be utilized as initial geometrical imperfections of the models, applied with the proposed tolerance level. Since stiffeners deformation is slightly higher than this of plate, maximum amplitude of 5,12 mm (L/200) is applied.

Models are imposed to pure uniaxial compression by subjecting displacement in longitudinal axis to the free to move RP. Simulation run using Rik's Method.

Hourglass Energy compared with Internal Energy of the model is shown in FIGURE 6.13 and FIGURE 6.14 for shell elements model and cubic elements model respectively. For shell elements model Hourglass Energy values are below 5% of Internal Energy as the element is shortening. Hourglass Energy values in cubic elements model are below 5% of Internal Energy for shortening strain up to 0,004 and range between 5% and 10% for strain up to

0,011. Cubic elements model is expected to behave more stiff compared to shell elements model due to higher Hourglass Energy

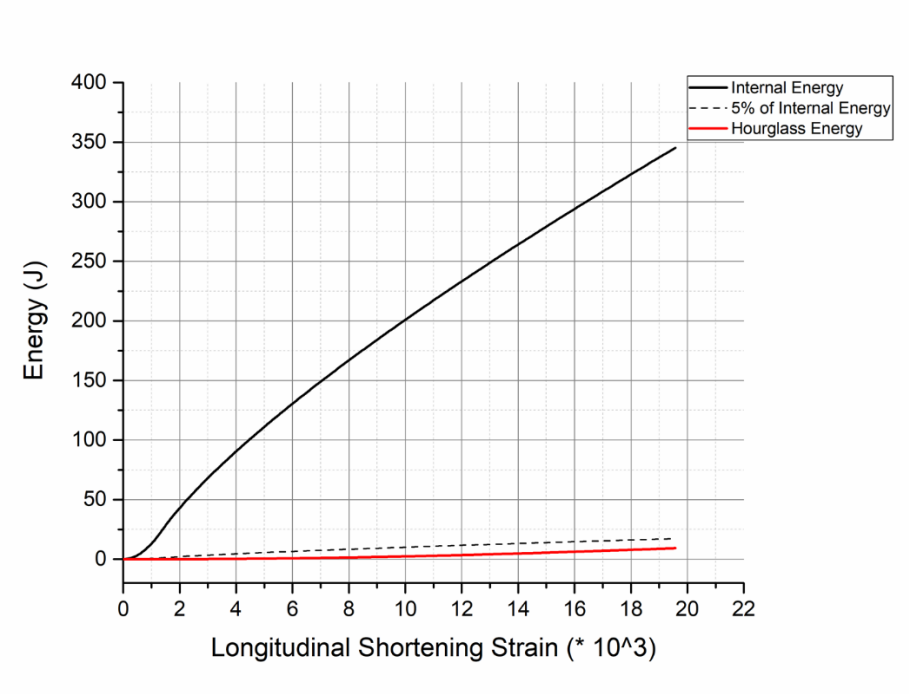

FIGURE 6.13 Internal and hourglass energy comparison for shell elements model

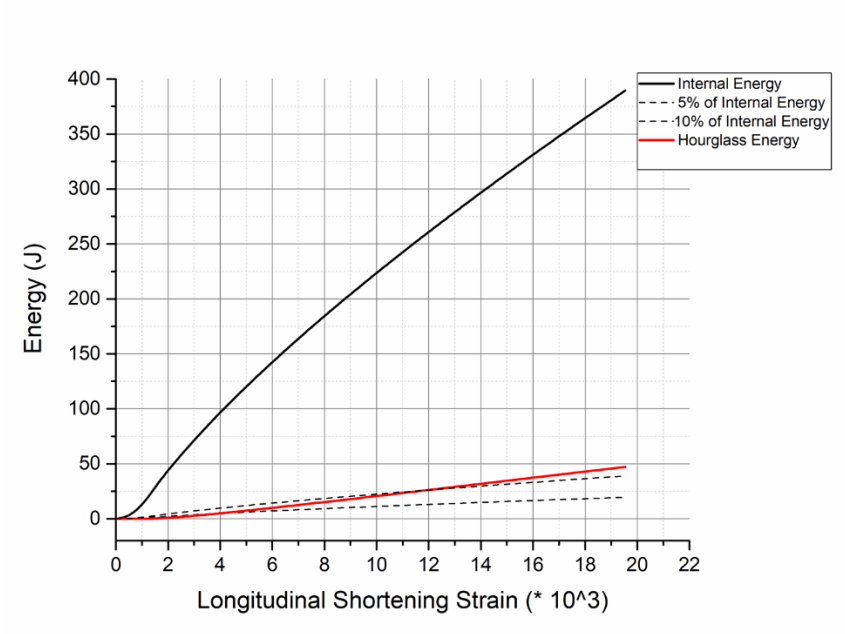

FIGURE 6.14 Internal and hourglass energy comparison for solid elements model

Linear Eigenvalue buckling analysis estimates a buckling load of 217 MPa for shell elements model and 214 MPa for cubic elements model. In FIGURE 6.15 it is observed that structure loses its stability after reaching peak value of 276 MPa for 0,00138 shortening strain and 279 MPa for a shortening strain of 0,00143 for shell and solid element models respectively. It must be noted that maximum load before structure collapses is higher than this estimated from linear buckling analysis on both cases (explained in Chapter 5.4.2). According to Common Structural Rules (CSR) maximum compressive stress the element can carry is 258 MPa for a shortening strain of 0,00153. Collapse mode predicted from CSR is similar with this acquired from FEM analysis, since CSR predicts that stiffeners lose stability under torsional buckling.

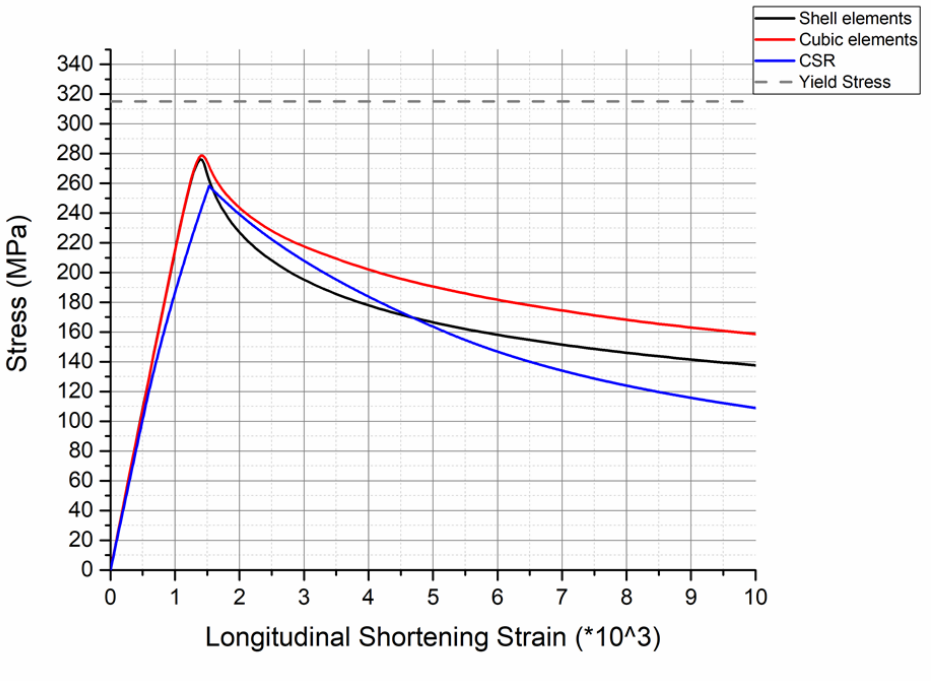

FIGURE 6.15 Stress-strain curves of single element

Both on the model of shell and solid elements, almost the whole of the element yields when instability occurs (FIGURE 6.16). Collapse mode of the whole element has no symmetry or antisymmetry in transverse direction, thus there is no symmetry or antisymmetry in the way von Mises stresses are distributed on the plating to the left and right of the stiffener. For each plate, stresses are distributed symmetrically in longitudinal direction.

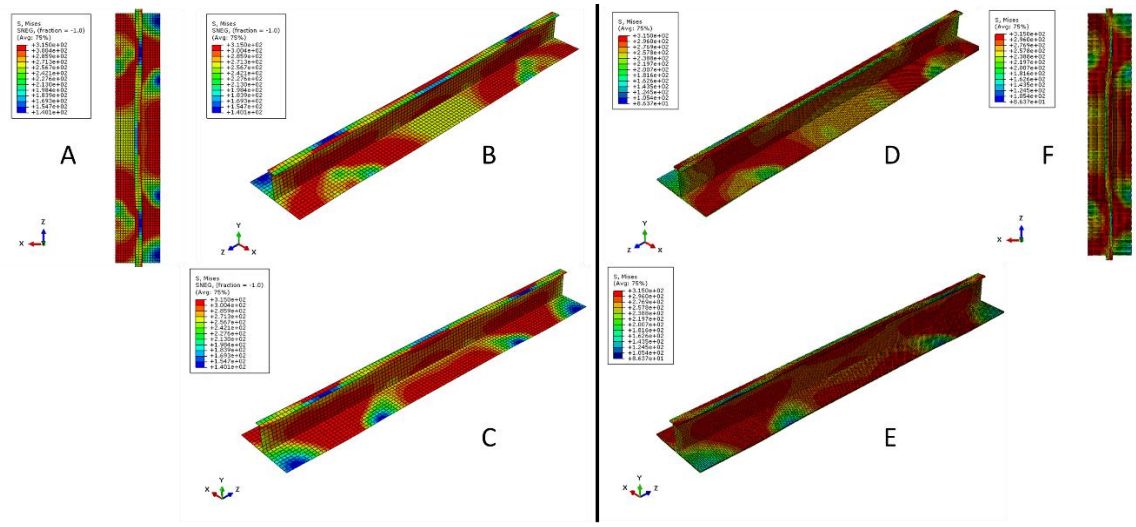

FIGURE 6.16 Von Misses Stress distribution for shell model (left), solid model (right) when element collapses

Maximum displacements when instability occurs shows a compilation of stiffener tripping with a slight topical buckling of the webs near the longitudinal ends of the stiffeners for both shell and cubic elements. Stiffeners' deformation seems to maximize in the middle of the stiffener. Buckling mode of plating between stiffeners differs from this predicted from linear eigenvalue analysis since the plates collapse forming five halfwaves (explained in Chapter 5.4.2). The exact same behavior and collapse mode encountered on stiffened plate with equivalent boundary conditions.

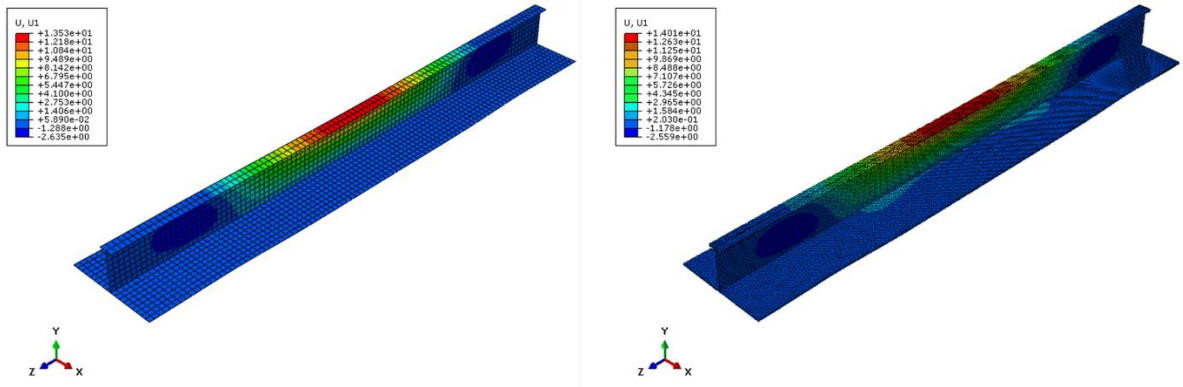

FIGURE 6.17 Transverse displacement for shell model (left), solid model (right) when element collapses

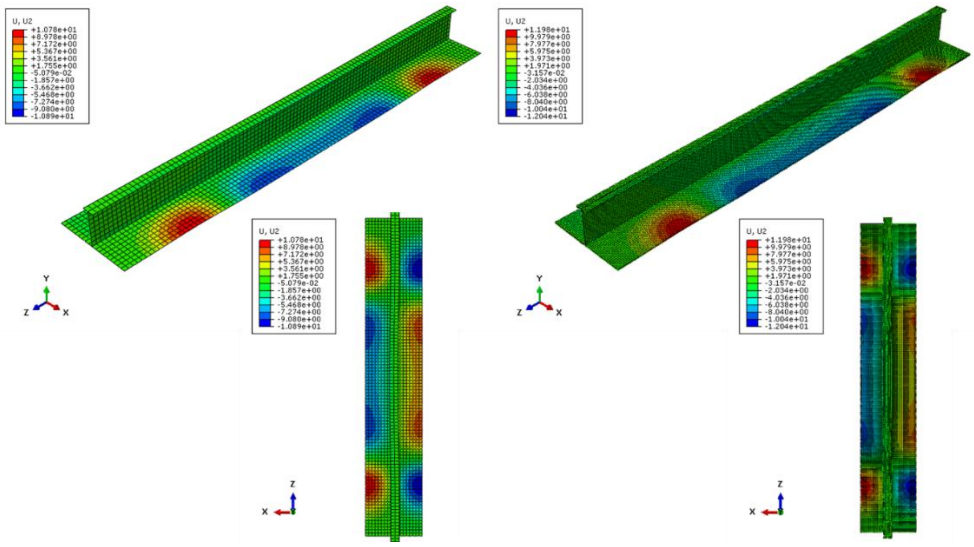

FIGURE 6.18 Vertical displacement for shell model (left), solid model (right) when element collapses

Stress-shortening strain curve of stiffened plate with 6 stiffeners is almost identical with the curve acquired from the analysis of a single element using shell finite elements. Thus, seems that estimating buckling capacity of a stiffened plate analyzing just one of its elements could lead to accurate results. Specifically, the stiffened plate with 6 stiffeners and equivalent boundary conditions reached its buckling load of 282MPa for a shortening strain of 0,0139 and the isolated element model reached its buckling load of 276/279 MPa for a shortening strain of 0,0138/0,0143 (shell/solid elements)

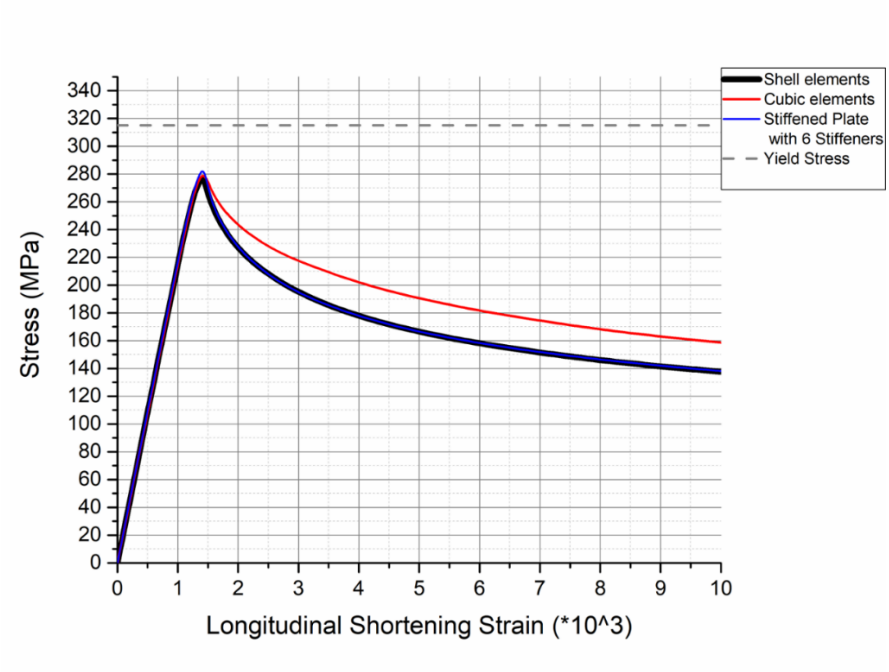

FIGURE 6.19 Single element and stiffened plate with 6 stiffeners comparison

7 Conclusions

This work is a study of the buckling and ultimate strength of a stiffened plate on a ship's deck and stiffened plate's element (stiffener and attached plating) under compressive loading conditions, which results from the sagging of the hull, using Finite Element Method. During the procedure, a series of 11 finite element models were studied. Firstly, a three-span model of a VLCC's hull subjecting to sagging was analyzed and the deformation of the transverse frames was monitored. The results of the analysis of the three-span model shown that vertical deformation of the frames is negligible. However, it is not clear whether transverse deformation of the frames is significant. Hence, for the analysis of a one-span model of the same hull under sagging, two different cases studied: 1) Nodes on transverse cross-section of the hull are free to move in transverse direction (transverse rigidity of transverse frames is underestimated) 2) Displacement of nodes of transverse cross-section of the hull is zero (transverse rigidity of transverse frames is overestimated). The results shown that the assumptions for the conditions encountered on the transverse cross-section of the hull, affects the behavior of deck's structural elements. Investigating the behavior of a stiffened plate with 24 stiffeners on the deck, was observed that transverse displacement of its longitudinal boundaries alters depending on the conditions on the transverse cross-section. Considering free transverse displacement of nodes on transverse cross-section, the nodes on longitudinal edges of the stiffened plate have common displacement in transverse direction. On the other hand, restricting the transverse displacement of nodes on transverse cross-section, the nodes on longitudinal edges of the stiffened plate barely move in transverse direction, hence their translation could be assumed zero. Therefore, two different sets of boundary conditions emerge for the analysis of an isolated stiffened plate. Those two different sets of boundary conditions were applied to an isolated one-span model of a stiffened plate with 24 stiffeners under compression. The analysis of the one-span model of the isolated stiffened plate shown that the applied boundary conditions simulate successfully the behavior of the stiffened plate as part of the equivalent one-span hull model.

Marine structures have plates with 5 to 10 stiffeners. A model of a stiffened plate with 6 stiffeners subjecting to uniaxial compression studied. The two aforementioned sets of boundary conditions were applied. Collapse mode, ultimate strength, stress distribution and load distribution along stiffened plate's elements were obtained for both of the cases. At the same time transverse displacement on the boundaries of the stiffened plate's elements for both of the cases were investigated. Hence, the appropriate boundary conditions representing realistically the behavior of an isolated stiffened plate element were acquired. As shown, the conditions an isolated element encounters on its boundaries, are affected by the boundary conditions of the plate it belongs to. Specifically, assuming a stiffened plate under uniaxial compression, whose nodes on the longitudinal boundaries have common transverse displacement, results in common transverse displacement for the nodes on the longitudinal boundaries of the stiffened plate's elements. Similarly, assuming a stiffened plate under uniaxial compression, whose nodes on the longitudinal boundaries have restricted transverse displacement, results in zero transverse displacement for the nodes on

the boundaries of the stiffened plate's elements. Finally, the behavior of an isolated stiffened plate's element was simulated, using shell and solid finite elements and setting the equivalent boundary conditions derive from the stiffened plate analysis. It is shown that through the analysis of an isolated stiffened plate's element, the collapse mode and ultimate strength of a stiffened plate could be approached acceptably.

From procedure described above the following conclusions made:

- When simplifying a three-span model of a hull to a one-span model with no transverse frame included, transverse rigidity of the transverse frame is either underestimated either overestimated. Those assumptions on boundary conditions affect the collapse mode and ultimate strength of deck's stiffened plates. For the stiffened plate of the VLCC studied in this work, the three-span hull model analysis predicted a collapse mode governed by local plate buckling and local buckling of stiffener's web. The ultimate strength of the stiffened plate was estimated 280 MPa. Underestimating transverse rigidity of transverse frames by setting free the transverse translation of the cross-sectional nodes in the one-span model of the same hull, lead to the same collapse mode with the three-span model for the stiffened plate, but ultimate strength was estimated 273 MPa (2,5% lower). Overestimating transverse rigidity of transverse frames, by suppressing transverse displacement of cross-sectional nodes in the one-span hull model, lead to a collapse mode for the plate which is a combination of local plate buckling and stiffener tripping. The ultimate strength calculated 291 MPa (4% higher). Underestimating the transverse rigidity of the frames, the ultimate strength of the deck's stiffened plate is also underestimated. Similarly, overestimating transverse rigidity of the transverse frames, overestimates the ultimate strength of the stiffened plate on deck.
- Transverse edge boundary conditions seem to have great impact on the response of the longitudinal boundaries of a stiffened plate. For the analysis of the one-span model of the hull, two different sets of boundary conditions assumed for the cross-sectional edge of the model: 1) Transverse cross-sectional nodes are free to move in transverse direction 2) Transverse displacement of transverse cross-sectional nodes is restricted. For the first set of boundary conditions, was observed that nodes on longitudinal edges of a stiffened plate on deck have common displacement in transverse direction. For the second set, was observed that nodes barely move in transverse direction.
- As a stiffened plate is subjected to uniaxial compression, its element's ultimate strength seems to differ. For the cases studied in this work, the ultimate strength of the stiffened plate's elements could differ up to 6,1% and 4,7% depending on the boundary conditions. Elements closer to stiffened plate's longitudinal edges, where boundary conditions are applied, was found to withstand higher loads before collapse.
- On a stiffened plate, suppressing transverse displacement of nodes on transverse and longitudinal edges and subjecting the plate to pure uniaxial compression, results

in biaxial compression with the ratio of loads acting on plate's edges changing as plate shortens. Different load ratios for biaxial compression lead to different collapse modes. Hence, for the aforementioned boundary conditions, collapse mode predicted from linear analysis might differ from the resulting collapse mode of nonlinear analysis.

- Boundary conditions simulating the behavior of an isolated stiffened plate's element seem to be dependent of the boundary conditions of the stiffened plate. The cases studied, reveal that for a stiffened plate whose nodes on transverse edges are free to move in transverse direction and nodes on longitudinal edges have common transverse displacement, restrictions for the transverse displacement of the equivalent nodes of its elements (stiffener with attached plate) are the same. Similarly, for a stiffened plate whose transverse translation of nodes on transverse and longitudinal edges is suppressed, the transverse translation of the equivalent nodes of its elements is zero.
- Shell and solid elements seem to be equally accurate estimating ultimate strength of an isolated stiffened plate's element. For the cases studied, models using cubic elements estimates a buckling stress 0,8% and 1,1% higher, depending on the boundary conditions, than the models using shell elements. Post buckling cubic elements seem to predict stiffer behavior of construction.
- Results acquired from the study of an isolated element of a stiffened plate, seem to be an acceptable estimation of a stiffened plate's buckling capacity. Comparing ultimate strength between a stiffened plate with 6 stiffeners and an isolated element was found that stresses predicted through the analysis of an isolated element are 4,4%/3,7% and 2,1%/1,1% lower, for models using shell/cubic elements, depending on boundary conditions. The collapse mode of the stiffened plate is estimated accurately through the analysis of an isolated element (stiffener with attached plate).

Model	Longitudinal span	Load	Element type	Mesh size	Comments on BC		Nonlinear Analysis			Chapter
					Transverse section nodes' transverse displacement (Stiffened Plate)	longitudinal edge nodes' transverse displacement (Stiffened Plate)	Maximum Stress MPa (Stiffened Plate)	Longitudinal Strain (Stiffened Plate)	Collapse mode	
VLCC's Hull	3 (L/2+L+L/2)	Pure Bending	S4R	250	_	_	280	0,00152	Local plate buckling, local web buckling	4.1
	1 (L)	Pure Bending	S4R	250	free	_	273	0,00144	Local plate buckling, local web buckling	4.2.3
	1 (L)	Pure Bending	S4R	250	suppressed	_	291	0,00142	Local plate buckling, stiffener tripping	4.2.4
VLCC's deck's stiffened plate with 24 stiffeners	1 (L)	Uniaxial Compression	S4R	250	free	common	269	0,00149	Local plate buckling, local web buckling	4.3.3
	1 (L)	Uniaxial Compression	S4R	250	suppressed	suppressed	285	0,00143	Local plate buckling, stiffener tripping	4.3.4
Stiffened plate with 6 stiffeners	1 (L)	Uniaxial Compression	S4R	50	free	common	270	0,00144	Local plate buckling, local web buckling	5.3
	1 (L)	Uniaxial Compression	S4R	50	suppressed	suppressed	282	0,00139	Local plate buckling, stiffener tripping	5.4
Single element of stiffened plate	1 (L)	Uniaxial Compression	S4R	50	free	common	258	0,00144	Local plate buckling, local web buckling	6.3
	1 (L)	Uniaxial Compression	S4R	50	suppressed	suppressed	276	0,00138	Local plate buckling, stiffener tripping	6.4
	1 (L)	Uniaxial Compression	C3D8R	20*20*4	free	common	260	0,00147	Local plate buckling, local web buckling	6.3
	1 (L)	Uniaxial Compression	C3D8R	20*20*4	suppressed	Suppressed	279	0,00143	Local plate buckling, stiffener tripping	6.4

TABLE 7.1 Table of results acquired from the study

References

[1] D. J. Eyres, (2007), *Ship Construction,* 6th ed.

[2] Yasuhisa Okumoto, Yu Takeda, Masaki Mano, Tetsuo Okada (2009), *Design of Ship Hull Structures,* Berlin: Springer-Verlag,

[3] Gilmer and Johnson (1987), *Introduction to Naval Architecture*

[4] Owen F. Hughes and Jeom Kee Paik, (2010), *Ship structural analysis and design,* Jersey City, New Jersey: The Society of Naval Architects and Marine Engineers, pp.14.1-15.26

[5] von Karman, T., Sechler, E., and Donnell, L. H. (1932). The strength of thin plates in compression. *Trans. ASME*, Vol. 54, 53.

[6] Sharp, M. L. (1966). Longitudinal stiffeners for compression members. *ASCE J. Struct. Div.*, Vol. 92, ST5.

[7] Timoshenko, S. P., and Gere, J. M. (1961). *Theory of elastic stability* (2nd ed.). New York: McGraw-Hill.

[8] https://www.steelconstruction.info/Stiffeners

[9] Cheng Yu, Benjamin W. Schafer (2016), *Stress Gradient Effect on the Buckling of Thin Plates*

[10] https://www.femto.eu/stories/linear-non-linear-analysis-explained/

[11] Simulia, *Abaqus 6.14, getting started with abaqus interactive edition,* p.8.2-8.5

[12] Nikolaos Vasios (2015), *Nonlinear Analysis of Structures, The Arc Length Method: Formulation, Implementation and Applications*, PhD thesis, University of Harvard

[13] http://www.aerospacengineering.net/buckling-theory-and-buckling-non-linear/

[14] Yao, T., & Fujikubo, M., (2016) *Buckling and Ultimate Strength of Ship and Ship-Like Floating Structures*

[15] IACS (2019), Common Structural Rules for Bulk Carriers and Oil Tankers

[16] ABS (2019), *Rules for building and classing, Marine vessels, Part 3 Hull construction and equipment, p. 388*